

1-1-2000

Material properties of novel polymeric films.

Gene Kim
University of Massachusetts Amherst

Follow this and additional works at: https://scholarworks.umass.edu/dissertations_1

Recommended Citation

Kim, Gene, "Material properties of novel polymeric films." (2000). *Doctoral Dissertations 1896 - February 2014*. 1004.
<https://doi.org/10.7275/zbz2-7c49> https://scholarworks.umass.edu/dissertations_1/1004

This Open Access Dissertation is brought to you for free and open access by ScholarWorks@UMass Amherst. It has been accepted for inclusion in Doctoral Dissertations 1896 - February 2014 by an authorized administrator of ScholarWorks@UMass Amherst. For more information, please contact scholarworks@library.umass.edu.

312066 0264 8337 8

MATERIAL PROPERTIES OF NOVEL POLYMERIC FILMS

A Dissertation Presented

by

GENE KIM

Submitted to the Graduate School of the
University of Massachusetts Amherst in partial fulfillment
of the requirements for the degree of

DOCTOR OF PHILOSOPHY

February 2000

Polymer Science and Engineering

© Copyright by Gene Kim 2000

All Rights Reserved

MATERIAL PROPERTIES OF NOVEL POLYMERIC FILMS

A Dissertation Presented

by

GENE KIM

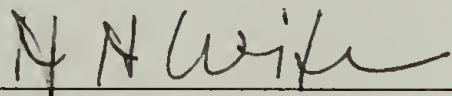
Approved as to style and content by:



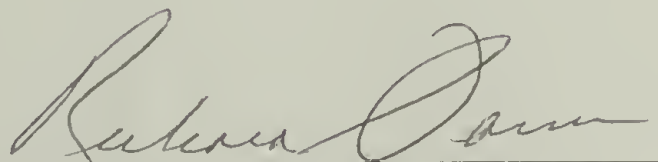
Richard J. Farris, Chair



Thomas J. McCarthy, Chair



Henning H. Winter, Member



Richard J. Farris, Department Head
Polymer Science and Engineering

ACKNOWLEDGMENTS

When I first arrived at the University of Massachusetts, I realized I had to adjust to a new set of rules, where there was no final or a mid-term where a limited amount of knowledge could get you a grade. The final exam here, as a graduate student, was going to cover everything that was going to happen over the period of my stay here in Amherst. It took me a while to get used to the idea that things weren't going to be graded in a short period of time, and patience was a virtue that I had to treasure to even attempt to take the final exam.

Now, looking back and getting ready for my final exam, I see how much tutoring has been done for me over the years. None of my achievements would have been possible without the help that I have received. Certainly, I had "the best of the best" when it came to tutors. My two research advisors, Dr. Thomas J. McCarthy and Dr. Richard J. Farris, served as the greatest minds in polymer science and polymer engineering for me. Their enthusiastic endeavors towards life, in general, were a great motivation for me, aside from their technical expertise. My other committee member, Dr. Henning H. Winter, has also been a great help for me with other aspects of my research and my life.

Tutoring didn't stop there. Dr. McCarthy's and Dr. Farris' post-doc's and students – past and present – have been a great help in learning graduate student life. I thank all of those who helped my stay here in Amherst be pleasurable.

Certainly being in the number one department in the United States (possibly the world) has its perks, and one of the biggest is the quality of the faculty. They have allowed me to have a solid foundation of polymer science and engineering second to

none, and I thank all of those who have helped me with my development as a polymer scientist and engineer. Another perk is having the best administrative staff in the world for tutoring me of ways around the department. Eileen, Eleanor, and Sophie – you’re the best! And the best perk of all is having great peers. I thank my classmates of ’94. You guys, although were nuts, have helped me in more ways than you can imagine. I have the utmost respect for all of you, I want you to know that.

I must mention some other names who have helped me throughout my graduate career. Thank you, Jack Hirsch, who has been instrumental in my development in and out of the department. Thank you, Wei Chen, Vipavee Phuvanartnuruks, and Padma Rajagopalan, for the daily gossiping and undivided moral support over the years. Thank you, Michael Yu, Young-je Kwark, and Jeong-han Kim, the talented Korean students in our department, who have been very supportive with my efforts, and helped me more than I can swallow. Thank you, Dr. Seo Hyun Cho, who has come at the nick of time to help my last two years of my research so exciting. And thank you, the rest of the Korean “Mafia” – a nickname given to the Koreans in our department by the department. You all know that I couldn’t have done it without you.

I thank all my friends who have been supportive of me over the years. I especially thank Jun-young Lee, Kwang-geun Chung, and Bryan Zelnik, and my posse in Korea, who have been the best of friends. May our friendship last forever!

Last but not least, I thank my family who has been there from the get-go, and pushed me to do my best in every occasion. I couldn’t ask for a better family even if I wanted to.

This thesis is dedicated to my biggest fan - my mom, Young-ja Kim. She didn't get to see me graduate due to her going off to a "better place". Thanks for looking out for me up there.

ABSTRACT

MATERIAL PROPERTIES OF NOVEL POLYMERIC FILMS

FEBRUARY 2000

GENE KIM, B.S., IOWA STATE UNIVERSITY

M.S., UNIVERSITY OF MASSACHUSETTS AMHERST

Ph.D., UNIVERSITY OF MASSACHUSETTS AMHERST

Directed by: Professors Richard J. Farris and Thomas J. McCarthy

This dissertation will study the material properties of two types of novel polymer films (polyelectrolyte multilayer films and photolithographic polymer films).

The formation of polyelectrolyte multilayer films onto functionalized aluminum oxide surfaces and functionalized poly(ethylene terephthalate) (PET) were studied. Functionalization of the aluminum oxide surfaces was achieved via silane coupling. Functionalization of PET surfaces was achieved via hydrolysis and amidation. Surface characterization techniques such as X-ray photoelectron spectroscopy (XPS) and dynamic contact angle measurements were used to monitor the polyelectrolyte multilayer formation. Mechanical properties of the aluminum oxide supported polyelectrolyte multilayer films were tested using a simplified peel test. XPS was used to analyze the surfaces before and after peel. Single lap shear joint specimens were constructed to test the adhesive shear strength of the PET-supported polyelectrolyte multilayer film samples with the aid of a cyanoacrylate adhesive. The adhesive shear strength and its relation with the type of functionalization, number of polyelectrolyte layers, and the effect of

polyelectrolyte conformation using added salt were explored. Also, characterization on the single lap joints after adhesive failure was carried out to determine the locus of failure within the multilayers by using XPS and SEM.

Two types of photolithographic polymers were formulated and tested. These two polymers (photocrosslinkable polyacrylate (PUA), and a photocrosslinkable polyimide (HRP)) were used to investigate factors that would affect the structural integrity of these particular polymers under environmental variables such as processing (time, UV cure, pressure, and temperature) and ink exposure. Thermomechanical characterization was carried out to see the behavior of these two polymers under these environmental variables. Microscopic techniques were employed to study the morphological behavior of the two polymer systems. Also, unique in-house characterization methods such as the vibrational holographic interferometry to measure residual stress in these polymer coatings upon processing, and the environmental tensile tester (ETT) to measure ink diffusion and swelling stresses were used to further characterize these two polymers.

TABLE OF CONTENTS

	<u>Page</u>
ACKNOWLEDGMENTS.....	iv
ABSTRACT.....	vii
LIST OF TABLES.....	xii
LIST OF FIGURES.....	xiii
LIST OF SCHEMES.....	xvii
CHAPTER	
1. LAYER-BY-LAYER ASSEMBLED ULTRATHIN POLYELECTROLYTE FILMS SUPPORTED ON MODIFIED ALUMINUM OXIDE SURFACES.....	1
Metal Oxide Surface Modification.....	1
Silane Coupling Reaction.....	1
Layer-by-layer Deposition.....	3
Polyelectrolyte Adsorption.....	6
Objective.....	10
Polymer Surface Analytical Techniques.....	10
X-ray Photoelectron Spectroscopy (XPS).....	10
Contact Angle.....	14
Experimental.....	16
Materials.....	16
Substrate Preparation.....	17
Silane Coupling Reaction.....	17
Layer-by-layer Deposition.....	17
Preparation of Specimens for the Simplified Peel Test.....	18
Characterization.....	19
Results and Discussions.....	19
Silane Coupling Reaction.....	19
Polyelectrolyte Deposition (kinetics, stratification, attenuation).....	21
Simplified Peel Test.....	35

Conclusions.....	36
References.....	36
 2. MECHANICAL PROPERTIES OF POLYELECTROLYTE MULTILAYER FILMS SUPPORTED ON MODIFIED POLY(ETHYLENE TEREPHTHALATE).....	40
Poly(ethylene terephthalate) (PET) Surface Modification.....	40
Previous Results.....	40
Objective.....	41
Single Lap Shear Test.....	42
Experimental.....	43
Materials.....	43
PET Substrate Preparation.....	43
Multilayer Formation.....	45
Single Lap Shear Assembly.....	45
Mechanical Testing.....	47
Results and Discussions.....	47
Adhesion and the Effect on Substrate Functionalization.....	47
Adhesion and the Effect of the Number of Layers.....	49
Adhesion and the Effect of Added Salt Incorporation.....	49
Determination of Locus of Failure.....	53
Conclusions.....	62
Future Work.....	62
References.....	63
 3. INVESTIGATION OF FACTORS GOVERNING THE STRUCTURAL INTEGRITY OF PHOTOLITHOGRAPHIC POLYMERS.....	65
Photolithographic Materials.....	65
Polymers in Photolithography.....	66
Limitations of the Polymeric Photosensitive Materials.....	66
Types of Photoresist Coatings.....	67
Requirements for Photoresist Polymer Coatings.....	67
Photolithographic Polymers in Adhesive Applications.....	69
Residual Stress in Coatings.....	70
Swelling Stresses and Diffusion of Small Molecules in Polymers.....	74
Objective.....	78
Experimental.....	79

Materials.....	79
Thermomechanical Studies.....	83
TGA Studies.....	85
Differential Scanning Calorimetry (DSC)	85
Dynamic Mechanical Thermal Analysis (DMTA)	85
Thermo-Mechanical Analysis (TMA)	86
Mechanical Properties.....	86
Phase Structure.....	86
Residual Stress Measurements.....	87
Swelling Stress and Stress Relaxation Behavior upon Ink Exposure.....	89
Results and Discussions.....	91
TGA Results.....	91
DSC Results.....	97
DMTA Results.....	104
TMA Results.....	111
Instron Tensile Testing.....	114
Phase Structure Studies.....	120
Residual Stress Measurements upon Processing.....	120
Swelling Stresses and Small Molecule Diffusion.....	124
Conclusions.....	128
Future Work.....	129
References.....	131

APPENDICES

A. XPS AND DYNAMIC CONTACT ANGLE DATA FOR THE POLYELECTROLYTE MULTILAYERS ASSEMBLED ONTO FUNCTIONALIZED ALUMINUM OXIDE.....	133
B. DERIVATION OF THE RELATIONSHIP BETWEEN NORMALIZED STRESS, STRAIN, AND MASS UPTAKE.....	134
C. OPTICAL MICROGRAPHS (REFLECTIVE MODE) OF FULLY PROCESSED POLY(URETHAN ACRYLATE) (PUA) AND POLY(AMIC ACID) METHACRYLIC ESTER (HRP) LITHOGRAPHIC PATTERNS.....	136
BIBLIOGRAPHY.....	137

LIST OF TABLES

Table	Page
1.1. XPS % atomic concentration and dynamic contact angle measurements for cleaned Al, and silane coupled Al (Al-NH ₃ ⁺).....	20
1.2. % atomic concentrations (via XPS, 75° take-off angle) for 24 and 25 polyelectrolyte layers on Al-NH ₃ ⁺ before and after the simplified peel test using a pressure sensitive adhesive (P.S.A.) tape (3M #810).....	35
3.1. Processing conditions for the poly(urethane acrylate) (PUA) and the poly(amic acid) methacrylic ester (HRP) films.....	83
3.2. Coefficient of thermal expansion measurements (TMA) for poly(urethane acrylate) (PUA) films processed at different UV cure conditions....	115
3.3. Coefficient of thermal expansion measurements (TMA) for poly(urethane acrylate) (PUA) films UV cured at 3.0 J/cm ² , thermally cured (220°C) at different cure times.....	115
3.4. Coefficient of thermal expansion measurements (TMA) for poly(urethane acrylate) (PUA) films UV cured at 3.0 J/cm ² , thermally cured (30 min.) at different cure temperatures.....	115
3.5. Mechanical properties of poly(urethane acrylate) (PUA) film UV cured at 3.0 J/cm ² obtained at different thermal cure conditions.....	118

LIST OF FIGURES

Figure	Page
1.1. Adsorbed amount of a weak acid ($pK_d=5$) as a function of pH for three fixed surface charges.....	7
1.2. Adsorption isotherm for 780K poly(styrene sulfonate) at two different salt concentrations.....	8
1.3. Average length and fraction of segments in trains, loops, and tails as a function of pH for a weak polyacid adsorbing onto a charged surface, $\sigma(0)=50 \text{ mC/m}^2$	9
1.4. XPS survey of silane coupled Al sample (75° take-off angle).....	20
1.5. %S atomic concentration (XPS) of the fifth polyelectrolyte monolayer (PSS) after various deposition times.....	22
1.6. %N atomic concentration (XPS) of the fifth polyelectrolyte monolayer (PSS) after various deposition times.....	23
1.7. XPS survey spectrum of a sample containing 6 polyelectrolyte layers deposited on Al-NH_3^+ (75° take-off angle).....	24
1.8. Nitrogen:Sulfur ratio (XPS) for polyelectrolyte multilayers deposited on Al-NH_3^+ ..	26
1.9. Dynamic contact angle measurements for polyelectrolyte multilayers deposited on Al-NH_3^+	27
1.10. Nitrogen:Sulfur ratio (XPS, 75° take-off angle) for polyelectrolyte multilayers constructed on Al-NH_3^+	29
1.11. Advancing contact angle measurements for polyelectrolyte multilayers constructed on Al-NH_3^+	30
1.12. %Al atomic concentration for polyelectrolyte multilayers deposited on Al-NH_3^+ ...	31
1.13. %Si atomic concentration for polyelectrolyte multilayers deposited on Al-NH_3^+ ...	32
1.14. Peak intensity plot for Si_{2p} upon increasing number of polyelectrolyte multilayers on Al-NH_3^+	33
1.15. Peak intensity plot for Al_{2p} upon increasing number of polyelectrolyte multilayers on Al-NH_3^+	34

2.1. Adhesive shear stress of single lap shear joint samples of polyelectrolyte multilayers constructed on modified PET.....	48
2.2. Change in adhesive shear stress for single lap shear joint samples of polyelectrolyte multilayers constructed on hydrolyzed PET.....	50
2.3. SEM micrographs of cyanoacrylate adhesive failure between two hydrolyzed PET lap shear joints (top: x 200 magnification, bottom: x 2000 magnification).....	54
2.4. Single lap shear joint specimens taken to adhesive failure.....	55
2.5. Single lap shear joint specimens taken to adhesive failure.....	56
2.6. %S atomic concentration (XPS, 75° take-off angle) for single lap shear joint samples of polyelectrolyte multilayers (with no added salt) constructed on PET-COO ⁻ after taken to adhesive failure.....	58
2.7. %S atomic concentration (XPS, 75° take-off angle) for single lap shear joint samples of polyelectrolyte multilayers (with added salt, manganese chloride) constructed on PET-COO ⁻ after taken to adhesive failure.....	59
2.8. %N atomic concentration (XPS, 75° take-off angle) for PET-COO ⁻ -supported polyelectrolyte multilayers (added salt) single lap shear joint samples taken to adhesive failure.....	60
2.9. N _{1s} spectrum (XPS, 75° take-off angle) of 21 polyelectrolyte layers (with added salt) on PET-COO ⁻	61
3.1. Typical holographic patterns observed for constructed membranes.....	73
3.2. TGA thermograms of poly(urethane acrylate) (PUA) films obtained under different processing conditions.....	92
3.3. TGA thermograms of poly(urethane acrylate) (PUA) films obtained under different UV curing conditions.....	94
3.4. TGA thermogram of the poly(amic acid) methacrylic ester (HRP) solution (20 wt%) in N-methyl pyrrolidinone (NMP).....	95
3.5. TGA thermogram of the poly(amic acid) methacrylic ester (HRP) film.....	96
3.6. DSC thermogram for poly(urethane acrylate) (PUA) macromonomer.....	98

3.7. DSC thermogram of PUA film obtained at different processing steps	100
3.8. DSC thermogram of PUA film obtained at different processing steps	101
3.9. DSC thermograms of PUA film obtained under different processing conditions...	102
3.10. X-ray diffractograms of PUA films obtained at different processing steps.....	103
3.11. Polarized optical micrographs of PUA film cured at 220 °C, 150 psi, 30 min.....	105
3.12. DSC thermogram of HRP film obtained after the 125 °C thermal cure.....	106
3.13. DSC thermogram of HRP film obtained after the 260 °C thermal cure.....	107
3.14. DMTA thermogram of poly(urethane acrylate) (PUA) polymer film UV cured at 3.0 J/cm ²	108
3.15. DMTA thermogram of poly(urethane acrylate) (PUA) polymer film UV cured at 5.0 J/cm ²	109
3.16. DMTA thermogram of poly(urethane acrylate) (PUA) polymer film UV cured at 3.0 J/cm ² + thermally cured (220 °C, 150 psi., 30 min.).....	110
3.17. DMTA thermogram of poly(amic acid) methacrylic ester (HRP) polymer film, thermally cured.....	112
3.18. TMA thermogram of poly(urethane acrylate) (PUA) polymer film UV cured at 3.0 J/cm ² + thermal cure at 220 °C, 150 psi. for 30 min.....	113
3.19. TMA thermogram of poly(amic acid) methacrylic ester (HRP) polymer film fully cured (CTE = 56 μm/m/°C).....	116
3.20. Stress-strain curve of poly(urethane acrylate) (PUA) films obtained at different processing conditions.....	117
3.21. Stress-strain curve of the fully cured poly(amic acid) methacrylic ester (HRP) film.....	119
3.22. TEM micrographs of poly(urethane acrylate) (PUA) films processed at different UV cure conditions.....	121
3.23. TEM micrographs of poly(urethane acrylate) (PUA) film processed at different conditions.....	122

3.24. Residual stress measurements (holographic interferometry) for poly(urethane acrylate) (PUA) film UV cured at 1.5, 3.0, 5.0 J/cm ²	123
3.25. Calibration curve for the Environmental Tensile Tester (ETT).....	125
3.26 Stress relaxation behavior of fully cured poly(urethane acrylate) (PUA) film upon introduction of WB60 ink.....	126
3.27. Stress relaxation behavior of fully cured poly(amic acid) methacrylic ester (HRP) film upon introduction of WB60 ink.....	127
C.1. Fully processed PUA lithographic patterns.....	136
C.2. Fully processed HRP lithographic patterns.....	136

LIST OF SCHEMES

Scheme	Page
1.1. Schematic representation of a silane coupling reaction with a functionalized triethoxysilane onto a metal oxide surface.....	2
1.2. Schematic representation of layer-by-layer deposition using two oppositely charged polyelectrolytes (washing steps are not included between each beaker).....	5
1.3. Schematic representation of X-ray Photoelectron Spectroscopy (XPS).....	13
1.4. Schematic representation of dynamic contact angle measurements (γ denotes the surface tension of each interface; S-solid, L-liquid, and V-vapor).....	15
1.5. Chemical formula for 3-aminopropyltriethoxysilane, poly(allyl amine) hydrochloride salt, and poly(styrene sulfonate) sodium salt.....	16
1.6. Side view of the simplified peel test samples used for XPS analysis.....	18
2.1. Surface functionalization of Mylar® poly(ethylene terephthalate) (PET) film.....	44
2.2. Single lap shear joint assembly configuration for the layer-by-layer deposited polyelectrolyte multilayer films.....	46
2.3. Pictorial representation of the single lap shear joint test.....	52
3.1. Simple diagram representing a free-radical initiated photopolymerization process.....	66
3.2. Two different types of photoresists.....	68
3.3. Processing of the poly(urethane acrylate) (PUA) system.....	81
3.4. Chemical compositions of the poly(urethane acrylate) (PUA) macromonomer.....	82
3.5. Chemical composition of the poly(amic acid) methacrylic ester (HRP) and its photoresist processing.....	84
3.6. Schematic set-up for the holographic interferometry.....	88
3.7. Schematic set-up of the environmental tensile tester (ETT).....	90

CHAPTER 1

LAYER-BY-LAYER ASSEMBLED ULTRATHIN POLYELECTROLYTE FILMS SUPPORTED ON MODIFIED ALUMINUM OXIDE SURFACES

Metal Oxide Surface Modification

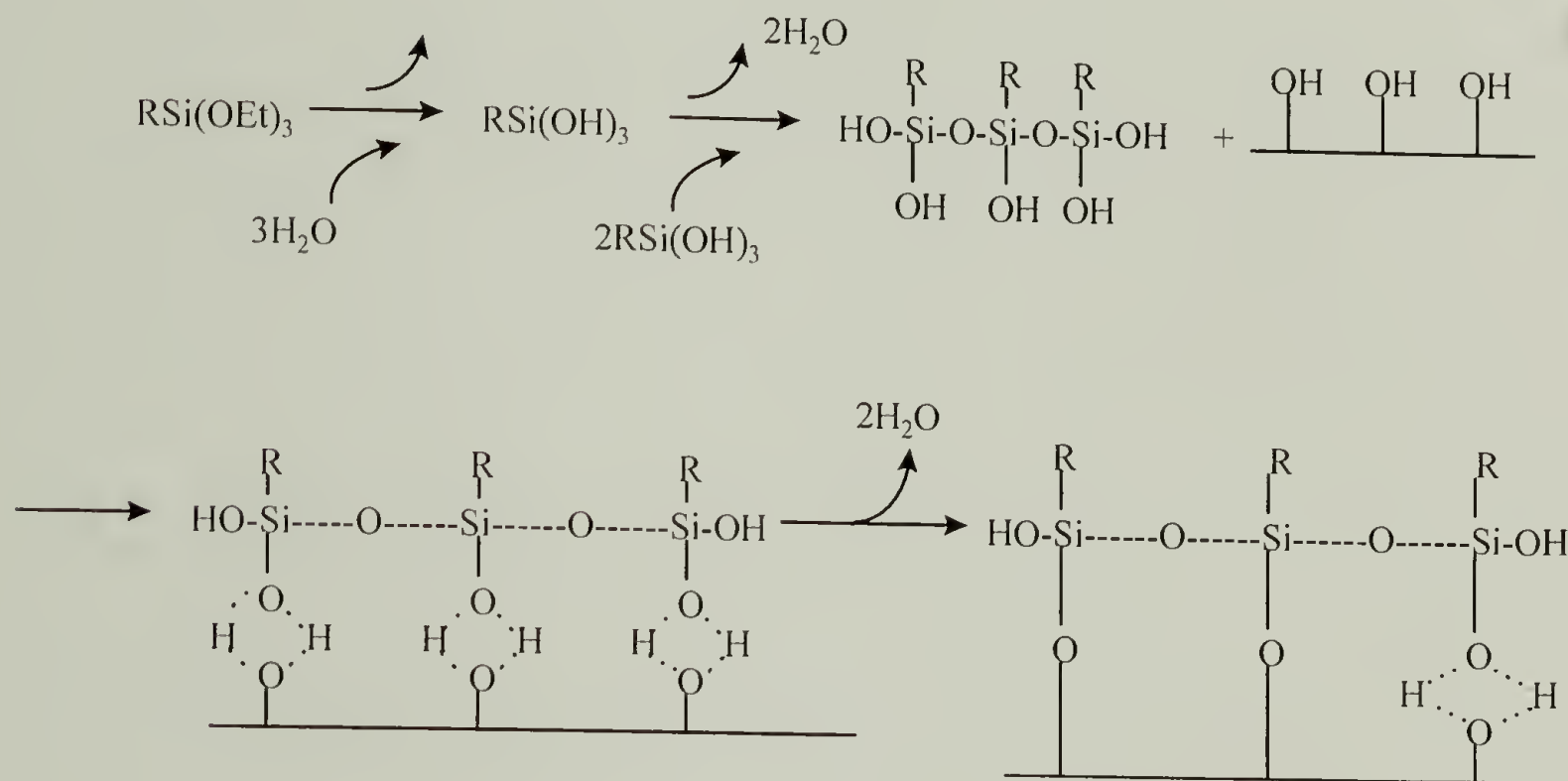
Structural joints consisting of metallic substrates and organic adhesives are inherently unstable in moist environments due to the change in the thermodynamic work of adhesion at the metal-adhesive interface (positive in dry conditions to negative when water is present).¹ This is due to the water gradually displacing organic adhesives at the interface that leads to a progressive increase in the de-bonded area. To improve the hydrothermal stability of these adhesive bonds, either (1) water must be prevented from migrating into the interface in sufficient amounts, or (2) primary bonding must be established across the interface to resist water.

Silane Coupling Reaction

Many efforts have been made to functionalize the metal oxide surface to achieve better adhesion towards organic species.² Organosilanes have been widely used to enhance the durability and wet strength of metal/adhesive joints. The effectiveness of a silane has been primarily attributed to its ability to interact chemically with metallic substrates.

A typical silane coupling reaction takes place as follows. The triethoxy-functionalized silane is hydrolyzed in the presence of water, and becomes trihydroxy-

functionalized. The hydroxyl groups react with each other to form a homopolymer, and this homopolymer when in contact with a metal oxide surface containing alcohol groups, will adsorb and form a hydrogen bond, which at the right conditions will become a covalent bond. This silane coupling reaction is illustrated in Scheme 1.1.



Scheme 1.1. Schematic representation of a silane coupling reaction with a functionalized triethoxysilane onto a metal oxide surface.

Gettings and Kinloch^{3,4} have shown that the environmental resistance of steel substrates bonded with epoxy adhesives is increased substantially by priming the substrate with γ -glycidylpropyltriethoxysilane; and that the durability of the joint is directly related to the presence or absence of a chemical bond, such as Fe-O-Si, at the interface.

Boerio and Gosselin⁵ have reported that single lap shear joints of aluminum, bonded with an amine-cured epoxy, exhibit better durability in a wet environment when the aluminum alloy substrates were primed with a 1% aqueous solution of γ -aminopropyltriethoxysilane (γ -APS). Furthermore, the improvement was greater when the solution pH was 8.5, compared to its natural pH of 10.4. Based on external reflection infrared spectroscopic studies, they attributed this pH dependence to structural variations of the adsorbed silane and to a greater interaction between the silane and the substrate when the pH of solution is 8.5.

In the failure analysis of double cantilever beams in a wet environment prepared from 2024 aluminum alloy and amine cured epoxy, Patrick *et al.*⁶ have reported that priming the substrate with a 0.01% aqueous γ -APS solution invariably led to cohesive failure in the epoxy adhesives. This compares with interfacial or mixed mode failures normally observed for the unprimed joints, suggesting that the interface is more resistant to moisture attack after γ -APS treatment.

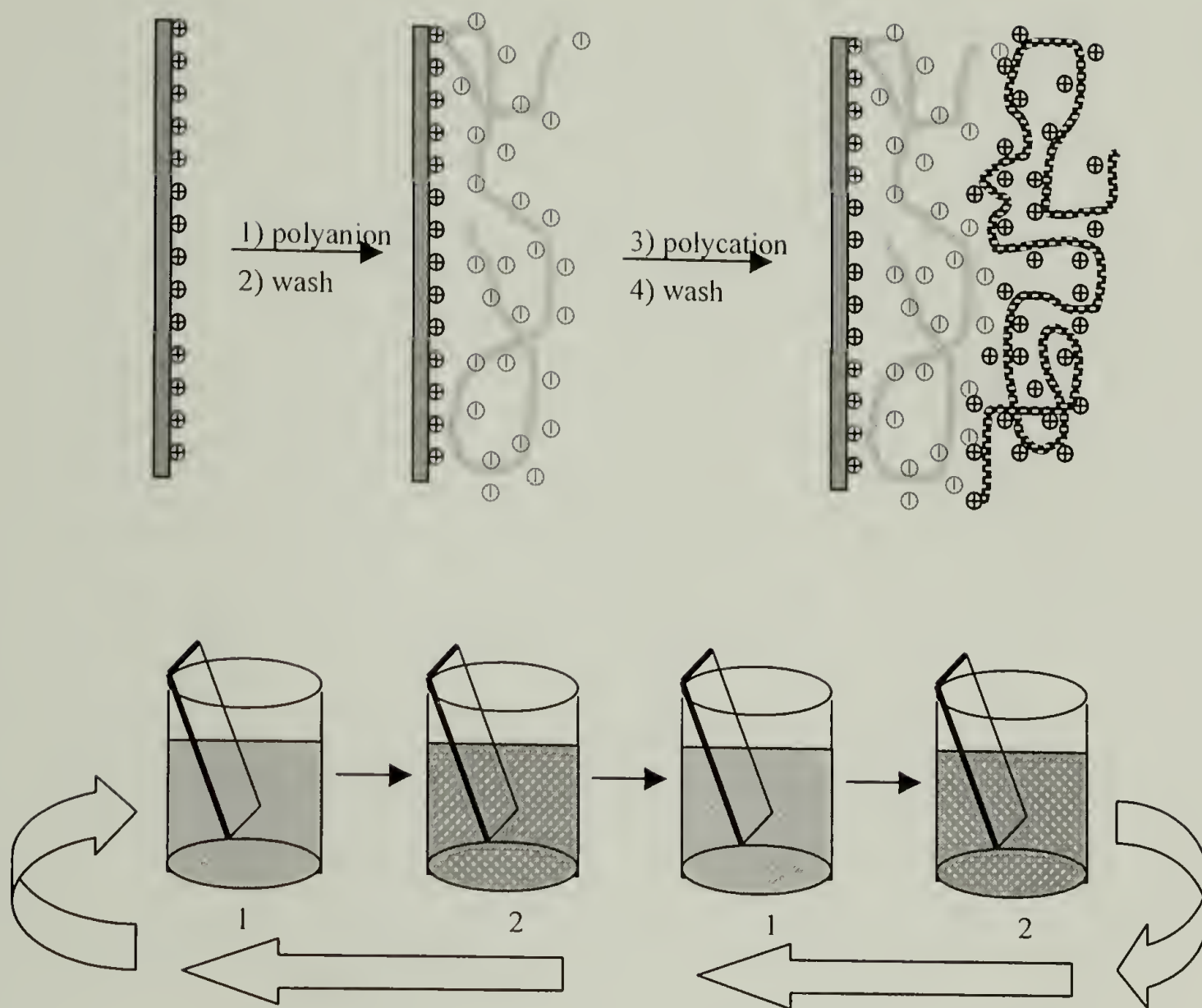
Layer-by-layer Deposition

Much attention has been received in the fabrication of polyelectrolyte multilayer films using a simple and versatile method called the layer-by-layer technique, pioneered by Decher.^{7,8} This relatively new technique of constructing multilayer assemblies involves sequential adsorption of anionic and cationic polyelectrolytes. An advantage over other classic adsorption techniques, such as the Langmuir-Blodgett technique⁹, is that the adsorption process is independent of the substrate size and topology. In this

technique, as opposed to the Langmuir-Blodgett technique, one can work with water-soluble molecules, which is required for many biological macromolecules.

The principle of the multilayer assembly is shown in Scheme 1.2¹⁰ and is described as follows. A solid substrate with a positively charged planar surface is immersed in a solution containing the anionic polyelectrolyte, and a layer of polyanions is adsorbed. Since the adsorption is carried out at a relatively high concentration of polyelectrolyte, a number of ionic groups remain exposed to the interface with the solution, and thus the surface charge is effectively reversed. After rinsing in pure water the substrate is immersed in a solution containing the cationic polyelectrolyte. Again a layer is adsorbed, but now the original surface charge is restored. By repeating both steps in a cyclic fashion, alternating multilayer assemblies are obtained. The complete reversal of surface charge is the crucial factor for a regular step-wise growth of the multilayer films. There is recent additional evidence that this charge reversal takes place at polymer concentrations above approximately 5 mg/ml.¹¹

Much work has been done using different types of polyelectrolytes,¹²⁻³⁹ and the formation of these multilayers on various surfaces.^{12,21,26,29-33,40-44} The technique is particularly interesting for industrial applications for several reasons. One reason is the simplicity of the technique. Another reason is the versatility of the technique. Still another reason is the environmental soundness of the technique that uses aqueous solutions - no organic solvents are involved. There have been promising results for this layer-by-layer deposition to be used as a tool for constructing films in applications such as conducting thin films,¹⁸⁻²¹ non-linear optics,⁴⁵ light-emitting and electrochromic thin



Scheme 1.2. Schematic representation of layer-by-layer deposition using two oppositely charged polyelectrolytes (washing steps are not included between each beaker).¹⁰

films,²²⁻²⁵ lithography,²⁶ sequential enzyme reactors,⁴⁶ biosensors,²⁷ humidity sensors,⁴⁷ and asymmetric gas separation membranes.⁴⁰

Polyelectrolyte Adsorption

The amount of polyelectrolytes adsorbed is controlled by surface charge density of the substrate, the pH and ionic strength of the solution, the polymer concentration and molecular weight, and on the adsorption time.

On a neutral surface, the amount of adsorption increases with molecular weight due to the increasing average size of loops and tails.⁴⁸⁻⁴⁹

On adsorption to a charged surface of an oppositely charged polyelectrolyte, conflicting results have been reported. Cosgrove⁵⁰ demonstrates that increasing surface charge decreases the adsorbed amount as the chains adsorb in a flat configuration using strong polyelectrolytes. Evers and Blaakmeer⁵¹⁻⁵² show, with a weak polyelectrolyte in a strong polyelectrolyte regime, that increasing surface charge increases the amount adsorbed due to the electrostatic contribution to the adsorption energy of the segments.

Varying the concentration and the solution pH, the adsorption behavior of weak polyelectrolytes can be controlled. At low concentrations, a high degree of ionization is attained and the adsorbed amount of polymer is low. At high pH's above the intrinsic dissociation constant, pK_o , the polyelectrolyte ionizes, behaving like a strong polyelectrolyte. This polyelectrolyte adsorption is independent of molecular weight and the pH increases with the salt content. By increasing the concentration, greater amounts of polymer adsorb. For low pH's, the behavior of the polyelectrolyte becomes that of a

neutral polymer, and the adsorption increases with molecular weight and decreases with solvent quality.⁵¹⁻⁵²

For a highly charged surface, adsorption decreases as the salt ions interfere with the adsorption process by preferentially adsorbing to the surface. At intermediate pH's (1-1.5 pH lower than pK_a), an adsorption maximum is observed due to the electrostatic attraction between the polymer segments and the surface being stronger than the repulsion between the polymer segments. Figure 1.1 illustrates the pH dependence on the polyelectrolyte adsorption behavior.⁵³

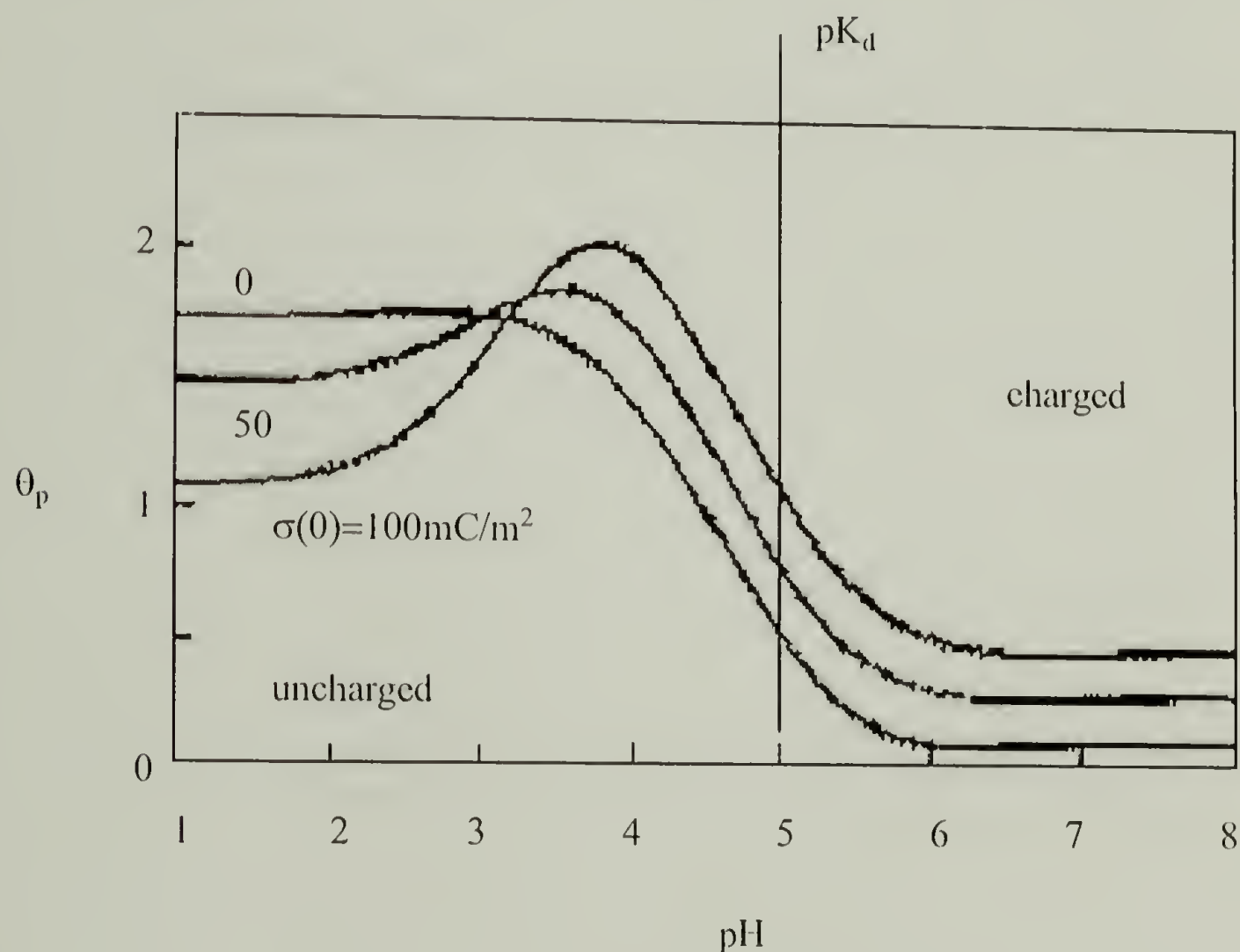


Figure 1.1. Adsorbed amount of a weak acid ($pK_a=5$) as a function of pH for three fixed surface charges.⁵³

The incorporation of salts in polyelectrolyte solutions can minimize the electrostatic forces present. Solutions not containing salts adsorb in a flat conformation, where 90% of the chains are in contact with the surface. Adding salt increases the ionic strength and, as a result, the repulsion between polymer segments is screened. This leads to more flexible chains that show more loops and a thicker adsorbed layer^{50,53,54} shown in Figure 1.2 and Figure 1.3.

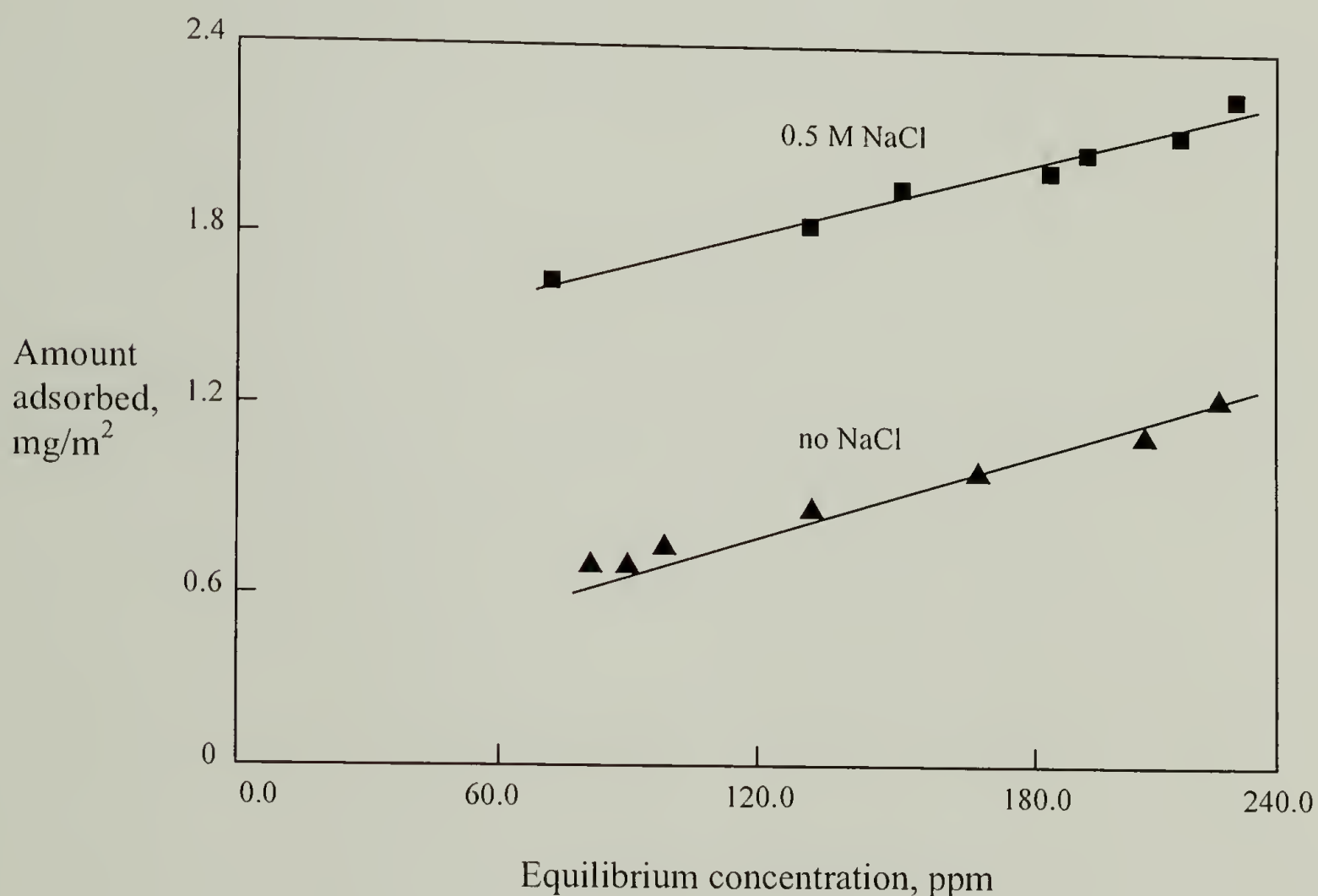


Figure 1.2. Adsorption isotherm for 780K poly(styrene sulfonate) at two different salt concentrations.⁵⁴

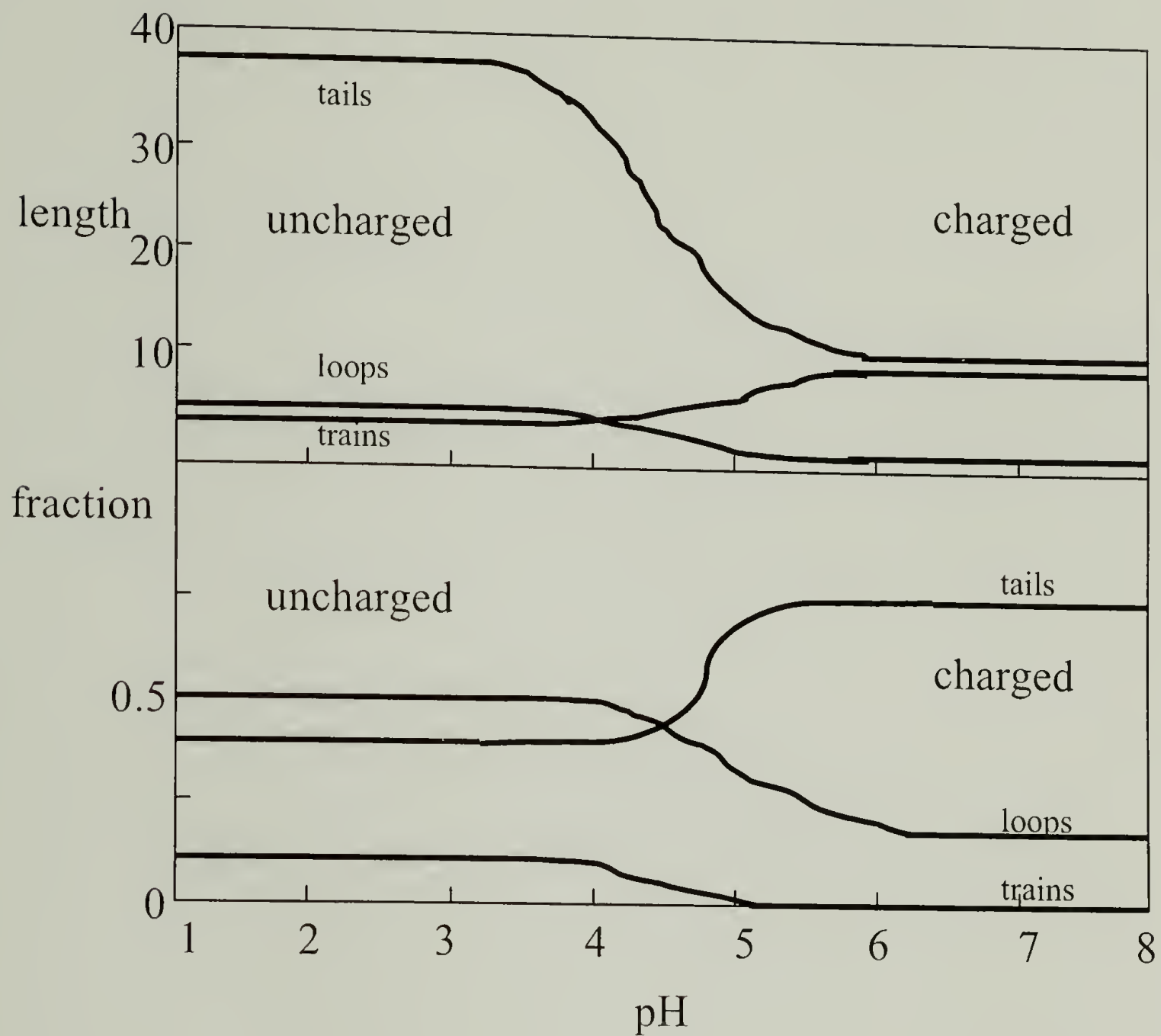


Figure 1.3. Average length and fraction of segments in trains, loops, and tails as a function of pH for a weak polyacid adsorbing onto a charged surface, $\sigma(0)=50 \text{ mC/m}^2$.⁵³

Adsorption on any substrate increases with ionic strength. For strong polyelectrolytes, the amount of adsorption increases as the polymer concentration is increased. Usually less than 20 minutes is required for complete polymer adsorption.

Objective

The extent to which layer-by-layer deposition will be effective as a technique for surface modification will depend on the structure and properties of the resulting multilayer assemblies. Significant effort has been expended on controlling and determining the structure of the polyelectrolyte multilayers, but little is known concerning their behavior as materials. If the process is to be used, for example, to modify a surface for adhesive bonding, the mechanical strength of the multilayer films must be significant. Our research group has reported the use of this technique as a general method for polymer surface modification⁴⁰⁻⁴¹ and as an approach for preparing asymmetric gas separation membranes.⁴⁰

Polymer Surface Analytical Techniques

Various surface characterization techniques can be applied to study the formation of these polyelectrolyte multilayer assemblies. Such techniques include ATR-IR, X-ray reflectivity, surface plasmon spectroscopy, X-ray photoelectron spectroscopy (XPS), and dynamic contact angle measurements. For this research, the two latter techniques mentioned above will be used (each of these characterization techniques will be explained).

X-ray Photoelectron Spectroscopy (XPS). X-ray photoelectron spectroscopy (XPS) reveals the atomic composition of the outer surface region of a material, ranging from depths of 10-100 Å^{55,57} or 200 Å⁵⁶, by utilizing the photoelectric effect. The sample is exposed to nearly monoenergetic soft x-rays under ultra-high vacuum and electrons are

ejected from the excited sample. The detector analyzes the kinetic energy of the core electrons (E_k) and determines the binding energy of an electron in an orbital of the source element (E_b) with

$$E_k = h\nu - E_b - \phi \quad (1.1)$$

where $h\nu$: energy of the x-ray photons, and

ϕ : the work function of the spectrometer.

Each atomic orbital of every element has a distinct binding energy, and XPS reveals the number of emitted electrons per element. Other factors are important in quantitative determination of surface atomic composition including sensitivity factor corrections. The photoelectric cross-sections of the atoms comprising the surface vary and peak sizes between elements cannot be compared directly. Atomic sensitivity factors compensate for differences in electron mean free paths and efficiencies of photoelectron generation and detection between elements.⁵⁵

The surface sensitivity of XPS can be ascribed to the finite escape depth of the ejected photoelectrons. Electrons travel only short distances through matter due to inelastic scattering, and as a result, XPS sensitivity decreases exponentially with depth. The number of electrons (N) detected relates to the number ejected (N_0) as

$$N = N_0 e^{-\left(\frac{z}{\lambda \sin \theta}\right)} \quad (1.2)$$

where z : the thickness of the material transversed (in the z direction),

λ : the mean free path of an electron in a given material, and

θ : the angle to the detector (from the plane of the sample surface).⁵⁶

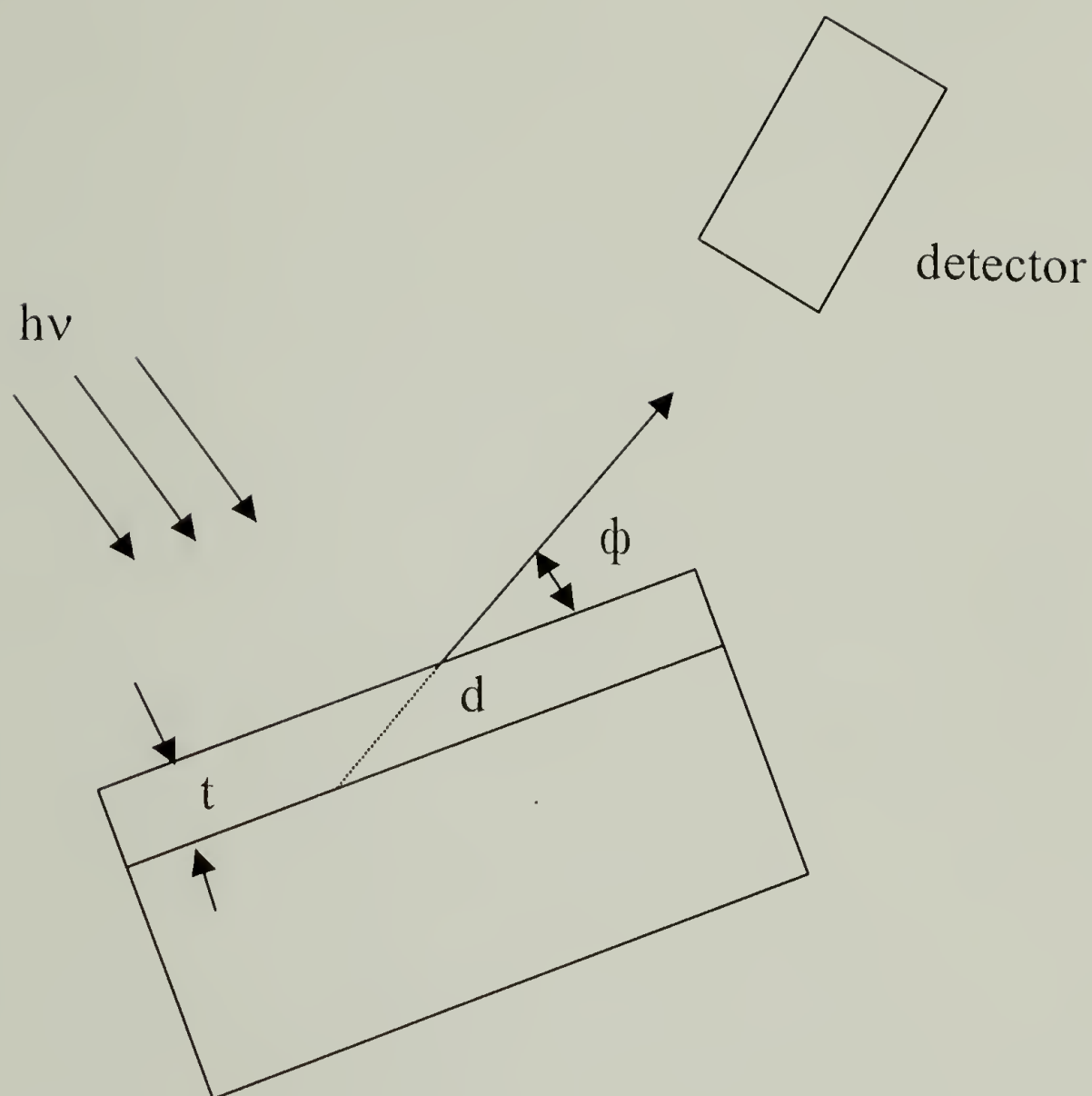
This exponential decrease in sensitivity indicates that XPS data will show higher values when functionality is concentrated in the outermost surface layers.

The mean free path of an electron in a material depends on its kinetic energy.⁵⁶

Using $\text{MgK}\alpha$ excitation, the mean free path for C_{1s} electrons has been determined to be 14 Å.⁵⁷ For XPS analysis of all film samples carried out in this dissertation, both $\text{MgK}\alpha$ and $\text{AlK}\alpha$ anodes were used, and 14 Å and 21 Å were used as mean free paths of Si_{2p} and Al_{2p} , respectively, for depth determinations.⁵⁴ The set-up of the XPS is shown in Scheme 1.3.

Variable take-off angle XPS analysis utilizes the dependence of the escape depth of ejected electrons on the angle between sample and detector, and assesses the vertical homogeneity of a sample. At shallow angles, electrons have to travel through more of the solid sample to reach the detector so only those emitted from the outermost layers are detected. At steeper angles, electrons ejected from deeper within the sample still reach the detector and this allows analysis of material at greater depths. All samples in this dissertation were analyzed at 15° and 75° take-off angles (between the plane of the sample and the detector).

From equation 1.2 within limits of 0 to thickness t , we can determine the intensity (or number (N) of electrons detected) as



Scheme 1.3. Schematic representation of X-ray Photoelectron Spectroscopy (XPS). X-ray beams ($h\nu$) are irradiated on a sample and excited photoelectrons from thickness t are detected at a variable angle (ϕ) from the sample to the detector.

$$N = k\lambda \sin \theta \left(1 - e^{-\left(\frac{t}{\lambda \sin \theta}\right)} \right) \quad (1.3)$$

where k is constant. Data from the 15° take-off angle geometry represent the atomic concentration of the top 11 \AA of the film sample and equation 1.3 indicates that 94% of the electrons detected originate from this region. Spectra recorded at the 75° take-off angle represent the composition of the outer 40 \AA of the surface and 95% of the electrons

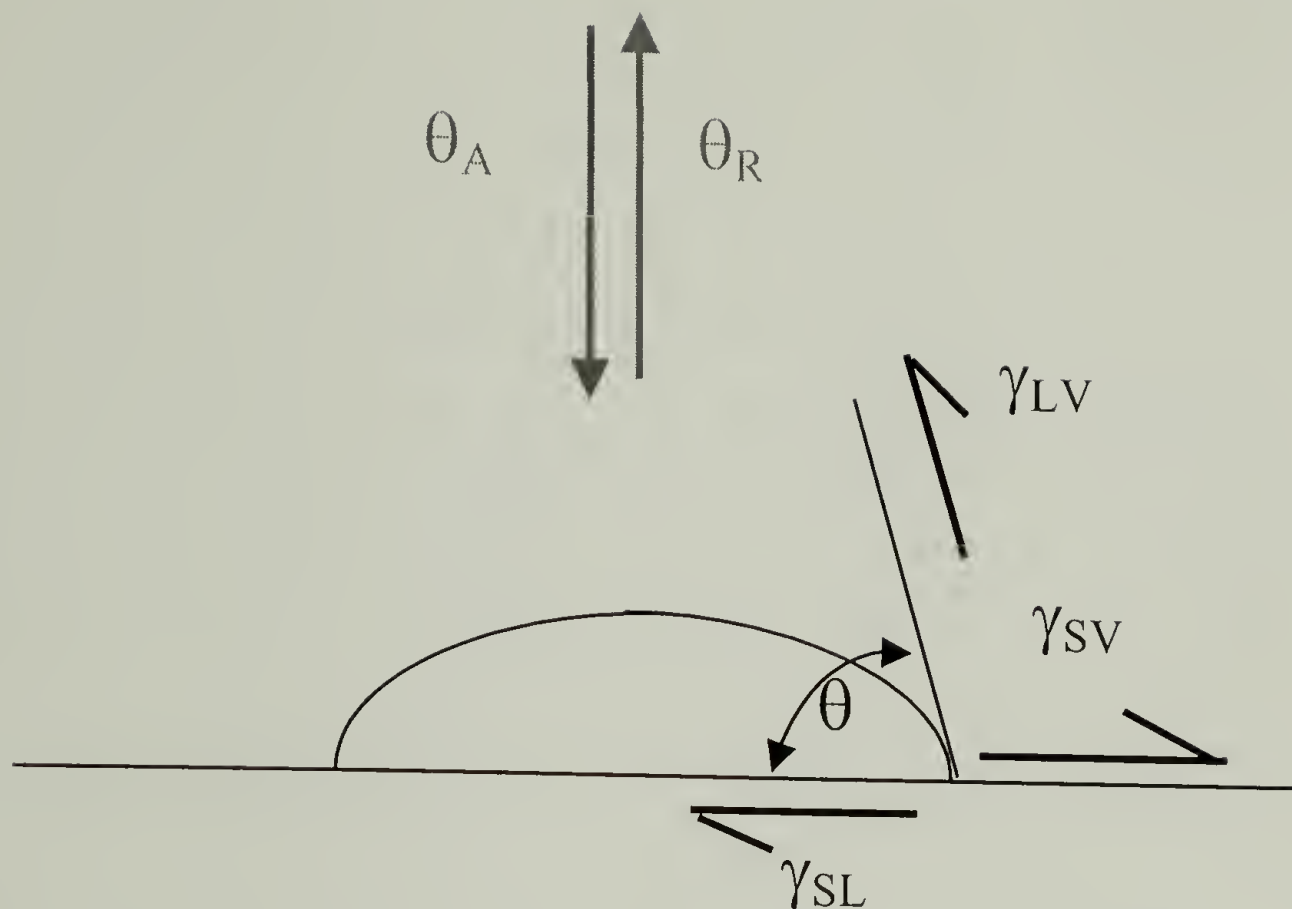
detected are emitted from this region. Roughly 54% of the photoelectrons measured at 75° actually originate in the top 11 Å of the material. For this reason, large discrepancies between data recorded at 15° and 75° can reveal information about the distribution of functionality in a sample.

Contact Angle Contact angle measurements provide the most surface-selective analysis of all the surface analytical techniques employed because only the outermost layers of the surface (few Å's) are sampled. Contact angle measurements are generally used to describe the surface tension of a material as well as give an indication of surface wettability. Young's equation⁵⁸

$$\gamma_{SV} - \gamma_{SL} = \gamma_{LV} \cos \theta \quad (1.4)$$

treats the angle formed by a liquid resting on a solid plane as a result of the mechanical equilibrium established as a balance of the three surface tensions involved, namely γ_{SL} of the solid-liquid interface, γ_{LV} of the liquid vapor interface and γ_{SV} of the solid-vapor interface. The set-up of the contact angle measurement is shown in Scheme 1.4.

For the dynamic measurements, water was used as the probe fluid, and advancing (θ_A) and receding (θ_R) angles were recorded as water was added to and withdrawn from the drop, respectively. In measuring dynamic contact angle, it is assumed that during the timeframe of the analysis, the surface is (1) completely smooth, (2) immobile, (3) nondeforming, (4) chemically homogeneous, and (5) that it does not interact with the probe fluid.⁵⁷ Within these requirements, a surface should have equal advancing and



θ_A : Advancing (adding probe fluid)

θ_R : Receding (subtracting probe fluid)

Scheme 1.4 Schematic representation of dynamic contact angle measurements (γ denotes the surface tension of each interface; S-solid, L-liquid, and V-vapor).

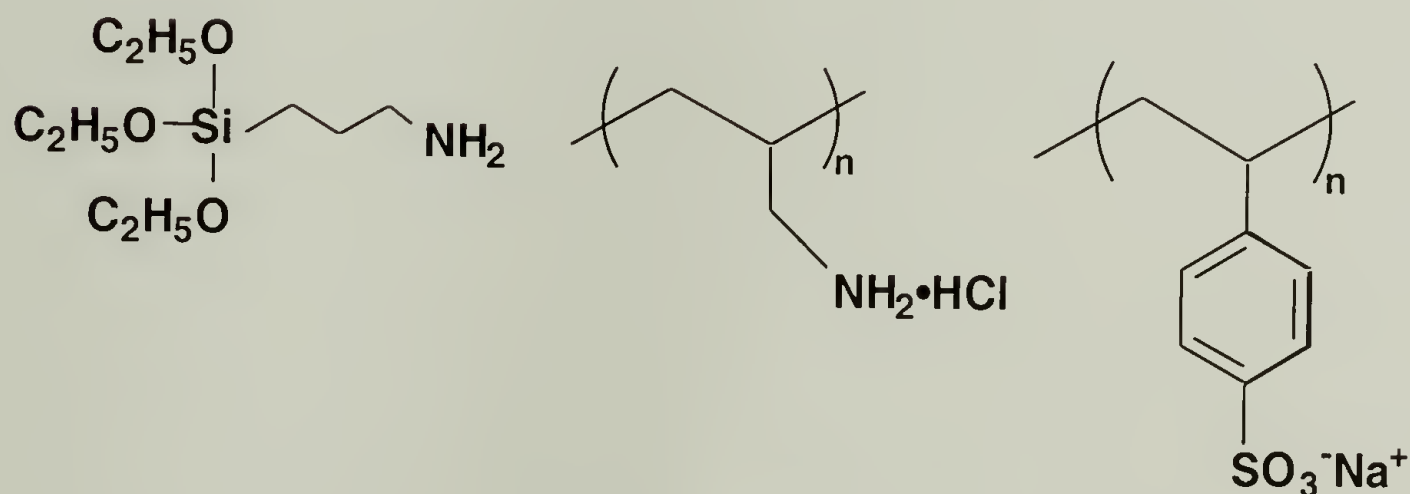
receding contact angles, but in reality, surfaces do not meet all of these requirements and the advancing and receding angles differ; this is termed contact angle hysteresis.

Hysteresis can stem from a variety (or combination) of causes such as chemical heterogeneity,⁵⁹ surface roughness,⁶⁰ or low mechanical properties of the surface.⁵⁷

Swelling of the surface layers with the probe fluid can also cause hysteresis.⁵⁷

Experimental

Materials. Aluminum sheets (Al 3003 alloy, 0.2 mm thickness) were obtained from McMaster-Carr. The sheet was cut into 0.5-inch square pieces. 3-aminopropyltriethoxysilane was purchased from Hüls America and used as received. Poly(allylamine hydrochloride) (PAH, $M_w=50,000-65,000$) and poly(sodium styrene sulfonate) (PSS, $M_w=70,000$) were obtained from Aldrich and used as received. Water was purified using a Millipore Milli-Q® system that involves reverse osmosis followed by ion-exchange and filtration steps. Solution pH's for the layer-by-layer adsorption studies were adjusted with small amounts of either HCl or NaOH aqueous solution using a Fisher 825MP pH meter. Chemical formulas of the two polyelectrolytes (PAH and PSS), along with the silane coupling agent (3-aminopropyltriethoxysilane) are shown in Scheme 1.5.



Scheme 1.5. Chemical formula for 3-aminopropyltriethoxysilane (left), poly(allyl amine) hydrochloride salt (center), and poly(styrene sulfonate) sodium salt (right).

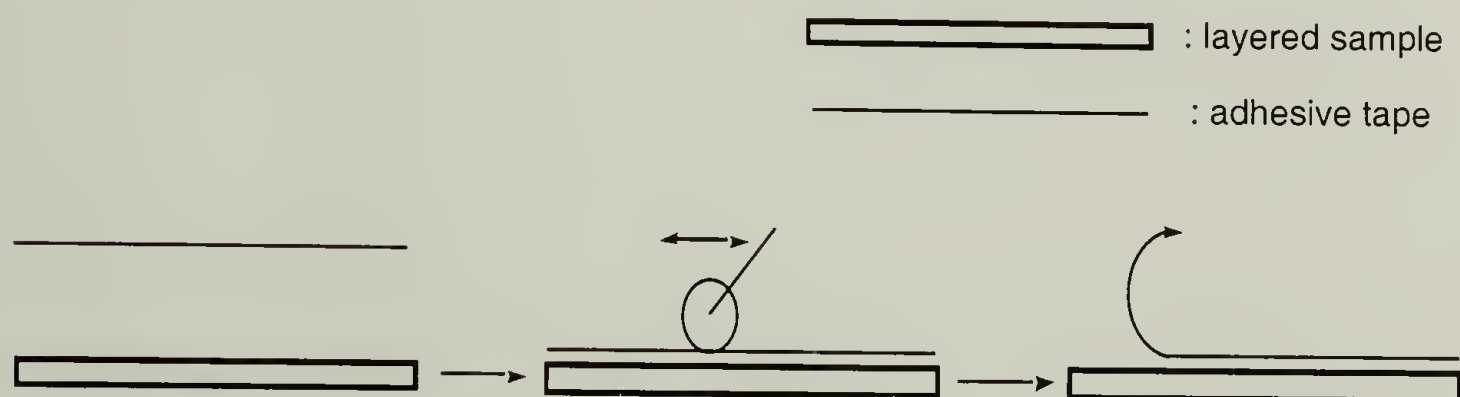
Substrate Preparation. The Al pieces were cleaned using the procedure recommended by Cave and Kinloch.⁶¹ The Al samples were immersed in 1.5 M NaOH (aq) at 50°C for 5 min. The samples were then taken out and rinsed with Milli-Q® water to eliminate the excess alkali. The samples were then immersed in a 10% nitric acid (aq) solution for 1 min. This step removes any etch residues. Excess nitric acid was removed by a subsequent Milli-Q® water wash. At this point, the water completely wets the Al surface. In order to minimize exposure of the cleaned surface to the atmosphere and subsequent contamination, the wet surfaces were initially immersed in ethanol to remove the water, and then immersed into chloroform. Excess chloroform was blown off of samples with a stream of N₂, and then the samples were immediately placed into the silane coupling solution.

Silane Coupling Reaction. The cleaned Al substrates were immediately immersed in a 0.1 M aqueous solution of 3-aminopropyltriethoxysilane (pH adjusted to 6.8). After 12 hours, the samples were removed, rinsed with aliquots of Milli-Q® water (x3), and dried at reduced pressure overnight.

Layer-by-layer Deposition. Polyelectrolyte adsorption was carried out at room temperature in stirred polyelectrolyte solutions that were prepared fresh every day. Samples that had been treated with 3-aminopropyltriethoxysilane (aq) and dried were immersed in 0.2 M (based on repeat units) poly(sodium styrene sulfonate) (PSS) solution (adjusted to pH 4.0) for 30 min. Afterwards, they were removed, rinsed with aliquots of Milli-Q® water (x3), and placed in a solution of 0.2 M (based on repeat units)

poly(allylamine hydrochloride) (PAH) (adjusted to pH 8.0) for 30 min. Multilayers were prepared by successive dippings into the two polyelectrolyte solutions. After every layer deposition, the samples were rinsed with Milli-Q® water three times. After the desired number of multilayers had been deposited, the Al-NH₃⁺-supported polyelectrolyte multilayer films were dried at reduced pressure overnight before characterization.

Preparation of Specimens for the Simplified Peel Test. Multilayer samples of 24 and 25 layers were prepared, and a pressure-sensitive adhesive tape (3M #810) was applied to their surfaces. The assembled specimens were rolled 20 times with a roller to achieve uniform contact before manually peeling the tape from the sample at a peel angle of 180° between the delaminated film surface and the tape. Both the multilayer samples and the tape (prior to and subsequent to the peeling experiment) were characterized by XPS. A schematic of this experiment is shown in Scheme 1.6.



Scheme 1.6. Side view of the simplified peel test samples used for XPS analysis. Both surfaces (layered sample and adhesive tape), before and after the peel test, were analyzed.

Characterization. X-ray photoelectron spectra (XPS) were recorded on a Perkin-Elmer-Physical Electronics 5100 Spectrometer with MgK α excitation (15 kV, 400 W). Spectra were recorded at two different take-off angles: 15° and 75° between the plane of the sample surface and entrance lens of the detector optics. Atomic concentration data were determined using sensitivity factors obtained from samples of known composition: C_{1s} 0.250; O_{1s} 0.660; N_{1s} 0.420; Si_{2p} 0.270; S_{2p} 0.540; Al_{2p} 0.185.

Contact angle measurements were made with a Ramé-Hart telescopic goniometer and a Gilmont syringe with a 24-gauge flat-tipped needle. Dynamic advancing (θ_A) and receding (θ_R) angles were recorded while the probe fluid (water) was added to and withdrawn from the drop, respectively.

Results and Discussions

Silane Coupling Reaction. Figure 1.4 shows an XPS survey spectrum of a silane-coupled Al sample (abbreviated Al-NH₃⁺). The substrate becomes positively charged in aqueous solutions of the appropriate pH and allows the initiation of layer-by-layer deposition. XPS atomic composition data for the Al-NH₃⁺ samples are reproducible and a representative sample (75° take-off angle) is shown in Table 1.1. The equal silicon and nitrogen content (which is expected from the coupling agent composition) was part of the basis for choosing these cleaning and reaction conditions. The presence of aluminum in the spectrum (75° take-off angle data represents the composition data for the outermost 40 Å) indicates that the silane coupling agent layer is monolayer-like in coverage.

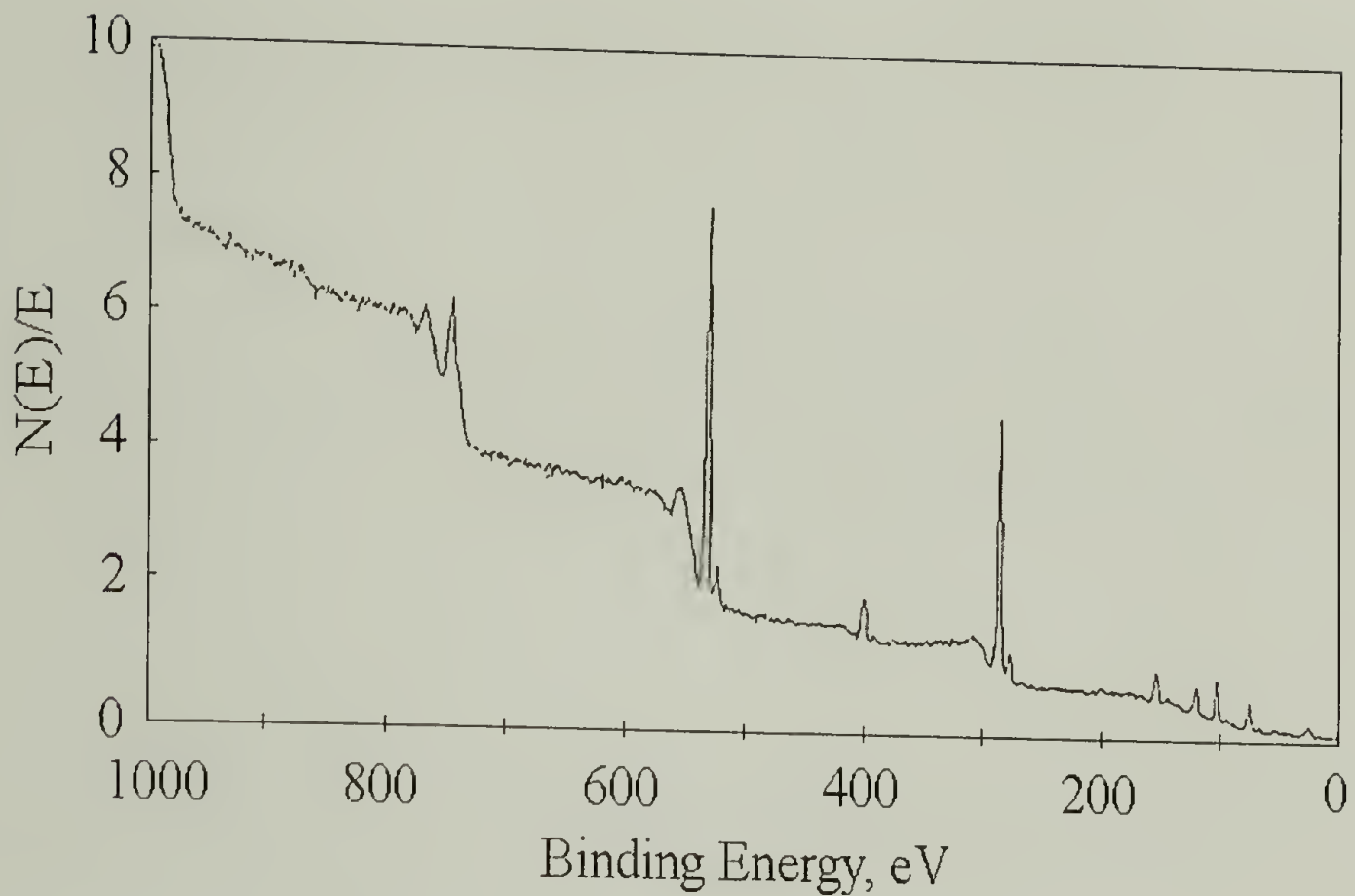


Figure 1.4. XPS survey of silane coupled Al sample (75° take-off angle). Peak assignments: 531 eV, O_{1s}; 402 eV, N_{1s}; 292 eV, C_{1s}; 153 eV, Si_{2s}; 119 eV, Al_{2s}; 102 eV, Si_{2p}; 74 eV, Al_{2p}.

Table 1.1. XPS % atomic concentration and dynamic contact angle measurements for cleaned Al, and silane coupled Al (Al-NH₃⁺). Top values denote 15° take-off angle data, and bottom values denote 75° take-off angle. Water was used as probe fluid for dynamic contact angle measurements (θ_A : advancing contact angle, θ_R : receding contact angle).

	element	Al _{2p}	O _{1s}	C _{1s}	Si _{2p}	N _{1s}	θ_A/θ_R
cleaned Al	15° take-off	10.54	40.01	47.54	1.92	-	93°/9°
	75° take-off	16.33	51.05	32.03	0.58	-	
Al-NH ₃ ⁺	15° take-off	4.39	21.64	63.28	5.66	5.03	50°/8°
	75° take-off	6.23	28.64	51.81	6.87	6.45	

Polyelectrolyte Deposition (kinetics, stratification, attenuation). Sequential adsorptions of poly(sodium styrene sulfonate) (PSS) and poly(allylamine hydrochloride) (PAH) onto Al-NH_3^+ samples were carried out at room temperature in open beakers. Attempts to obtain reproducible kinetics for the first (PSS) and second layer (PAH) adsorptions were unsuccessful. The XPS results show that the final state structures are formed within approximately 20 min., but also indicate that desorption of a portion of the first layer likely occurs during the second layer adsorption and that the first bilayer (Al-NH_3^+ -PSS-PAH) is not stratified with the PAH layer on top of the PSS layer. This inconsistent behavior was not observed using other substrates (both inorganic and organic) in our laboratories,^{40,41} and we suspect that a portion of the silane coupling agent layer is adversely affected by the polyelectrolyte adsorption conditions. We note that silicon is observed at low concentrations in the XPS spectra for even the thick multilayer assemblies and thus must be mobile during the multilayer assembly process.

The multilayer deposition process, however, becomes more well-behaved after multiple adsorptions; apparently defects are healed during the deposition process. Reproducible kinetics were obtained for the fifth layer (PSS) adsorption after 4 layers were built up with 30 min. adsorption times and pronounced stratification was also observed. Sulfur and nitrogen atomic concentrations level off after 30 min (see Figures 1.5 and 1.6). We conclude that 30 min. is best for constructing polyelectrolyte multilayers, and use an adsorption time of 30 min. for all subsequent polyelectrolyte adsorption.

Figure 1.7 shows an XPS survey spectrum of a 6-layer film on Al-NH_3^+ (PAH is top layer). All the features of interest are present in this spectrum: the PSS and PAH

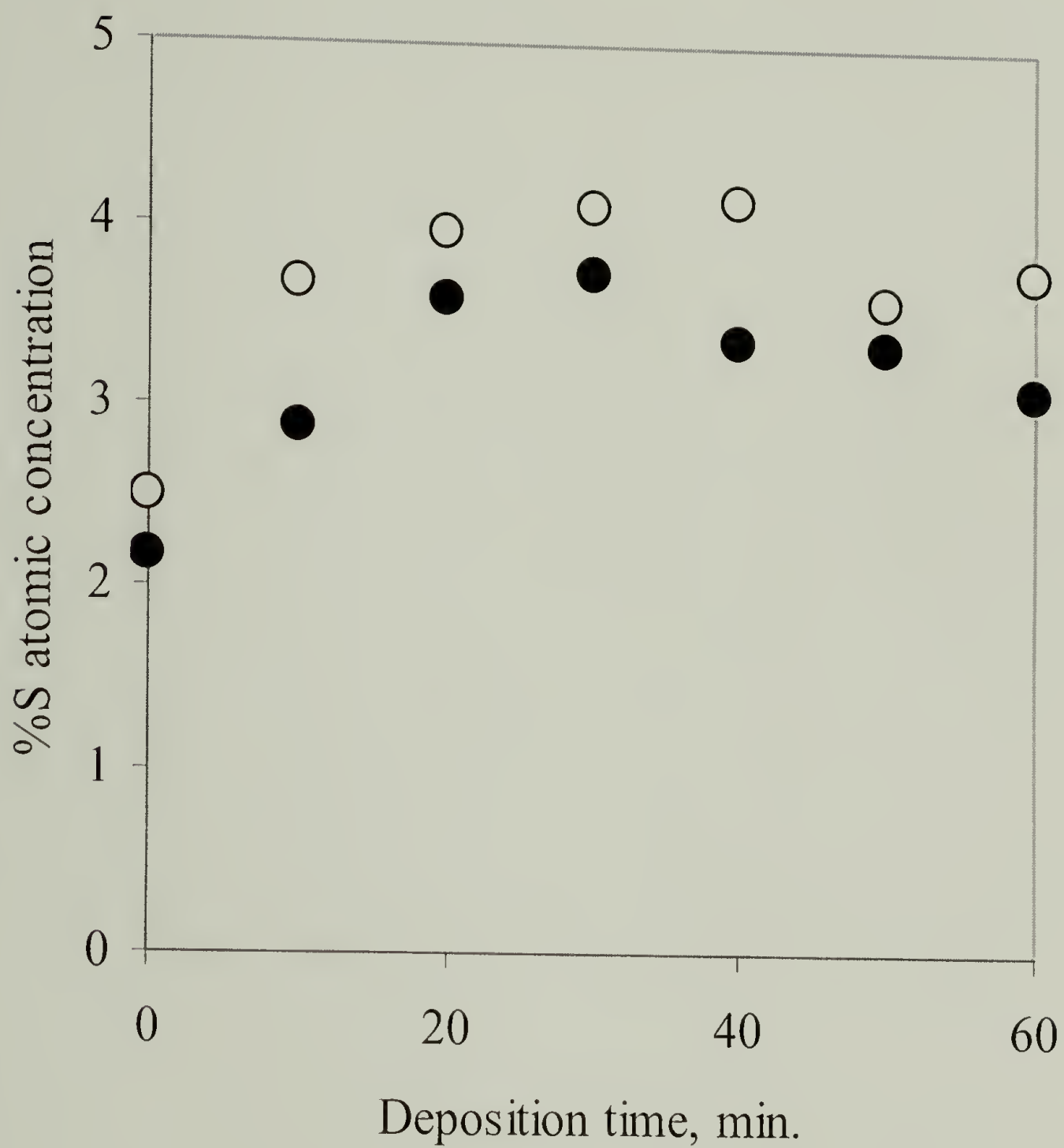


Figure 1.5. %S atomic concentration (XPS) of the fifth polyelectrolyte monolayer (PSS) after various deposition times. Zero time denotes four polyelectrolyte layers on Al-NH_3^+ , deposited for 30 min. each (●: determined from 15° take-off angle data, and ○: determined from 75° take-off angle data).

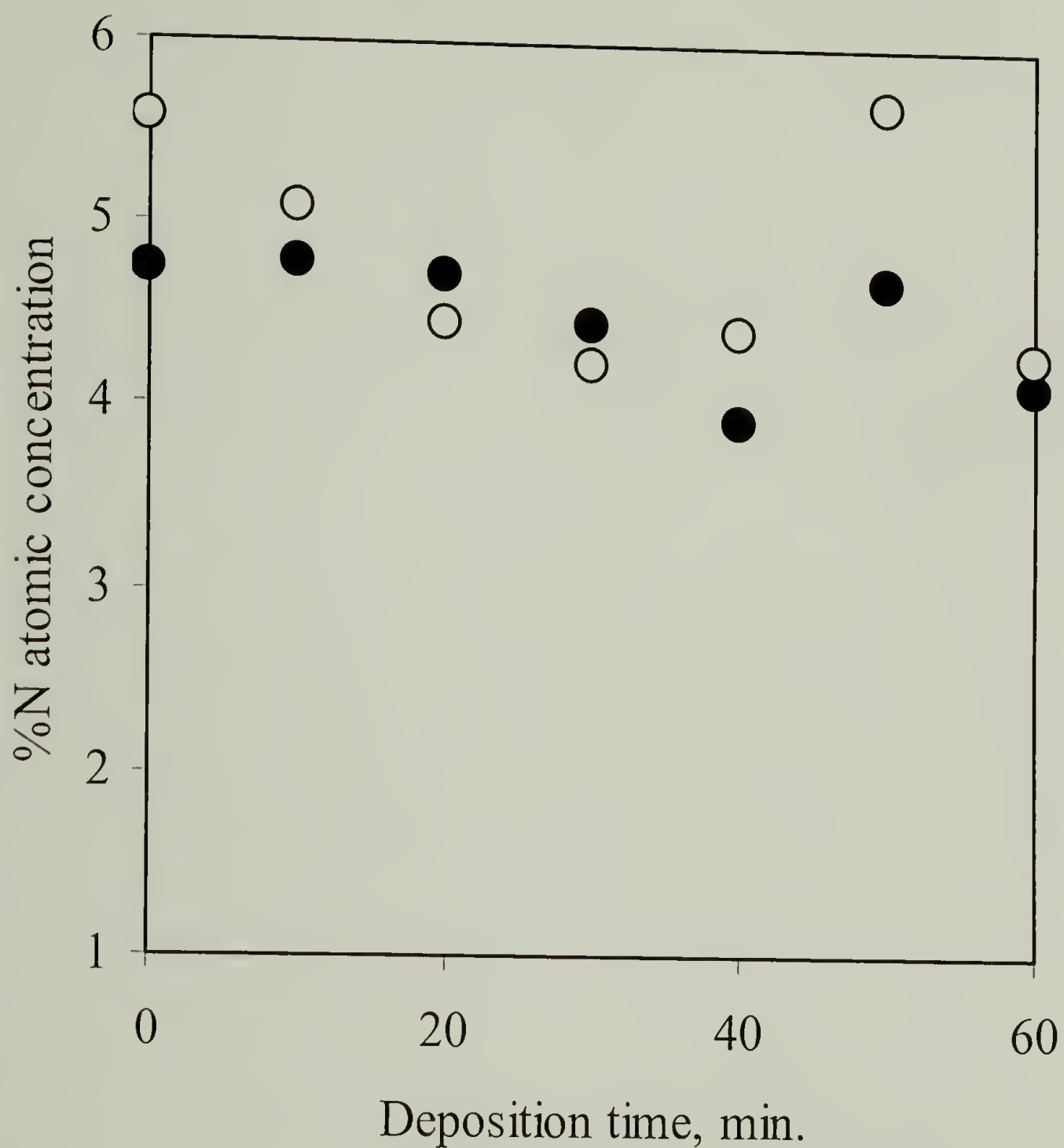


Figure 1.6. %N atomic concentration (XPS) of the fifth polyelectrolyte monolayer (PSS) after various deposition times. Zero time denotes four polyelectrolyte layers on Al-NH_3^+ , deposited for 30 min. each (●: determined from 15° take-off angle data, and ○: determined from 75° take-off angle data).

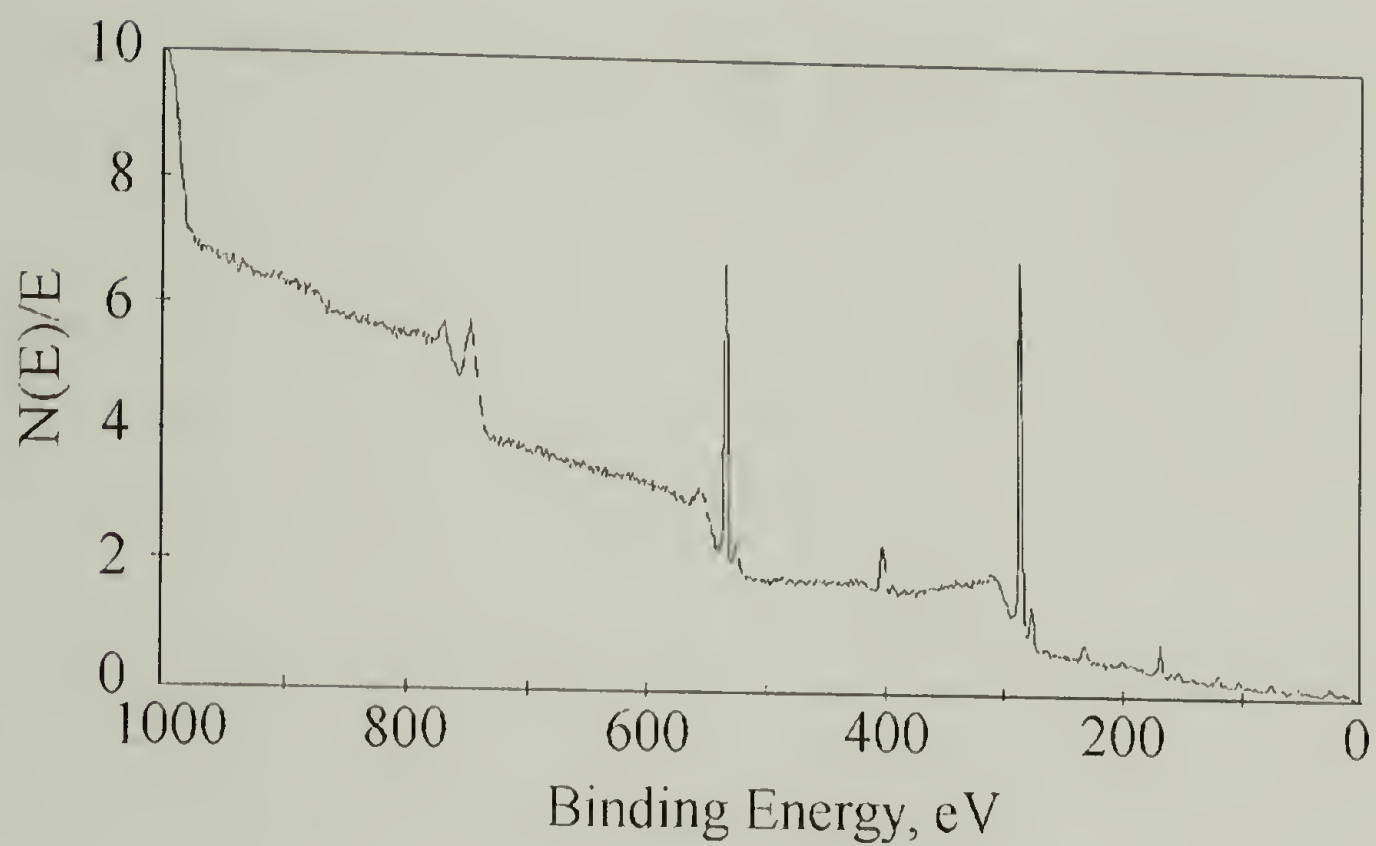


Figure 1.7. XPS survey spectrum of a sample containing 6 polyelectrolyte layers deposited on Al-NH_3^+ (75° take-off angle). Peak assignments: 531 eV, O_{1s} ; 402 eV, N_{1s} ; 292 eV, C_{1s} ; 229 eV, S_{2s} ; 165 eV, S_{2p} ; 153 eV, Si_{2s} ; 119 eV, Al_{2s} ; 102 eV, Si_{2p} ; 74 eV, Al_{2p} .

layers are identified by the sulfur (229 and 165 eV) and nitrogen (402 eV) photoelectron lines, respectively, and the Al-NH_3^+ substrate is observed by the aluminum (119 and 74 eV) and silicon (153 and 102 eV) signals.

Figure 1.8 shows nitrogen to sulfur ratios for a series of multilayer assemblies. Note that there is a pronounced odd-even trend in the data that persists to high layer number, where the addition of one more PSS or PAH layer does not greatly affect the composition of the multilayer assembly. The N:S ratio is relatively high when the outermost layer is PAH and relatively low when the outer most layer is PSS. These results suggest that the layers are stratified. The stoichiometry of the assembly process (ammonium ion: sulfonate ion ratios) is also evident from these data and we note that the ratio of ammonium ions to sulfonate ions is 3:2 (N:S ratio is 1.5). Few (and often no) counterions (sodium or chloride) are observed (in the dry state during XPS measurements) and this indicates that PAH must be present as the free base. The self-assembly process exerts its own stoichiometric control and a particular stoichiometry is not required.

Water contact angle data also indicate the stratified structure of the multilayer assemblies with an odd-even trend.^{40,41} Figure 1.9 shows dynamic contact angle data for a series of Al-NH_3^+ -supported PSS/PAH multilayer assemblies. Stratification is apparent for the advancing contact angle data. Receding angles are consistently low due to the wetting of the polyelectrolytes after the water drop has advanced over the surface. The values are high compared to the values that are usually seen with other systems. This may be due to the inherent roughness of the aluminum substrate, or the re-adsorption of the

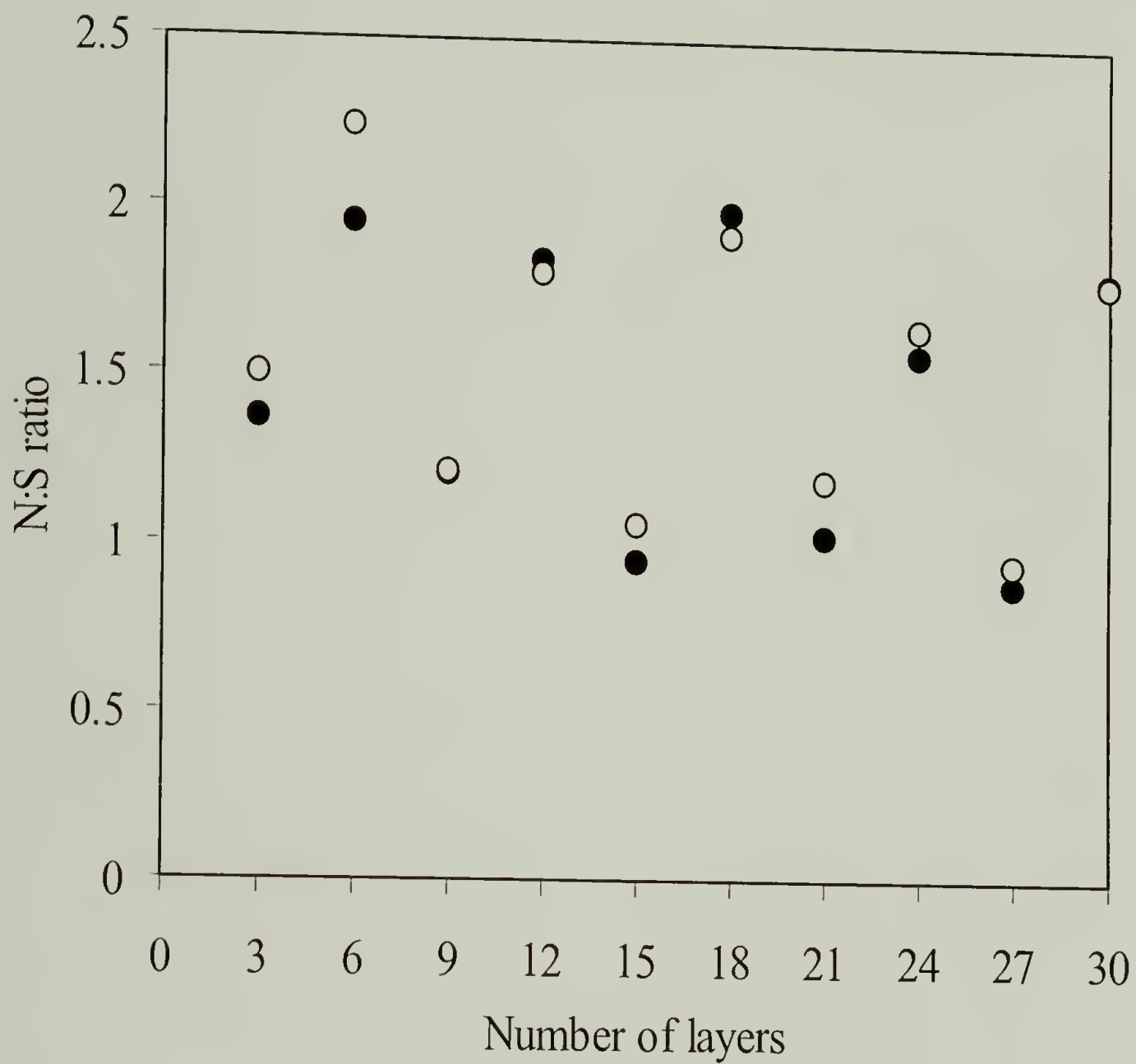


Figure 1.8. Nitrogen:Sulfur ratio (XPS) for polyelectrolyte multilayers deposited on Al-NH_3^+ . Each set of x values are a multiple of 3 (●: determined from 15° take-off angle data, and ○: determined from 75° take-off angle data).

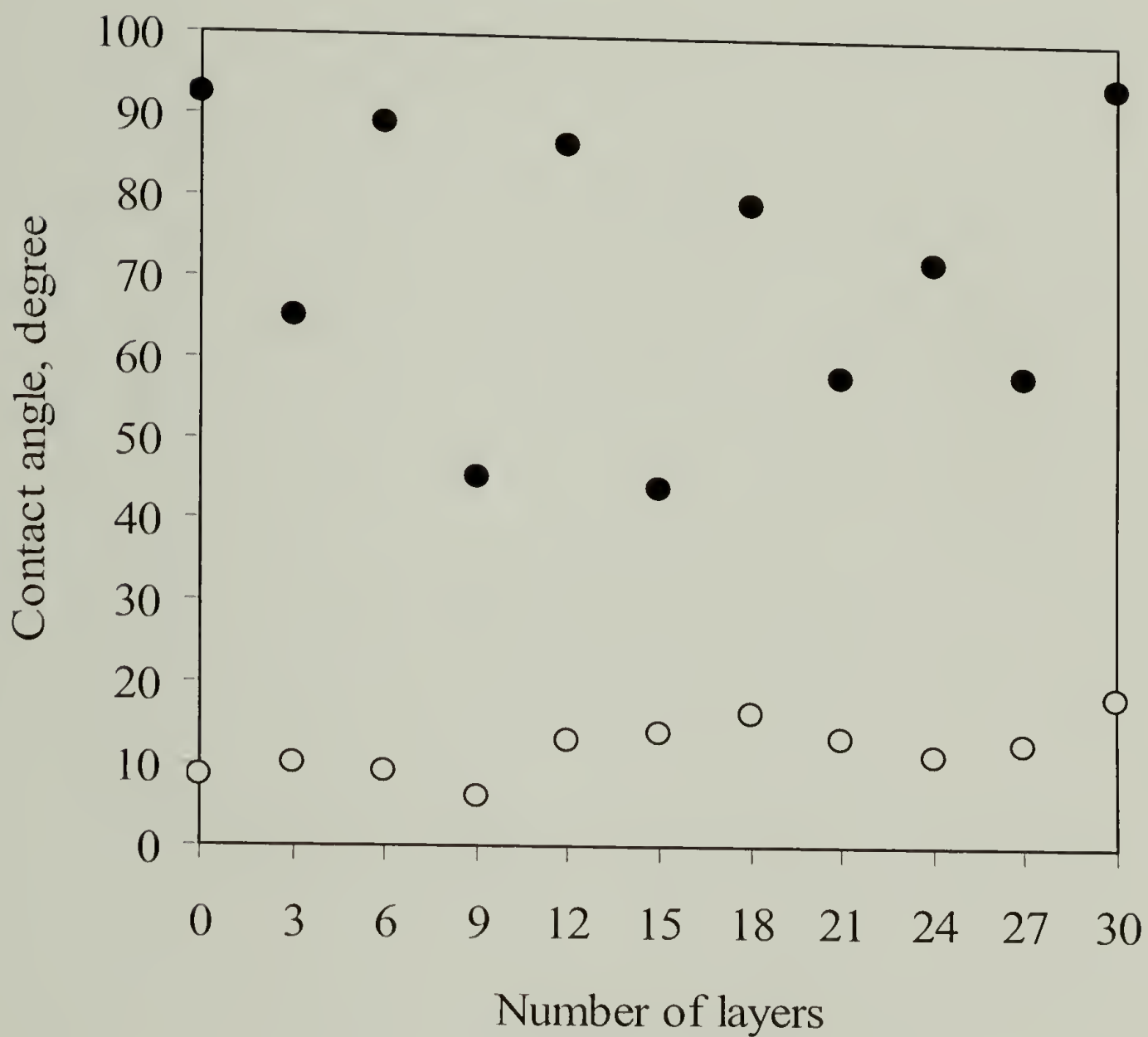


Figure 1.9. Dynamic contact angle measurements for polyelectrolyte multilayers deposited on Al-NH_3^+ . Each set of x values are a multiple of 3 (●: determined from advancing contact angle data, and ○: determined from receding contact angle data).

silane coupling agent during the alternate deposition process. Nevertheless, multilayer assemblies can be prepared with up to 100 layers on the Al-NH_3^+ substrate, and their stratified features mentioned above hold true (see Figure 1.10 and 1.11).

We can estimate by XPS (we could calculate if the mean free paths were known) the thickness of the multilayer assemblies and individual layers from the decrease in intensity of the substrate photoelectron lines (aluminum and silicon). Figures 1.12 and Figure 1.13 show atomic concentration data for aluminum and silicon versus the number of layers deposited for a series of Al-NH_3^+ -supported multilayer films, respectively. The aluminum and silicon signals are almost completely attenuated after 9 layers have been deposited. An average polyelectrolyte monolayer thickness can be accurately measured by plotting peak intensity of the Al and Si signals upon increasing number of polyelectrolyte multilayers using the following equation:

$$-\ln(N / N_0) \sin \theta = nz / \lambda \quad (1.5)$$

The plots generated from this equation are shown in Figure 1.14 and 1.15. This allows us to measure a slope that can be used to determine the average polyelectrolyte monolayer thickness. From the slope of the Al signals, an average monolayer thickness was measured to be $\sim 5 \text{ \AA}$ thick, using an average mean free path length of 14 \AA . By comparison with X-ray reflectivity results, we see that the adsorption of these polyelectrolytes are comparable to other systems. The small, but finite amount of silicon observed in thick layers has been discussed above.

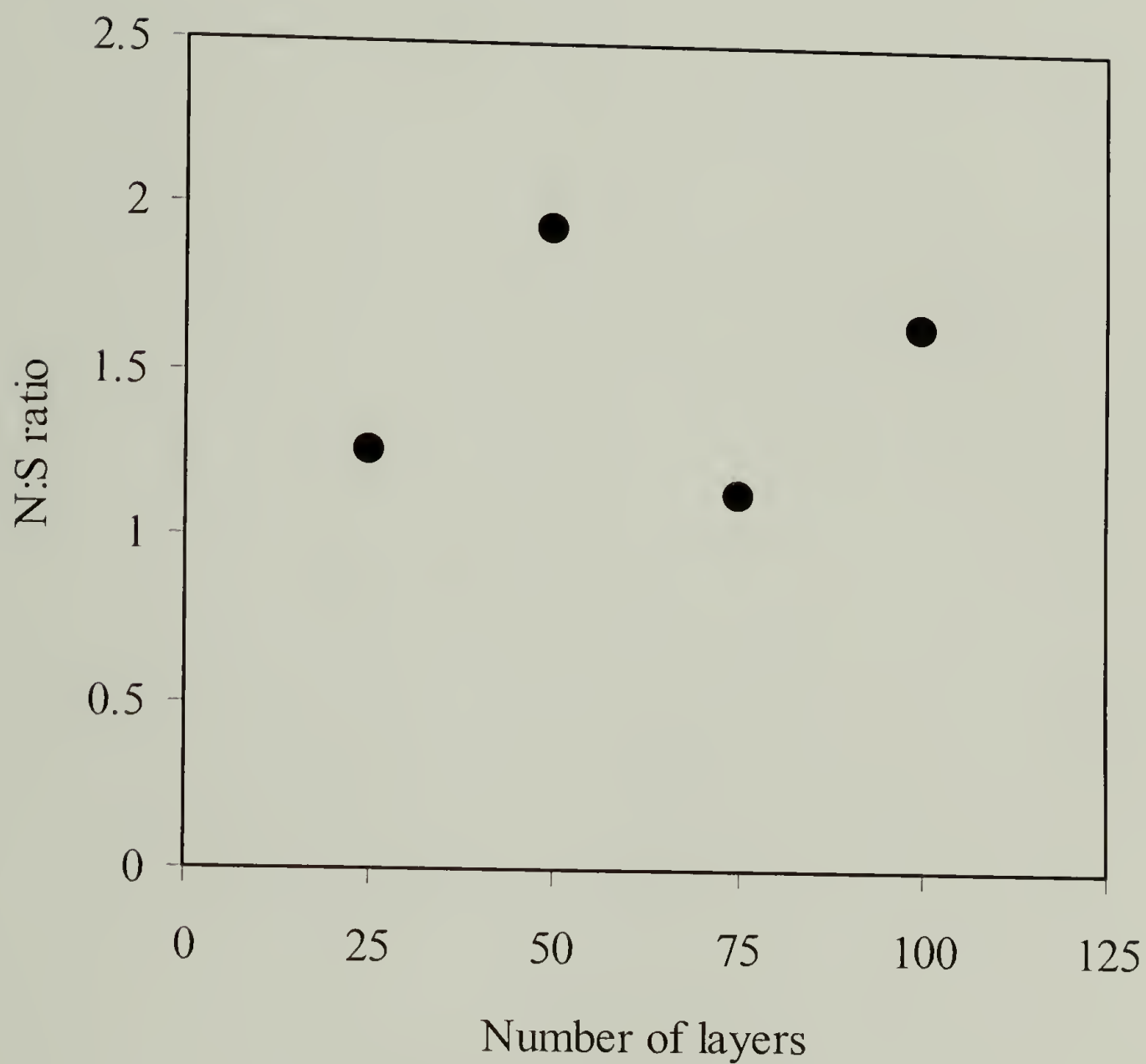


Figure 1.10. Nitrogen:Sulfur ratio (XPS, 75° take-off angle) for polyelectrolyte multilayers constructed on Al-NH_3^+ . Each point represents a multiple of 25 layers.

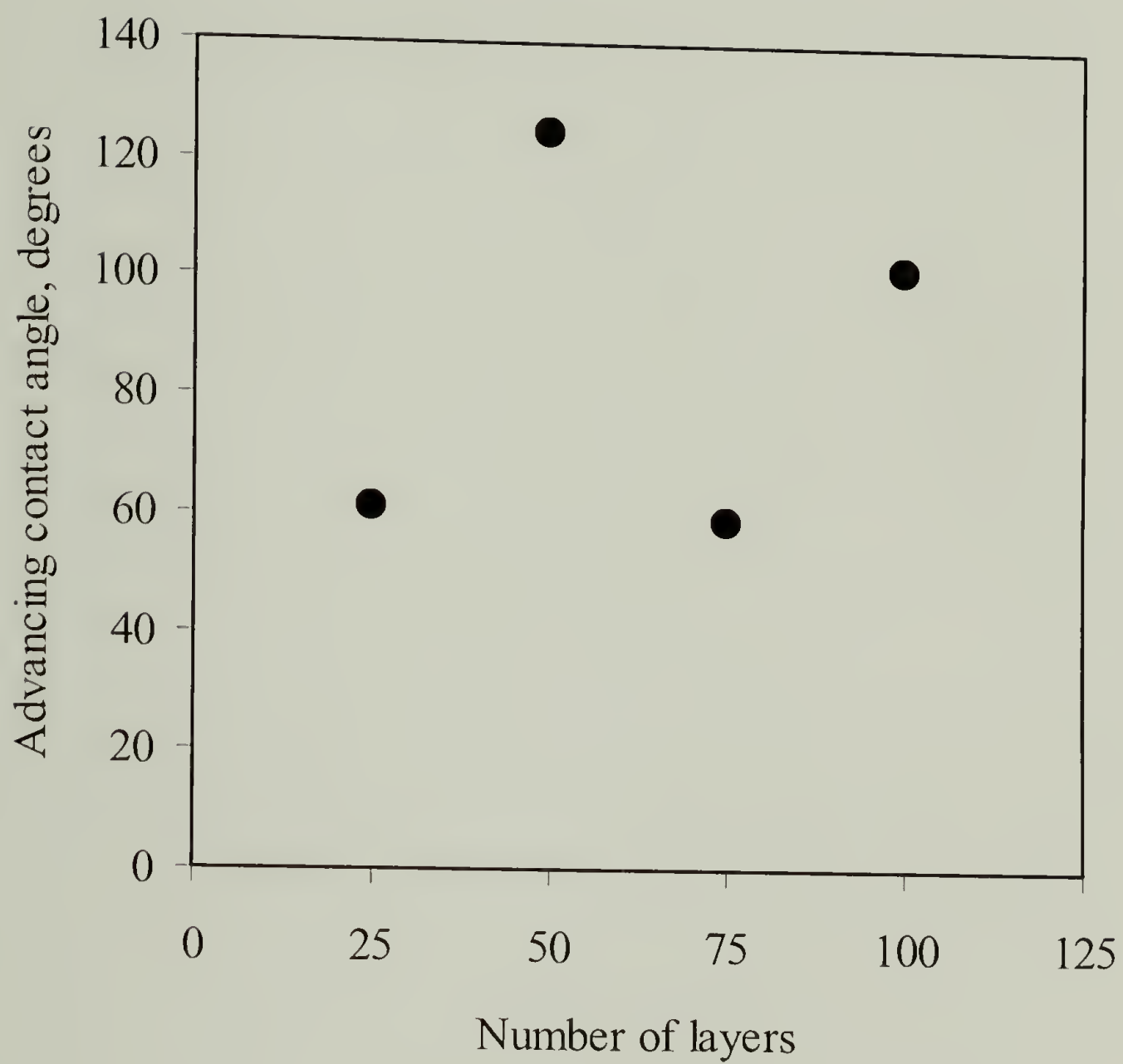


Figure 1.11. Advancing contact angle measurements for polyelectrolyte multilayers constructed on Al-NH_3^+ . Each point represents a multiple of 25 layers.

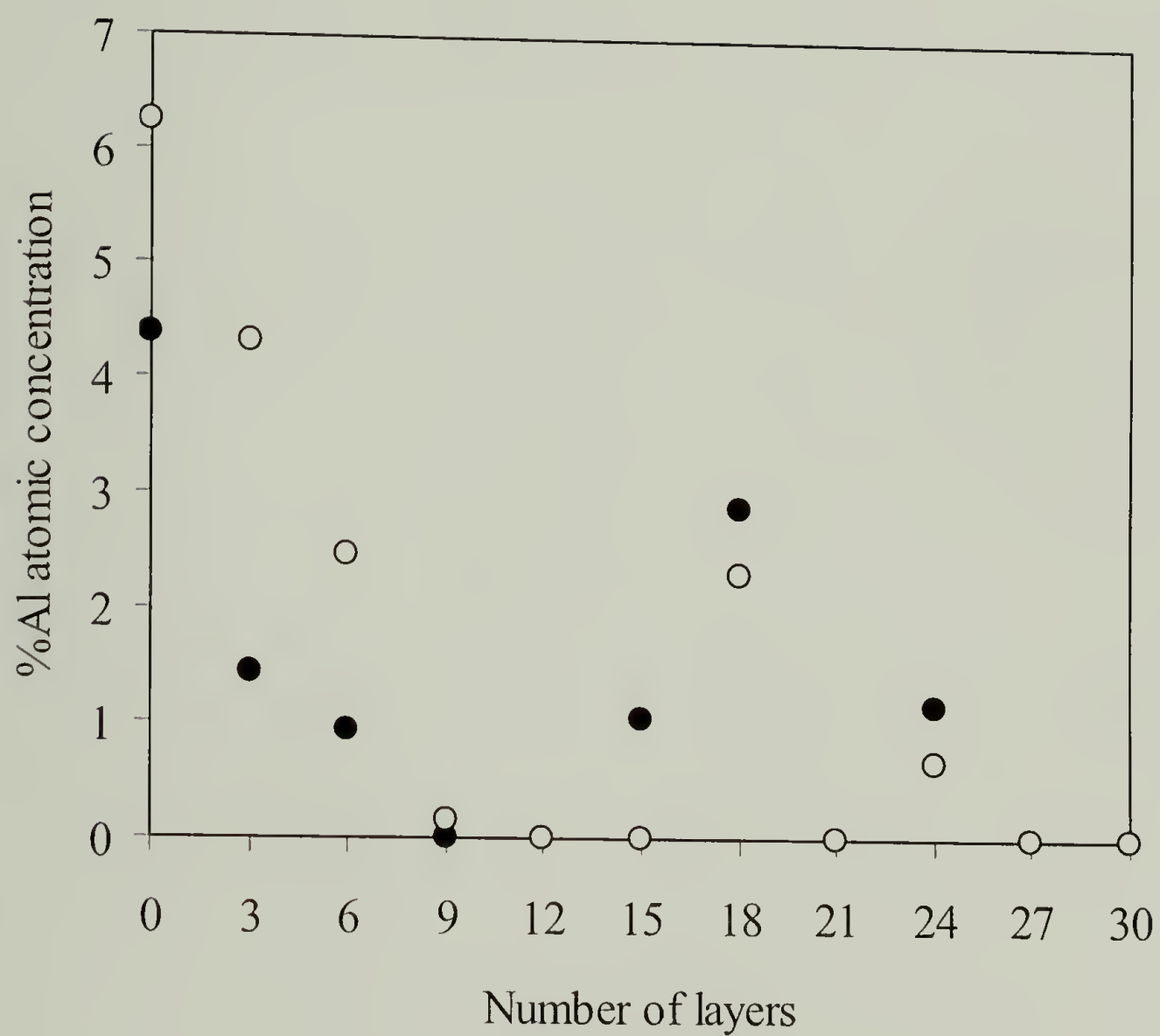


Figure 1.12. %Al atomic concentration for polyelectrolyte multilayers deposited on Al-NH_3^+ . Each set of x values are a multiple of 3 (●: determined from 15° take-off angle data, and ○: determined from 75° take-off angle data).

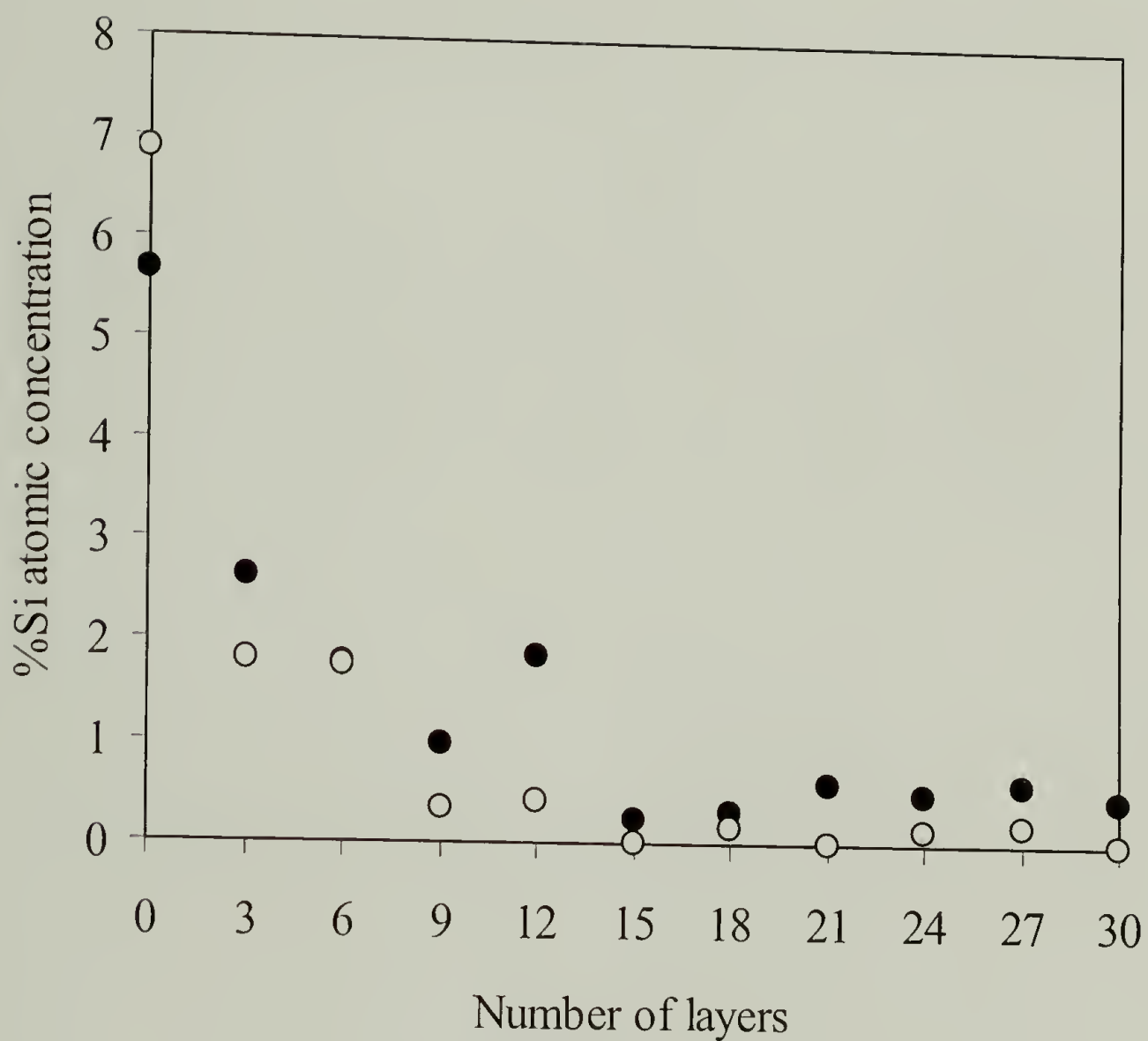


Figure 1.13. %Si atomic concentration for polyelectrolyte multilayers deposited on Al-NH_3^+ . Each set of x values are a multiple of 3 (●: determined from 15° take-off angle data, and ○: determined from 75° take-off angle data).

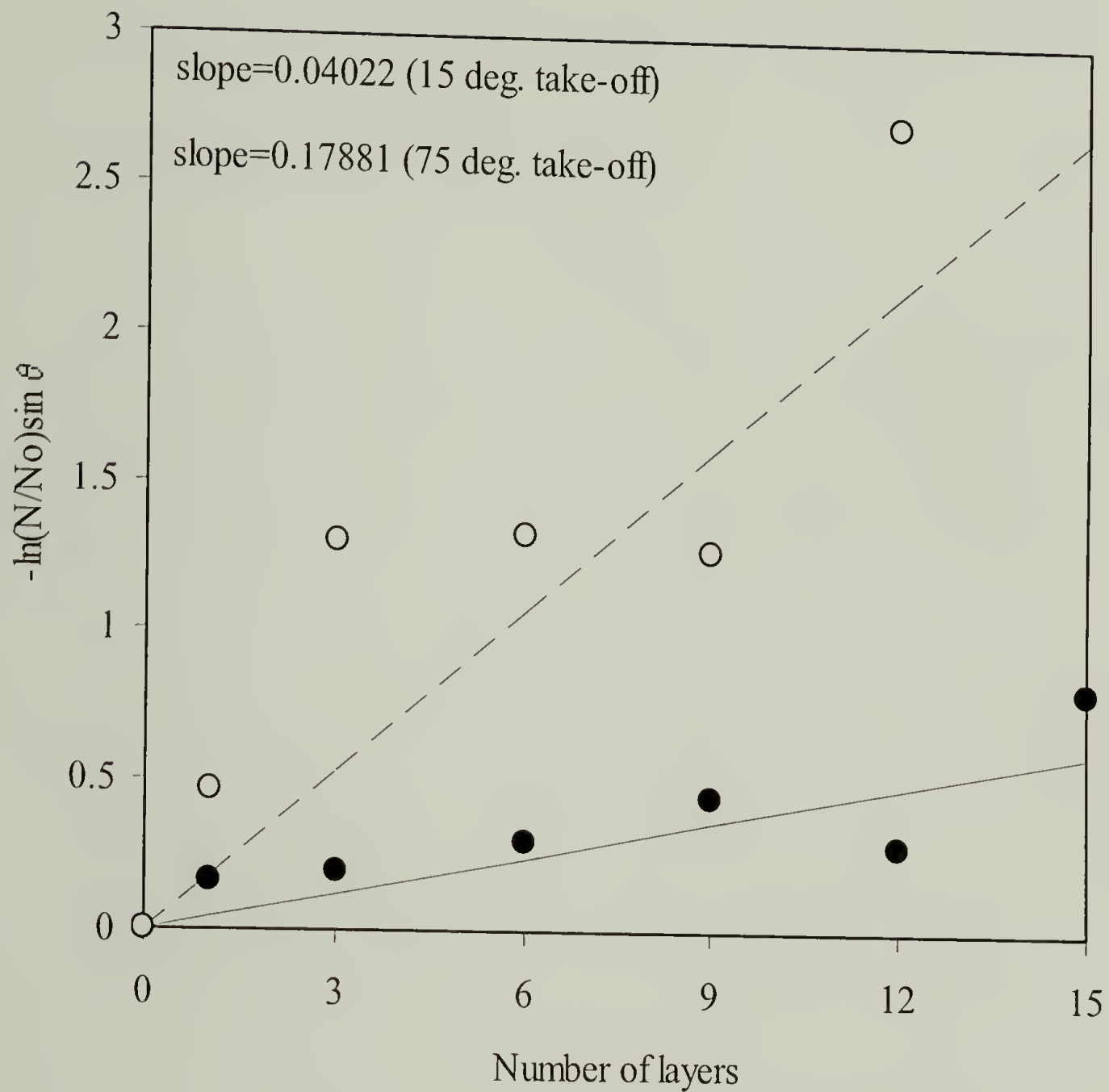


Figure 1.14. Peak intensity plot for Si_{2p} upon increasing number of polyelectrolyte multilayers on Al-NH_3^+ . ●: 15° take-off angle data, solid line: slope generated from 15° take-off angle data, ○: 75° take-off angle data, dotted line: slope generated from 75° take-off angle data.

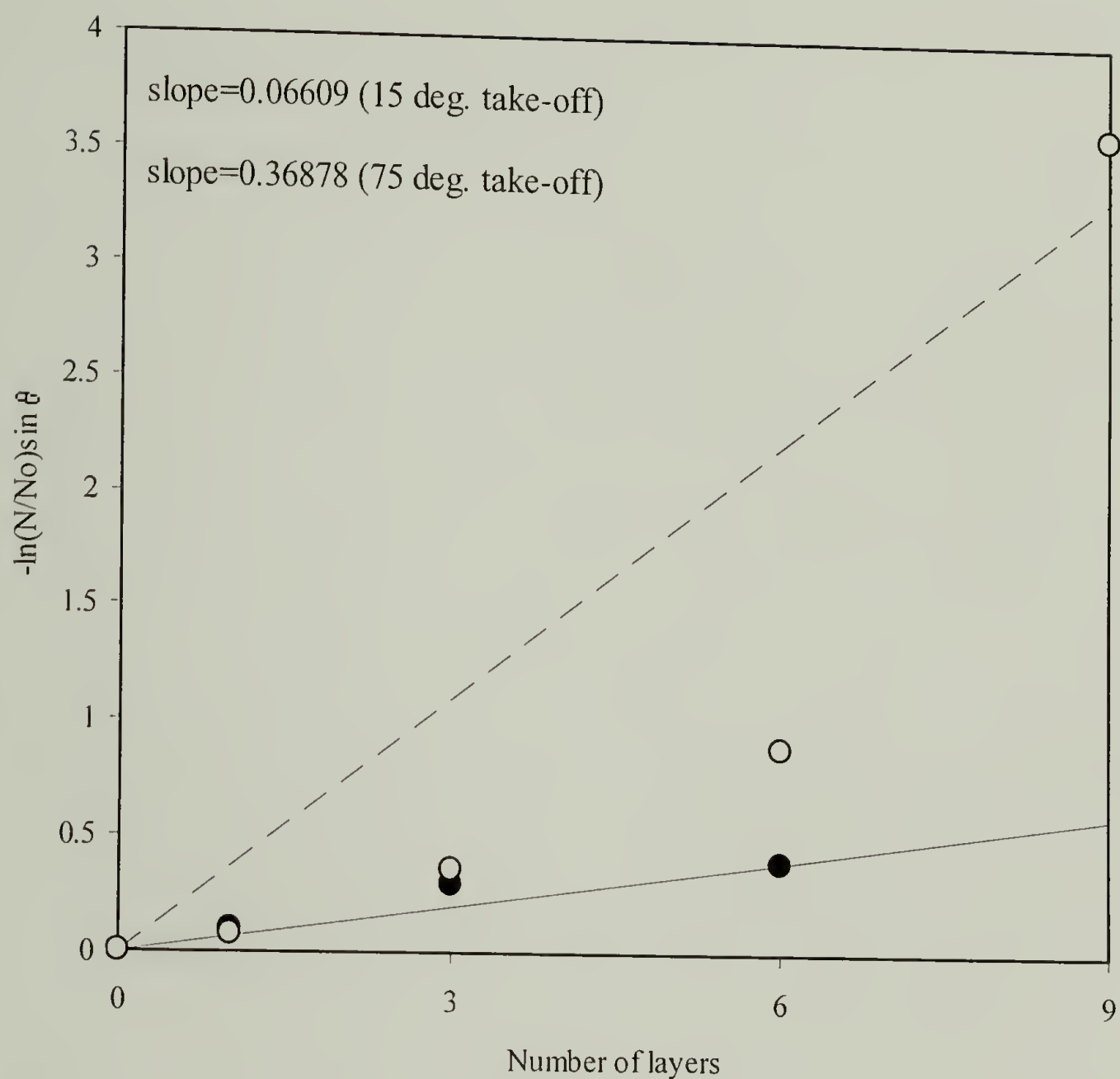


Figure 1.15. Peak intensity plot for Al_{2p} upon increasing number of polyelectrolyte multilayers on Al-NH_3^+ . \bullet : 15° take-off angle data, solid line: slope generated from 15° take-off angle data, \circ : 75° take-off angle data, dotted line: slope generated from 75° take-off angle data.

Simplified Peel Test. Peel tests were performed on samples with 24 (PAH top layer) and 25 (PSS top layer) layers using 3M #810 adhesive tape. XPS analysis of the tape indicates that only carbon and oxygen is detected; the samples contain nitrogen and sulfur so XPS analysis of the locus of failure was straightforward. Tabulated results of this experiment are shown in Table 1.2. In all cases cohesive failure in the tape was observed indicating that the mechanical strength of the multilayer assemblies and the adhesive strength of the bonds between the multilayers and the charged substrate are stronger than the cohesive strength of the pressure sensitive adhesive tape.

Table 1.2. % atomic concentrations (via XPS, 75° take-off angle) for 24 and 25 polyelectrolyte layers on Al-NH_3^+ before and after the simplified peel test using a pressure sensitive adhesive (P.S.A.) tape (3M #810).

	% C _{1s}	% O _{1s}	% N _{1s}	% S _{2p}	N:S
P.S.A. (before)	85.4	14.6	0.00	0.00	?
P.S.A. (after 24)	83.45	15.13	0.00	0.00	0.00
24 layers (before)	71.55	17.50	5.68	3.62	1.569
24 layers (after)	68.12	22.29	3.53	2.42	1.459
P.S.A. (after 25)	84.35	14.47	0.00	0.20	0.00
25 layers (before)	70.36	21.04	3.41	3.00	1.137
25 layers (after)	72.59	18.89	3.59	3.26	1.101

Conclusions

Silane coupling reactions with aqueous 3-aminopropyltriethoxysilane onto aluminum oxide surfaces were successful. The silane coupling layer is monolayer-like according to XPS analysis.

Sequential polyelectrolyte adsorptions onto silane coupled aluminum oxide surfaces were successful. Kinetics of the polyelectrolyte adsorption suggests that 30 min. is ample time needed for maximum adsorption. Notable features due to the nature of the two oppositely charged polyelectrolytes shown using XPS and contact angle include; (1) stratification upon increasing number of polyelectrolyte layers due to the outermost polyelectrolyte layer governing the surface characteristics of the multilayer assembly, and (2) attenuation of the starting surface upon increasing number of polyelectrolyte layers due to the increase in thickness with increasing number of polyelectrolyte layers.

Simplified peel tests using pressure sensitive adhesive tape suggest that the mechanical integrity of the polyelectrolyte multilayers constructed on Al-NH_3^+ are stronger than the cohesive strength of the adhesive tape, for we see cohesive failure of the tape, which transfers over to the polyelectrolyte multilayers.

References

1. Kinloch, A.J., Dukes, W.A., Glandhill, R.A. *Adhesion Science and Technology*, Plenum Press, New York, 1975.
2. Plueddemann, E.P., *Silane Coupling Agents*, 2nd ed., Plenum Press, New York, 1990.
3. Gettings, M., Kinloch, A.J., *J. Mater. Sci.* **1977**, *12*, 2511.
4. Gettings, M., Kinloch, A.J., *Surface Interface Analysis* **1979**, *1*, 189.

5. Boerio, F.J., Gosselin, C.A., 36th Ann. Conf. Reinf. Plast/-Composites Inst., SPI Paper 2G, 1981.
6. Patrick, R.L., Brown, J.A., Cameron, N.M., Gehman, W.G., *Appl. Polym. Symp.* **1971**, 12, 87.
7. Decher, G., Hong, J.D., European Patent 0472 990 A2, 1992.
8. Decher, G., Hong, J.D., *Ber Bunsenges. Phys. Chem.* **1991**, 95, 1430.
9. Roberts, G. G., *Langmuir-Blodgett Films*, Plenum Press, New York, 1990.
10. Decher, G., Eckle, M., Schmitt, J., Struth, B *Current Opinion in Colloid & Interface Science* **1998**, 3, 32.
11. Berndt, P., Kurihara, K., Kunitake, T., *Langmuir* **1992**, 8, 2486.
12. Decher, G., Hong, J. -D., Schmitt, J. *Thin Solid Films* **1992**, 210, 831.
13. Decher, G., Schmitt, J. *Progr. Colloid. Polym. Sci.* **1992**, 89, 160.
14. Lvov, Y., Decher, G., Möhwald, H. *Langmuir* **1993**, 9, 481.
15. Decher, G., Lvov, Y., Schmitt, J. *Thin Solid Films* **1994**, 244, 772.
16. Sukhorukov, G. B., Schmitt, J., Decher, G. *Ber. Bunsenges. Phys. Chem.* **1996**, 100, 948.
17. Decher, G., Ed., *Multilayer Films(Polyelectrolytes)*; CRC Press: Boca Raton; 1996, p. 4540.
18. Ferreira, M., Rubner, M.F. *Macromolecules* **1995**, 28, 7107.
19. Fou, A. C., Rubner, M.F. *Macromolecules* **1995**, 28, 7115.
20. Cheung, J. H., Stockton, W.B., Rubner, M.F. *Macromolecules* **1997**, 30, 2712.
21. Stockton, W. B., Rubner, M.F. *Macromolecules* **1997**, 30, 2717.
22. Fou, A. C., Onitsuka, O., Ferreira, M., Rubner, M.F., Hsieh, B.R. *J. Appl. Phys.* **1996**, 79, 7501.
23. Onoda, M., Yoshino, K. *Jpn. J. Appl. Phys.* **1995**, 34, L260.
24. Stepp, J., Schlenoff, J.B. *J. Electrochem. Soc.* **1997**, 144, L155.

25. Laurent, D., Schlenoff, J.B. *Langmuir* **1997**, *13*, 1552.
26. Hammond, P. T., Whitesides, G.M. *Macromolecules* **1995**, *28*, 7569.
27. Caruso, F., Niikura, K., Furlong, D.N., Okahata, Y. *Langmuir* **1997**, *13*, 3427.
28. Lvov, Y., Haas, H., Decher, G., Möhwald, H., Kalachev, A. *J. Phys. Chem.* **1993**, *97*, 12835.
29. Schmitt, J., Grunewald, G., Decher, G., Pershan, P.S., Kjaer, K., Losche, M. *Macromolecules* **1993**, *26*, 7058.
30. Watanabe, S., Regan, S.L. *J. Am. Chem. Soc.* **1994**, *116*, 8855.
31. Lvov, Y., Ariga, K., Kunitake, T. *Chem. Lett.* **1994**, 2323.
32. Caruso, F., Niikura, K., Furlong, D.N., Okahata, Y. *Langmuir* **1997**, *13*, 3422.
33. Delcorte, A., Bertrand, P., Wischerhoff, E., Laschewsky, A. *Langmuir* **1997**, *13*, 5125.
34. Kleinfield, E. R., Ferguson, G.S. *Science* **1994**, *265*, 370.
35. Lvov, Y., Ariga, K., Ichinose, I., Kunitake, T. *Langmuir* **1996**, *12*, 3038.
36. Delcorte, A., Bertrand, P., Arys, X., Jonas, A., Wischerhoff, E., Mayer, B., Laschewsky, A. *Surface Science* **1996**, *366*, 149.
37. Lvov, Y., Haas, H., Decher, G., Möhwald, H. *Langmuir* **1994**, *10*, 4232.
38. Lvov, Y., Decher, G., Sukhorukov, G. *Macromolecules* **1993**, *26*, 5397.
39. Tsukruk, V. V., Rinderspacher, F., Bliznyuk, V. *Langmuir* **1997**, *13*, 2171.
40. Leväsalmi, J.-M., McCarthy, T.J. *Macromolecules* **1997**, *30*, 1752.
41. Chen, W., McCarthy, T.J. *Macromolecules* **1997**, *30*, 78.
42. Phuvanartnuruks, V., McCarthy, T.J. *Polym. Prepr. (Am. Chem. Soc. Div. Polym. Chem.)* **1997**, *38(1)*, 961.
43. Dias, A. J., McCarthy, T.J. *Macromolecules* **1987**, *20*, 2068.
44. Ferreira, M., Cheung, J.H., Rubner, M.F. *Thin Solid Films* **1994**, *244*, 806.

45. Laschewsky, A., Bayer, B., Wischerhoff, E., Arys, X., Bertrand, P., Delacorte, A., Jonas, A. *Thin Solid Films* **1996**, 284, 334.
46. Onoda, M., Lvov, Y., Ariga, K., Kunitake, T. *J. Ferment. Bioeng.* **1996**, 82, 502.
47. Kleinfield, E. R., Ferguson, G.S. *Chem. Mater.* **1995**, 7, 2327.
48. Marra, J., van der Schee, H.A., Fleer, G.J., Lyklema, J., Ed., *Adsorption from Solution*; Academic Press: New York; 1983, p.245.
49. Papenhuijzen, J., Fleer, G.J., Bijsterbosch, B.H. *J. Colloid Interface Sci.* **1985**, 104, 530.
50. Cosgrove, T., Obey, T.M., Vincent, B. *J. Colloid Interface Sci.* **1986**, 111(2), 409.
51. Evers, O. A., Fleer, G.J., Scheutjens, J.M.H.M., Lyklema, J. *J. Colloid Interface Sci.* **1986**, 111(2), 446.
52. Blaakmeer, J., Böhmer, M.R., Cohen Stuart, M.A., Fleer, G.J. *Macromolecules* **1990**, 23, 2301.
53. van der Schee, H. A., Lyklema, J. *J. Phys. Chem.* **1984**, 88, 6661.
54. Böhmer, M. R., Evers, O.A., Scheutjens, J.M.H.M. *Macromolecules* **1990**, 23, 2288.
55. Muilenberg, G.E., *Handbook of X-ray Photoelectron Spectroscopy*, Perkin-Elmer Corp., 1979.
56. Andrade, J.D., Gregonis, D.E., Smith, L.M., *Surface and Interfacial Aspects of Biomedical Polymers*, Plenum Press, New York, 1986.
57. Clark, D.T., Thomas, H.R., *J. Polym. Sci., Polym. Chem. Ed.* **1977**, 15, 2843.
58. Zisman, W.A., *Adv. Chem. Ser.* **1964**, 68, 1744.
59. Johnson, R.E., Dettre, R.H. *J. Phys. Chem.* **1964**, 68, 1744.
60. Huh, C., Mason, S.G. *J. Colloid Interface Sci.*, **1977**, 60, 11.

CHAPTER 2

MECHANICAL PROPERTIES OF POLYELECTROLYTE MULTILAYER FILMS SUPPORTED ON MODIFIED POLY(ETHYLENE TEREPHTHALATE)

Poly(ethylene terephthalate) (PET) Surface Modification

PET is an economically important thermoplastic that is used in photographic film, magnetic recording tape, packaging material, and electronic insulation.¹ PET has been surface modified by a variety of techniques including plasma,² corona discharge,³ ion beam,⁴ laser treatment,⁵ photoinitiated graft polymerization,⁶ saponification,⁷ aminolysis,⁸⁻⁹ reduction,⁹⁻¹⁰ and entrapment of poly(ethylene oxide).¹¹ PET was chosen as the substrate for modification studies for several reasons: (1) it contains carbonyl groups that are capable of hydrogen bonding, (2) the surface can be readily hydrolyzed to introduce carboxylic acid (as well as alcohol) functionality that can support negative charge (PET-CO₂⁻) in sufficiently basic solution, and (3) the surface can react with polyamines to incorporate amine functionality that can support positive charge (PET-NH₃⁺) in non-basic solution.

Previous Results

Surface modification of PET has been developed recently by a previous group member using amidation to create cationic functionalities, and hydrolysis to create anionic functionalities.¹² XPS and contact angle data indicate that the layers formed are

extremely thin (2 - 6 Å) and are stratified. Wettability characteristics of the polyelectrolyte multilayer films are controlled by the outermost polyelectrolyte layer and the thickness of the individual layers. Depending on the surface chemistry, the thickness and the stoichiometry (ammonium cation : sulfonate anion ratio) is influenced. The effect of the ionic strength of the polyelectrolyte solutions was also studied for the neutral PET surface. The ionic strength was controlled by incorporating added salt (manganese chloride MnCl_2) into the polyelectrolyte solutions. Both the individual layer thickness and the deposition stoichiometry are affected by the change in ionic strength. Simplified peel tests were performed to show that the multilayer assemblies have significant mechanical strength.

Objective

Our objective is to use previous results obtained from functionalizing PET surfaces by constructing polyelectrolyte multilayers on these surfaces, and examine in detail the mechanical strength of these constructed multilayers with conventional mechanical tests. The fabrication of polyelectrolyte multilayers and the controlling variables for the polyelectrolyte adsorption on surfaces have been discussed in Chapter 1. Testing these materials will give us a better understanding of the mechanical integrity of these polyelectrolyte multilayers and the potential application of this process for adhesion promotion. By evaluating these polyelectrolyte multilayers in a conventional test such as the single lap shear joint test, the adhesive shear strength of the material can be measured. The effect of adhesive shear strength of these multilayer assemblies with different functional PET surfaces is of interest. Also, the effect of increasing the number of

polyelectrolyte multilayers, and its relation with the adhesive shear strength of the multilayer assembly is of interest. The effect of ionic strength, adjusted by the incorporation of added salt (manganese chloride), on the adhesive shear strength of the polyelectrolyte multilayer assemblies will also be investigated.

Single Lap Shear Joint Test

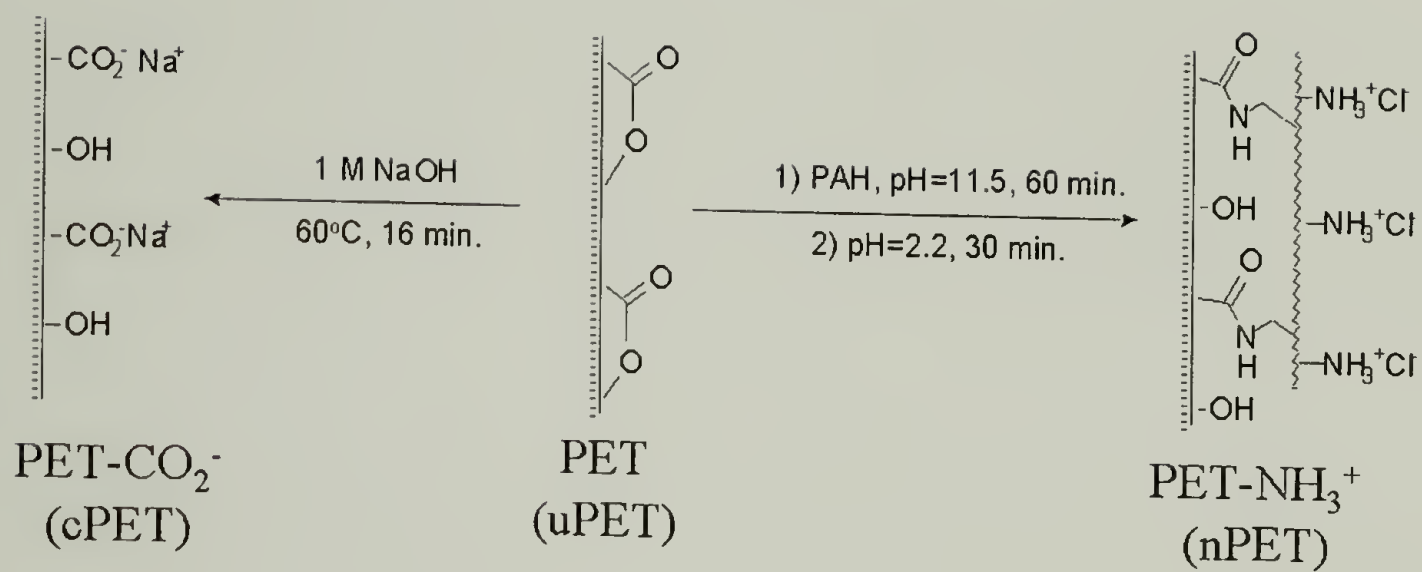
Of the various geometries and methods of loading, the single lap joint has received the most attention from the stress analysts. There are two main reasons for this interest. Firstly, a lap joint, which consists of two sheets of the substrates joined by a simple overlay, is one of the most common joint designs employed in industry and secondly, it is a simple and convenient test geometry for evaluating adhesive joints.

The lap shear test is typically used to determine adhesive shear strengths. However, because it was designed for use with metals, there are several limitations to it when applied to plastic substrates. Because plastics have much lower tensile strength than metals, plastic lap shear specimens are more likely to fail within the substrate than the metal lap shear joints. This makes the analysis for plastics much more difficult because many of the adhesives will achieve substrate failure. Another disadvantage of using the lap shear method for plastics are the lower moduli compared to metals. This causes the plastic substrate to deform more during testing, which introduces significant peel and cleavage forces on the joint. The lower the modulus of the plastic, the more the specimen will deform under load, and the less representative the experimental shear strength will be of the actual shear strength.

Experimental

Materials. Poly(allylamine hydrochloride) (PAH, $M_w=50,000-65,000$) and poly(sodium styrene sulfonate) (PSS, $M_w=70,000$) were obtained from Aldrich. Sodium chloride, $MnCl_2 \cdot 4H_2O$, 1.0 M HCl, sodium hydroxide, methanol (HPLC grade) and hexane (HPLC grade) were purchased from Fisher. All materials were used as received. Water was purified using a Millipore Milli-Q® system that involves reverse osmosis followed by ion exchange and filtration steps. Solution pH's for layer-by-layer adsorption studies were adjusted with either HCl or NaOH solution using a Fisher 825MP pH meter. Poly(ethylene terephthalate) film (DuPont Mylar®), 5 mil thick (1 mil = 25 μm), was used in this study. The films were cut up into 10 mm x 50 mm strips for their use as single lap joints. A room-temperature cure, gel type cyanoacrylate adhesive (Loctite 454) was received from Loctite.

PET Substrate Preparation. Functionalization of the PET film has been done previously in our research group.¹³ A schematic is shown in Scheme 2.1. The films were rinsed with distilled water and methanol, extracted in refluxing hexane for 2 hours, and then dried (room temperature, 0.01 mmHg, overnight). PET-CO₂⁻ was prepared by introducing the cleaned PET films to 1 M NaOH aqueous solution for 16 min at 60°C. The films were subsequently rinsed with 0.1 M HCl, distilled water (x2), methanol, hexane, and then dried at reduced pressure. PET-NH₃⁺ was prepared by immersing the cleaned PET films in a PAH solution (167 mg of PAH in 120 ml of water, pH=11.5) for 1 hr. at room temperature. The film was removed from the solution, rinsed with water (x3),

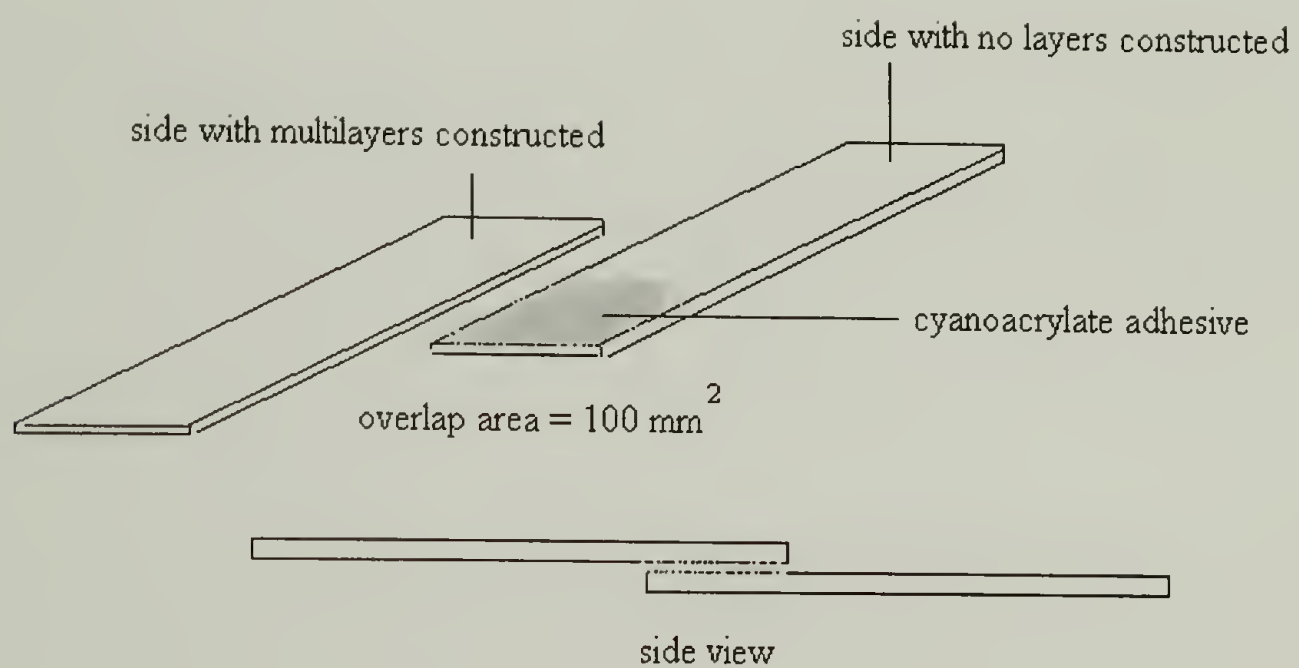


Scheme 2.1. Surface functionalization of Mylar® poly(ethylene terephthalate) (PET) film. Left: hydrolysis, right: amidation.¹³

and introduced to pH=2.2 water for 30 min. After rinsing with water (x3), the PET-NH₃⁺ films were dried at reduced pressure.

Multilayer Formation. The film samples (either unmodified or modified), after the steps described above, are then ready for layer-by-layer deposition. Each adsorption is carried out at room temperature in an open beaker containing an unstirred polyelectrolyte solution that was prepared fresh for each new batch of samples. The first polycation layer deposition is carried out using the unmodified and hydrolyzed PET by immersing the films into a 0.2 M (based on repeat units) PAH solution (pH=8.0) and then waiting for 20 minutes for the system to reach steady-state. The PET strips are then washed with aliquots of Milli-Q® water (x3). The first polyanion layer deposition is carried out using the amidated PET by immersing the films into a 0.2 M (based on repeat units) PSS solution (pH=4.0), and then after 20 minutes, taken out of the solution for another Milli-Q® water wash (x3). The process is continued (immersion-20min-take out and wash) by alternating between the two beakers containing the oppositely charged polyelectrolyte solutions until the desired number of layers is deposited. Upon reaching the desired number of layers, the strips are washed in aliquots of Milli-Q® water (x3), and vacuum dried under reduced pressure overnight.

Single Lap Shear Assembly. A multilayer-assembled strip is paired with a PET strip that has only gone through the surface functionalization step (i.e., PET-CO₂⁻/(PSS-PAH)_n paired with PET-CO₂⁻). This is shown in Scheme 2.2. This is to aid us in finding the locus of failure of the multilayers upon adhesive failure. The strips are adhered



Scheme 2.2. Single lap shear joint assembly configuration for the layer-by-layer deposited polyelectrolyte multilayer films.

together using a room-temperature cure gel type cyanoacrylate adhesive over a bond area of 100 mm^2 (10 mm x 10 mm). The reason for using this particular type of cyanoacrylate adhesive is to minimize complications in the curing and permeation of the adhesive through the multilayer assemblies as much as possible. The average thickness of the adhesive applied was 25 microns. The lap joint specimens were left to cure in ambient air for at least 72 hours before running mechanical tests.

Mechanical Testing. The single lap shear joint specimens were subjected to tension in order to measure the adhesive joint strength and the effect the multilayers have on the adhesive joint strength. An Instron tensile tester (Model 5564) was used with a 10 N load cell. A crosshead speed of 10 mm/min. was used. All samples were taken to failure and at least 5 samples for each case were tested for reproducibility. All values reported for adhesive shear strength values in this experiment show a standard deviation of 15%.

Results and Discussions

Adhesion and the Effect on Substrate Functionalization. Figure 2.1 shows the lap shear strength of the multilayer/adhesive specimens upon increasing number of multilayers for the unmodified and modified PET-supported test samples. No noticeable trend is observed for the unmodified and amidated PET samples. The adhesive shear strength of these particular samples shows a weak interaction between the substrate, the polyelectrolyte multilayers, and the cyanoacrylate adhesive. For the hydrolyzed PET samples, however, we observe that the initial adhesive shear strength between the

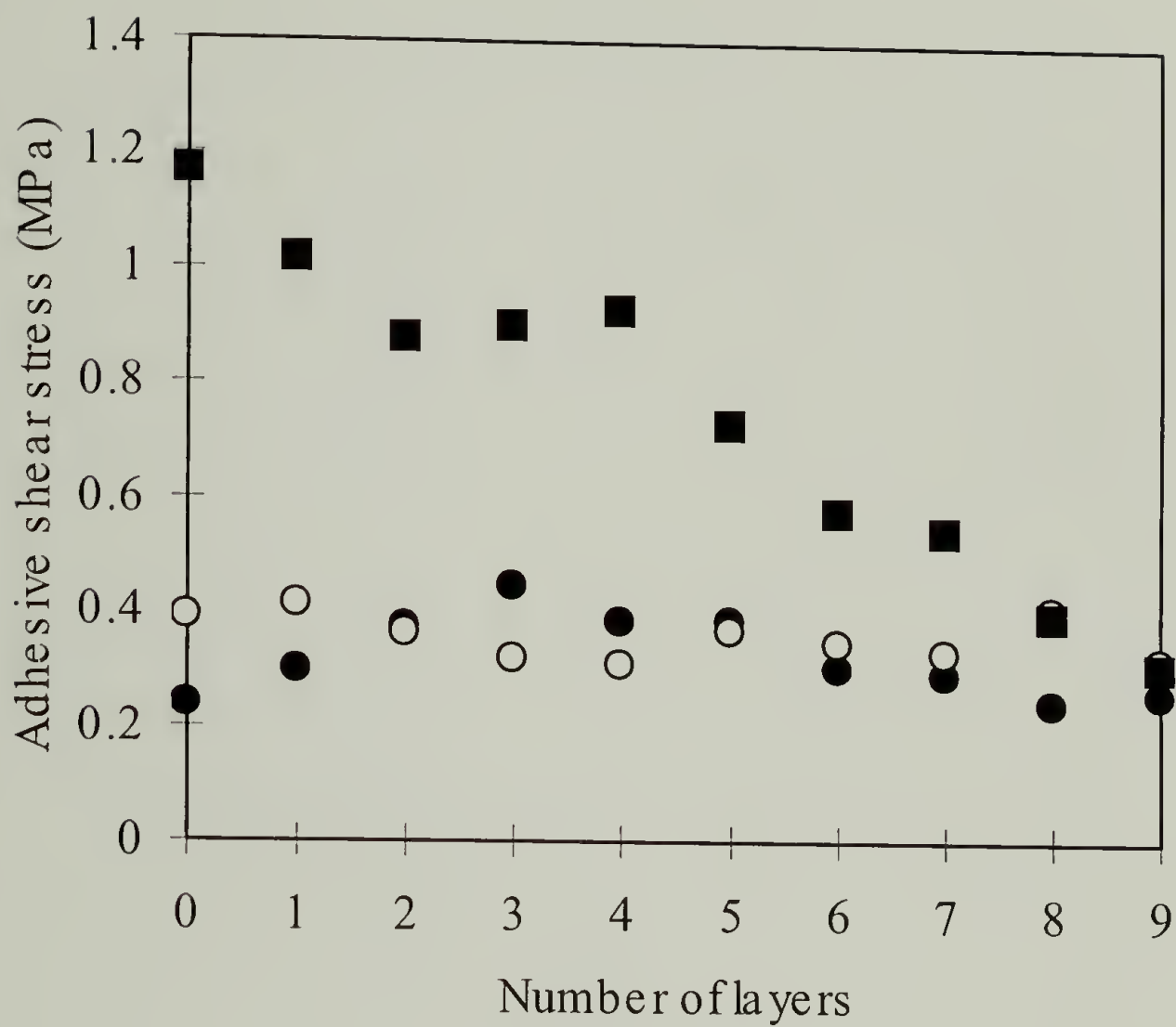


Figure 2.1. Adhesive shear stress of single lap shear joint samples of polyelectrolyte multilayers constructed on modified PET. ●: polyelectrolyte multilayers constructed on untreated PET; ○: polyelectrolyte multilayers constructed on amidated PET (PET-NH₃⁺); ■: polyelectrolyte multilayers constructed on hydrolyzed PET (PET-COO⁻).

cyanoacrylate adhesive and the two hydrolyzed PET lap shear joints is greater than in either the unmodified or the amidated PET (some hydrolyzed samples showed substrate failure before bond failure). This result is significant in itself because we can conclude that by hydrolyzing PET, we can obtain better adhesion characteristics.

Adhesion and the Effect of the Number of Layers. Another noticeable trend in Figure 2.1 is the decreasing adhesive shear strength of the lap shear joint specimens upon increasing number of polyelectrolyte multilayers. One possible explanation for this behavior is that the polyelectrolyte multilayers prevent the cyanoacrylate adhesive from permeating through the multilayers and interacting with the hydrolyzed PET surface by increasing the number (i.e., thickness) of the multilayers. As the probability of the adhesive interacting with the original PET surface decreases, and the probability of the adhesive interacting with the polyelectrolyte multilayers increases, the weaker the adhesive shear strength of those particular specimens. This result shows that the polyelectrolyte multilayers are inherently weak, and that they do not reinforce the adhesion characteristics with their ionic-strength interactions as was originally envisaged.

Adhesion and the Effect of Added Salt Incorporation. Figure 2.2 shows the comparison between the adhesive shear strength of the lap shear joint specimens that have polyelectrolyte multilayers constructed with no added salt (top curve) and lap shear joint specimens that have polyelectrolyte multilayers constructed with added salt (MnCl_2 added to both polyelectrolyte solutions). The incorporation of salt into the individual polyelectrolyte solution changes the conformation of the polyelectrolyte to allow a more

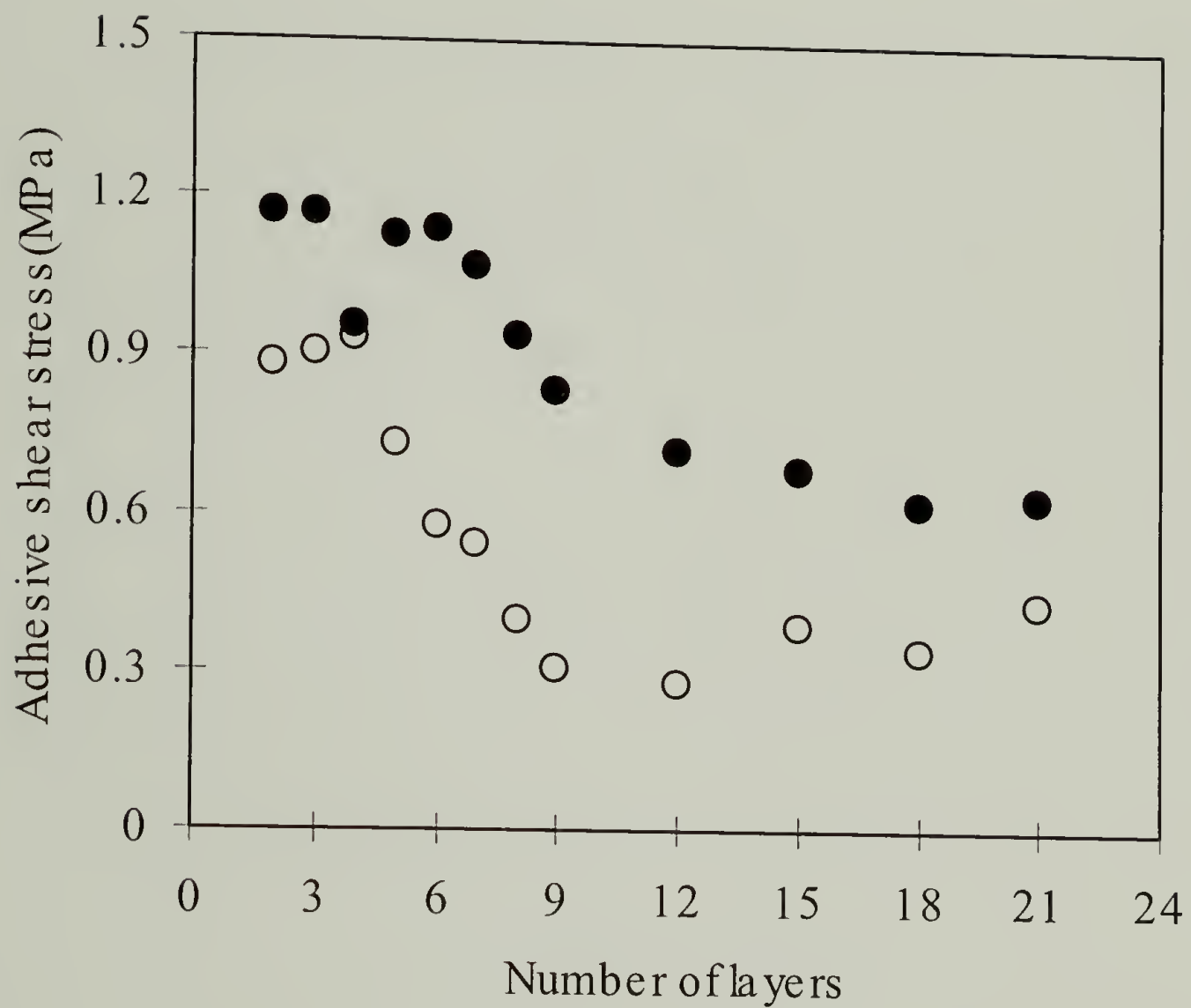
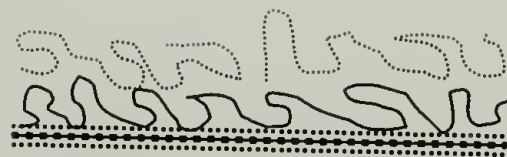


Figure 2.2. Change in adhesive shear stress for single lap shear joint samples of polyelectrolyte multilayers constructed on hydrolyzed PET. ●: polyelectrolyte multilayers with no added salt in the polyelectrolyte solutions; ○: polyelectrolyte multilayers with added salt (manganese chloride, MnCl_2) in the polyelectrolyte solutions.

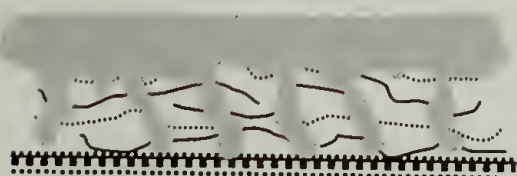
globular structure due to charge screening than in the case of more linear conformations when no salt is added. This added salt in the polyelectrolyte solution translates into thicker individual polyelectrolyte monolayers. However, as seen in Figure 2.2, the adhesive strength towards the cyanoacrylate adhesive for these polyelectrolyte multilayers with added salt indicates a weaker adhesive shear strength value than in the case of the polyelectrolyte multilayers with no added salt. This can be explained: even though the polyelectrolyte multilayers with added salt are thicker, the adhesion between these polyelectrolyte multilayers and the hydrolyzed PET substrate decreases due to the charge screening effect. Another interesting trend is both the polyelectrolyte multilayers with and without added salt show a plateau after a certain number of multilayers. We conclude that this is from the cyanoacrylate adhesive no longer interacting with the original PET substrate, and that we are seeing only the interaction between the cyanoacrylate adhesive and the polyelectrolyte multilayers. Therefore, the adhesive shear strength values at the plateau region for both sets coincide with the adhesive shear strength of the multilayers. The reason for the difference in the number of layers where the plateau region begins (~12 layers for added salt, and ~18 layers for no added salt) is due to the surface coverage of these two differently adsorbed multilayer assemblies. For the polyelectrolyte multilayers with no added salt, the more linear conformation of the polyelectrolytes allows them to cover surfaces in a tighter network with fewer imperfections that allow permeation of the adhesive to occur. For the polyelectrolyte multilayers with added salt, the more globular conformation of the polyelectrolytes covers surfaces in a looser network with more imperfections that allow permeation of the adhesive to occur rather easily. This is pictorially depicted in Scheme 2.3.



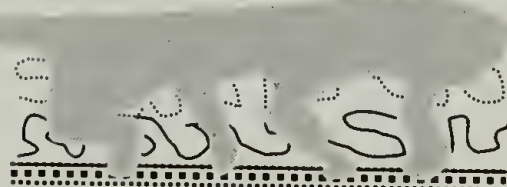
Polyelectrolyte assembly
(no added salt)



Polyelectrolyte assembly
(added salt, MnCl_2)



Thin, tighter
network structure



Thick, looser
network structure



Harder to pull off:
strong adhesion between
polyelectrolyte multilayers



Easier to pull off:
weak adhesion between
polyelectrolyte multilayers

Scheme 2.3. Pictorial representation of the single lap shear joint test. Solid and dotted lines represent the oppositely charged polyelectrolytes. ■ denotes the cyanoacrylate adhesive.

We are aware that some of the results involved in comparing the two systems may be faulted by the fact that the cyanoacrylate chemistry for polymerization is sensitive to the acidity/basicity of the surfaces that the adhesive is applied towards. Knowing that the pH values for the polyelectrolyte solutions with added salt (both solutions' pH~2.2) and for the polyelectrolyte solutions with no added salt (pH=4.0 for PSS, and pH=8.0 for PAH) are significantly different, this may well have an effect on the adhesion properties of the cyanoacrylate adhesive. However, the general trends that are observed are still valid in that most of the results are effects of the polyelectrolyte multilayers interacting with the PET surface and the cyanoacrylate adhesive, and not the simple effect of pH on the performance of the cyanoacrylate adhesive. Also, we believe the washing step between each polyelectrolyte deposition helps in neutralizing the surface charges and does away with most the added salt within the polyelectrolyte multilayers. We believe that the effect of the performance of the cyanoacrylate adhesive due to the pH of the polyelectrolyte solutions should be minimal.

Determination of Locus of Failure. Figure 2.3 shows SEM micrographs of the lap shear joint specimens of the cyanoacrylate adhesive after adhesive failure. Figures 2.4 and 2.5 show SEM micrographs of the lap shear joint specimens of 9 polyelectrolyte multilayers constructed on PET-COO⁻ after adhesive failure. Each individual picture shows that the failure is complex, in that there is no apparent interface the assembly prefers to fail at. This is due to the adhesive permeating through the thickness of the multilayers. This behavior, however, diminishes with increasing number of layers, where

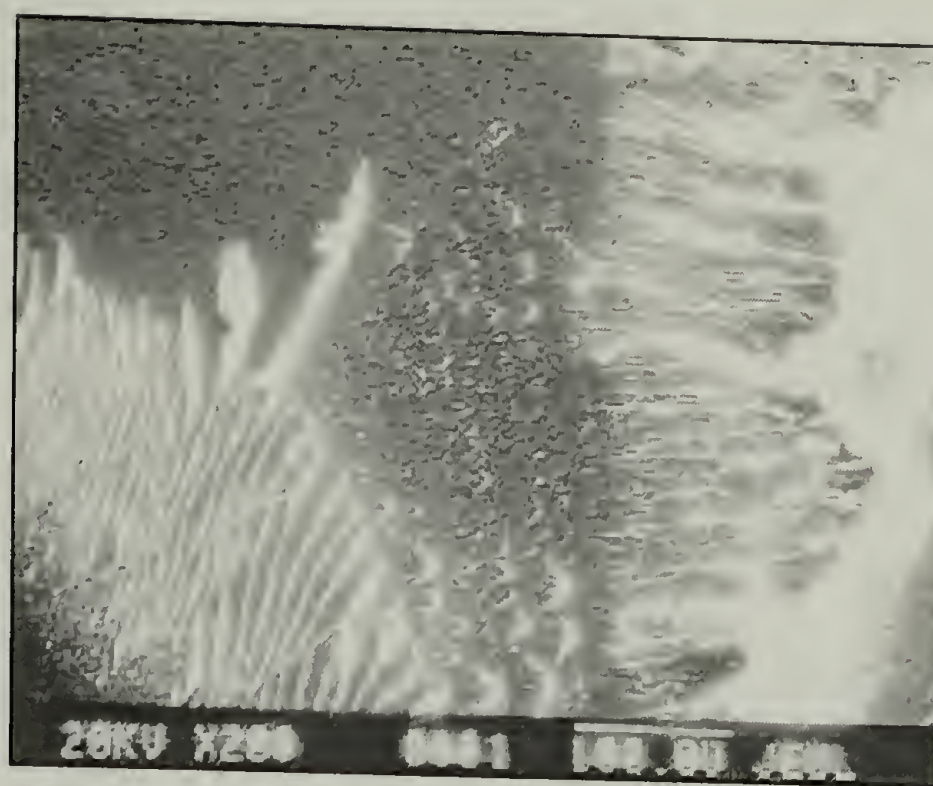


Figure 2.3. SEM micrographs of cyanoacrylate adhesive failure between two hydrolyzed PET lap shear joints (top: x 200 magnification, bottom: x 2000 magnification).

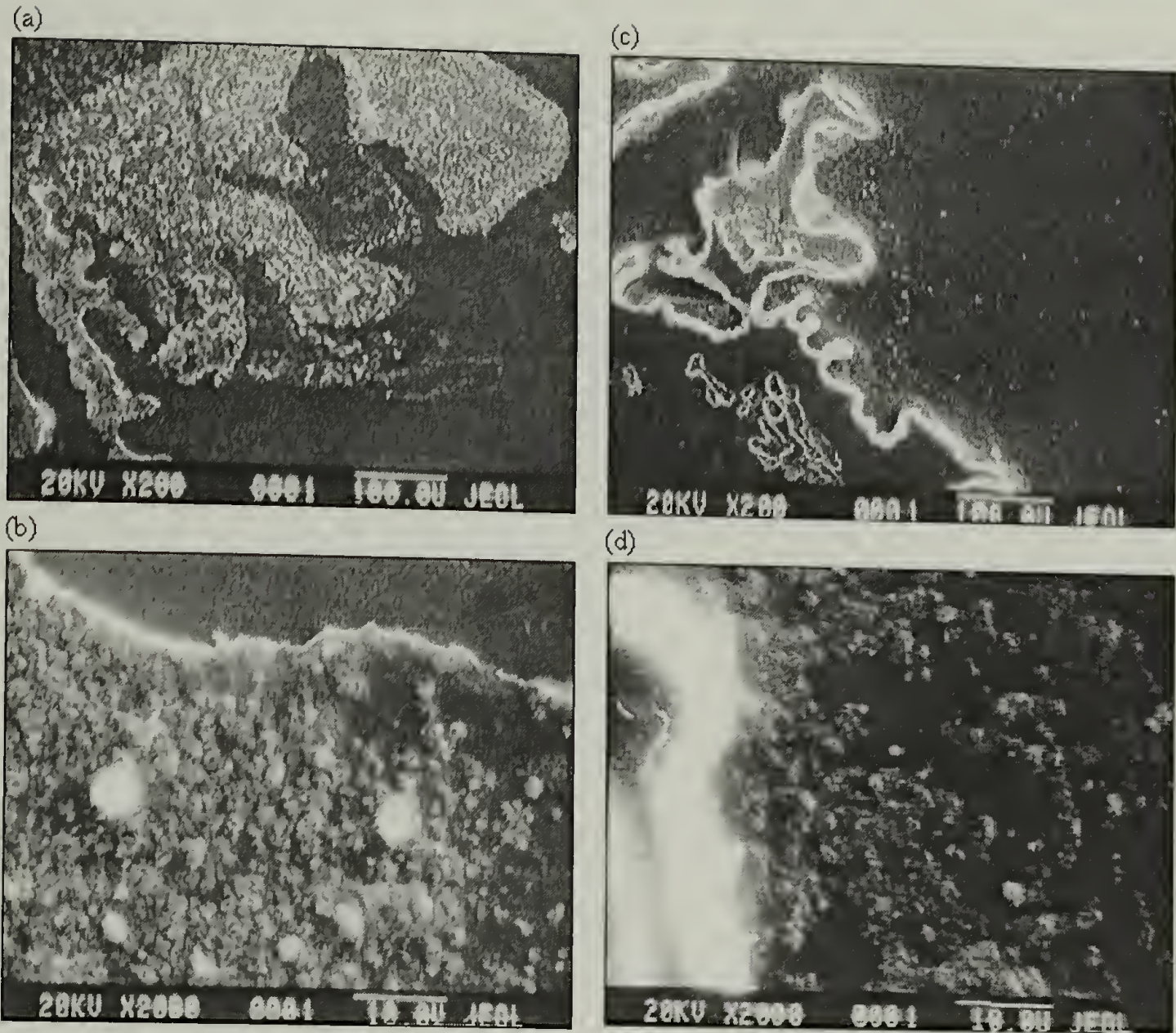


Figure 2.4. Single lap shear joint specimens taken to adhesive failure. (a) layer side, 9 polyelectrolyte layers, added salt (manganese chloride)(x 200 magnification); (b) same layer side (x 2000 magnification); (c) zero side, 9 polyelectrolyte layers, added salt (manganese chloride)(x 200 magnification); (d) same zero side (x 2000 magnification).

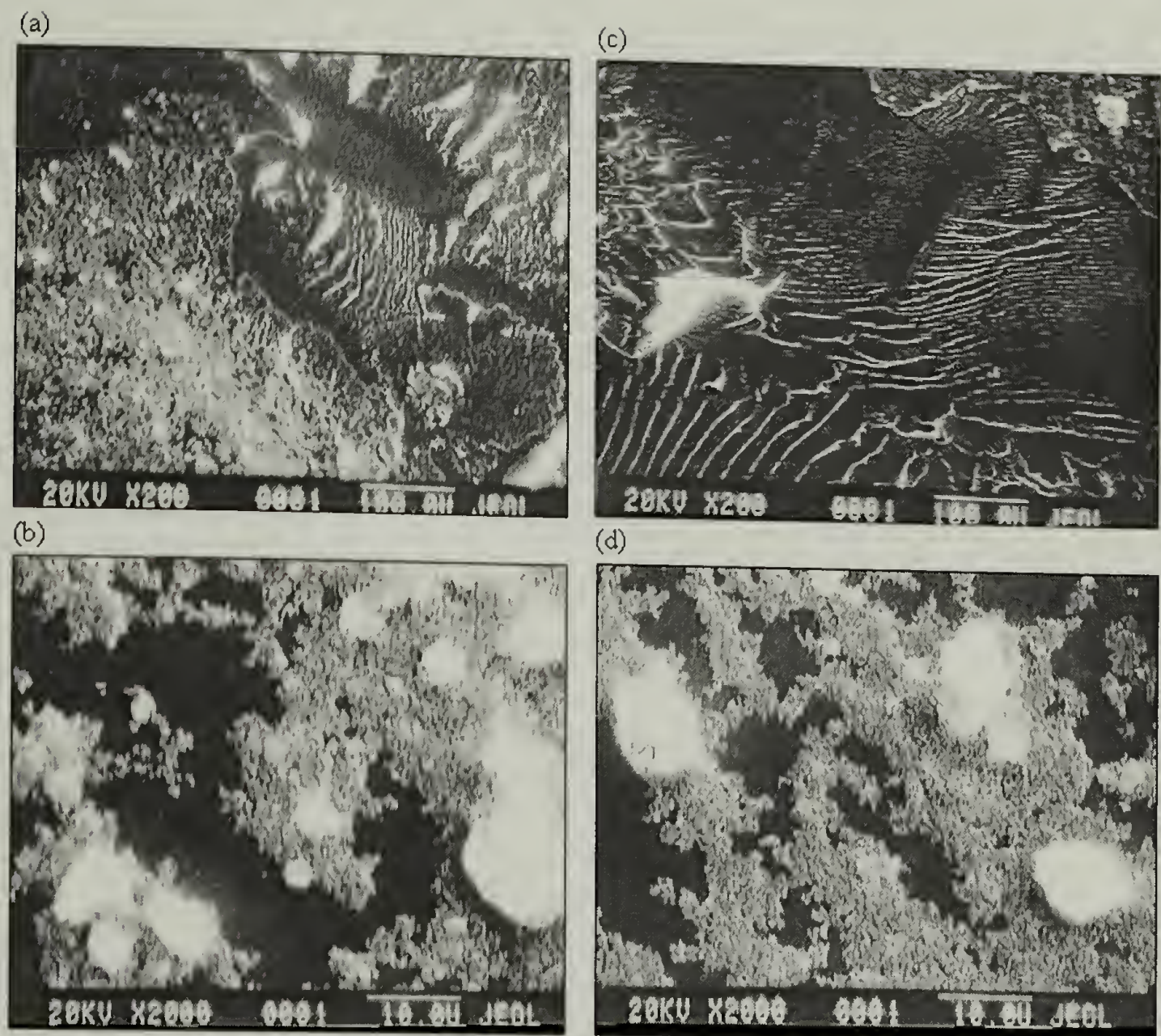


Figure 2.5. Single lap shear joint specimens taken to adhesive failure. (a) layer side, 9 polyelectrolyte layers, no added salt (x 200 magnification); (b) same layer side (x 2000 magnification); (c) zero side, 9 polyelectrolyte layers, no added salt (x 200 magnification); (d) same zero side (x 2000 magnification).

the adhesive doesn't contact the substrate anymore, and interacts only with the multilayers.

XPS results also agree with this analysis. Figures 2.6 and 2.7 show the %S content of the two sides of the lap shear joint specimens after failure upon increasing number of layers for both the added salt and the no added salt case. Although no general trend is noticeable with the increasing number of polyelectrolyte multilayers, there is a higher percentage of S atoms that shows up on the side that had no polyelectrolyte multilayers assembled on the PET before the lap shear test. This means that the adhesive permeates the polyelectrolyte multilayers, and pulls out the multilayers over to the side where no polyelectrolyte multilayers were constructed. Pull-out is eminent due to the preferred adhesion characteristics the cyanoacrylate adhesive has with the hydrolyzed PET side with no polyelectrolyte multilayers constructed on it. The same type of behavior is shown with the %N content (see Figure 2.8). A higher percentage of N atoms is shown on the hydrolyzed PET side with no polyelectrolyte multilayers constructed on them. N_{1s} Spectra for the 21 layer samples (for both added salt and no added salt) show no real conclusive evidence on whether there is a definite interface where the failure occurs. Therefore, we conclude that the failure mode for the lap shear joint samples tested is complex, with no preferable interface that wants to form when subjected to failure. Comparing the N_{1s} spectrum for the 21 layer sample shown in Figure 2.9, we see that the 403 eV peak, which is predominantly from the cyanoacrylate adhesive, generally shows a higher affinity toward the lap shear joint side with no polyelectrolyte layers constructed on it (zero side). This suggests that the adhesive exhibits a higher affinity towards the zero-layer side.

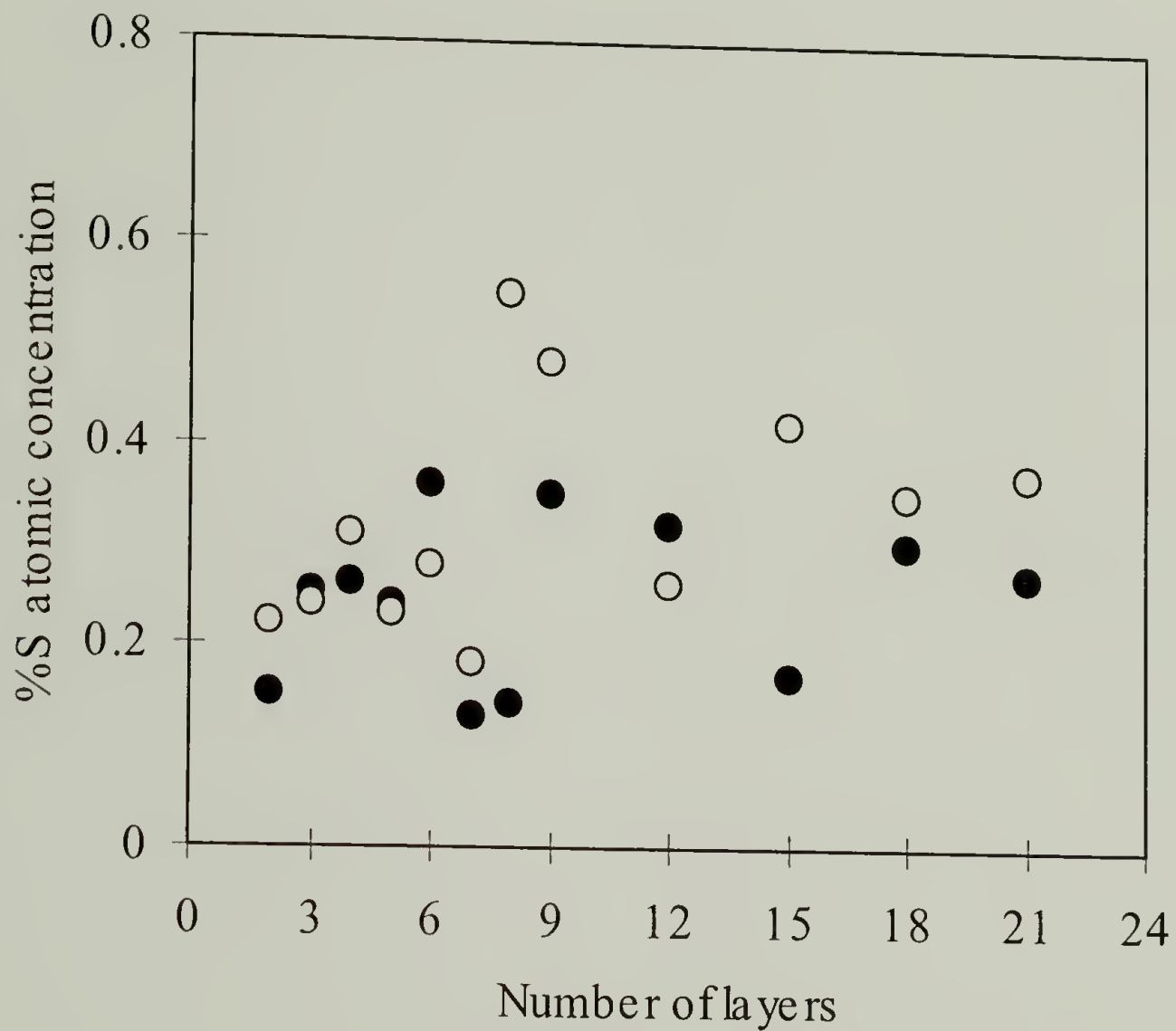


Figure 2.6. %S atomic concentration (XPS, 75° take-off angle) for single lap shear joint samples of polyelectrolyte multilayers (with no added salt) constructed on PET-COO⁻ after taken to adhesive failure. ●: lap shear joint originally with multilayers constructed on them, ○: lap shear joint originally with no multilayers on them.

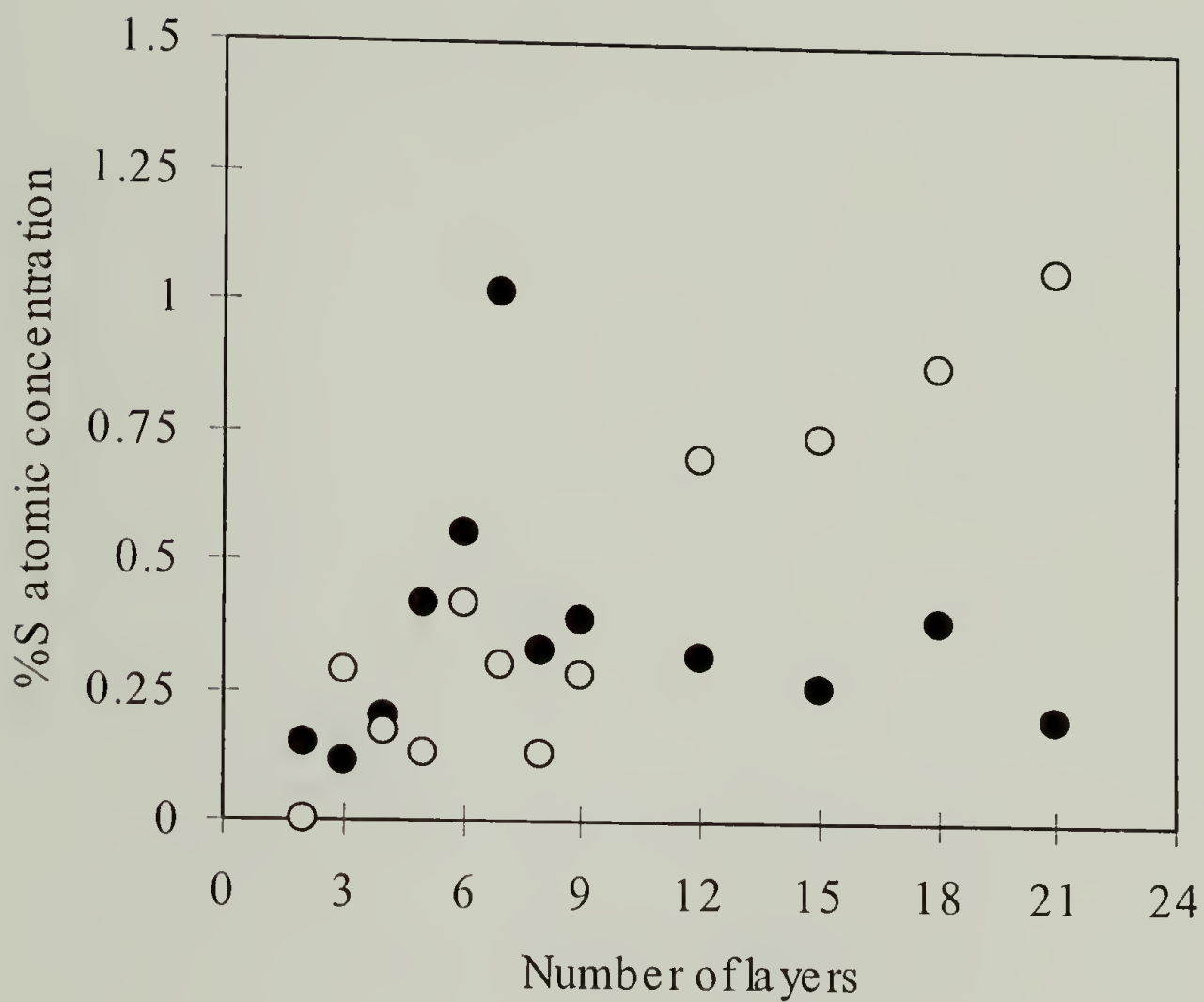


Figure 2.7. %S atomic concentration (XPS, 75° take-off angle) for single lap shear joint samples of polyelectrolyte multilayers (with added salt, manganese chloride) constructed on PET-COO⁻ after taken to adhesive failure. ●: lap shear joint originally with multilayers constructed on them, ○: lap shear joint originally with no multilayers on them.

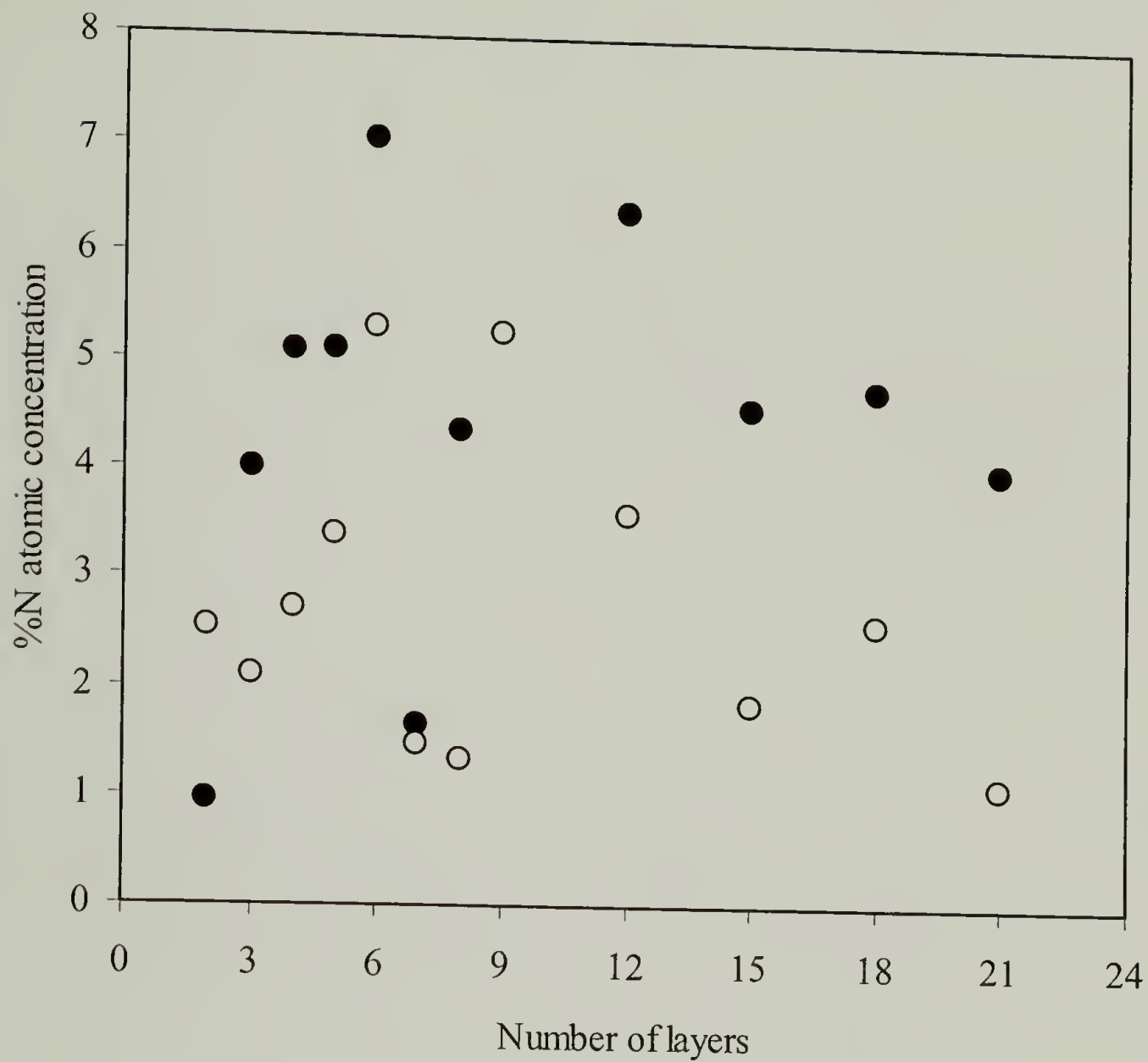


Figure 2.8. %N atomic concentration (XPS, 75° take-off angle) for PET-COO⁻-supported polyelectrolyte multilayers (added salt) single lap shear joint samples taken to adhesive failure. ●: single lap shear joints without polyelectrolyte multilayers constructed on them (zero side), ○:single lap shear joints with polyelectrolyte multilayers constructed on them (layer side).

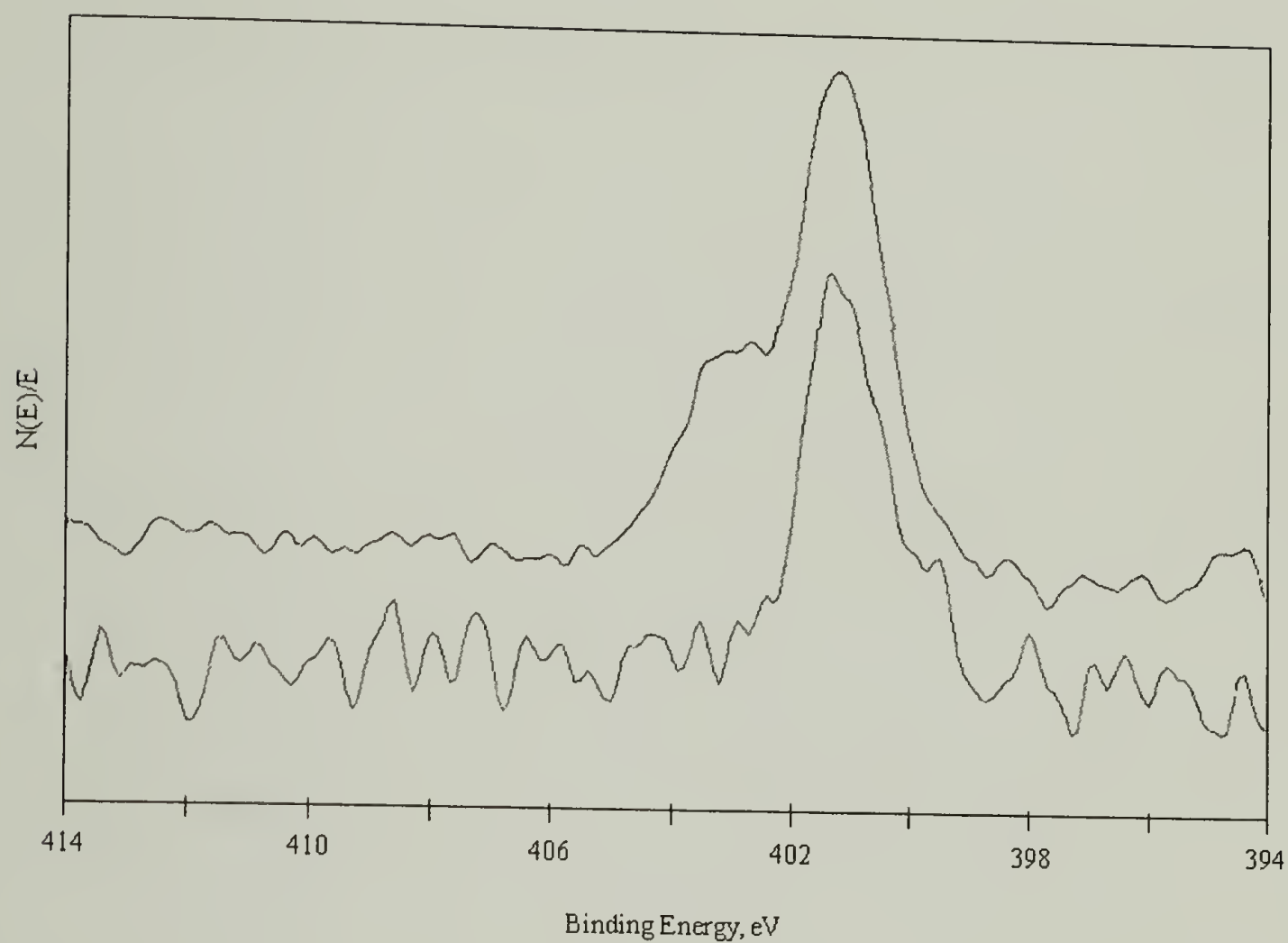


Figure 2.9. N_{1s} spectrum (XPS, 75° take-off angle) of 21 polyelectrolyte layers (with added salt) on PET-COO⁻ (top graph: zero side, bottom graph: layer side).

Conclusions

The adhesive joint strength of polyelectrolyte multilayers supported on unmodified and modified PET substrates using a commercial cyanoacrylate adhesive has been measured by a single lap shear joint test. Formation of the multilayers was monitored using XPS and dynamic contact angle measurements. Hydrolyzed PET single lap shear joint specimens showed the highest adhesive shear strength, which leads us to conclude that the hydrolysis of PET enhances the adhesion characteristics of PET towards cyanoacrylate adhesives. The polyelectrolyte multilayers are weak in strength, unlike the way we envisaged, and show decreasing adhesive shear strength upon increasing number of layers and increasing individual layer thickness using added salt. Using SEM and XPS, we see that the failure is complex, with the multilayers favorably transferred over to the non-multilayer side due to the permeation and interaction of the adhesive with the polyelectrolytes.

Future Work

For the layer-by-layer deposition to have any commercial significance, the technique should likely involve dynamic processes at high velocities. Since the process of constructing multilayers was carried out in near-quiescent conditions on the laboratory scale, there is the possibility that the multilayers could form differently when carried out under dynamic, non-equilibrium conditions. In many applications, the formation of an adsorbed layer is an important process step. For a layer to be efficiently adsorbed, the rate at which the layer forms is crucial. Also, the polymer layers are often exposed to shear

and collisions in highly dynamic situations during processing. Hence, the behavior of polymers at and near the interface under non-equilibrium conditions is an important field of study.¹⁴⁻²²

References

1. Werner, E., Janocha, S., Hopper, M.J., MacKenzie, K.J., *Encyclopedia of Polymer Science and Engineering*, John Wiley & Sons, New York, 1989.
2. Wang, J., Feng, D., Wang, H., Remhold, M., Fritz, T., *J. Appl. Polym. Sci.* **1993**, 50, 585.
3. Strobel, M., Lyons, C.S., Strobel, J.M., Kapaun, R.S., *J. Adhes. Sci. Technol.* **1992**, 6, 429.
4. Bertrand, P., DePuydt, Y., Beuken, J.M., Lutgen, P., Feyder, G., *Nucl. Instrum. Methods Phys. Res., Sect. B* **1987**, B19-20, 887.
5. Arenholz, E., Heitz, J., Wagner, M., Baeuerle, D., Hibst, H., Hagenmeyer, A., *Appl. Surf. Sci.* **1993**, 69, 16.
6. Yao, Z.P., Rånby, B., *J. Appl. Polym. Sci.* **1990**, 41, 1459.
7. Dave, J., Kumar, R., Srivastava, H.C., *J. Appl. Polym. Sci.* **1987**, 33, 455.
8. Avny, Y., Reubenfeld, L., *J. Appl. Polym. Sci.* **1986**, 32, 4009.
9. Bui, L.N., Thompson, M., McKeown, N.B., Romaschin, A.D., Kalman, P.G., *Analyst* **1993**, 118, 463.
10. Collin, R.J., U.S. Pat. 2,955,954, 1964.
11. Desai, N.P., Hubbell, J.A., *Macromolecules* **1992**, 25, 226.
12. Robinson, R.A., *CRC Handbook of Chemistry and Physics*, CRC Press, Boca Raton, 1986.
13. Chen, W., McCarthy, T.J. *Macromolecules* **1997**, 30, 78.
14. Keller, A., Odell, J.A. *Colloid Polymer Sci.* **1985**, 263, 181.

15. Besio, G. J., Prud'homme, R.K., Benziger, J.B. *Macromolecules* **1988**, 21, 1070.
16. Cohen, Y. *Macromolecules* **1988**, 21, 494.
17. Lee, J. J., Fuller, G.G. *Macromolecules* **1984**, 17, 375.
18. Atkinson, J., Goh, C.J., Phan-Tien, N. *J. Chem. Phys.* **1984**, 80, 6305.
19. Gramain, P., Myard, P. *Macromolecules* **1981**, 14, 180.
20. Bagassi, M., Chauveteau, G., Lecourtier, J., Englert, J., Tirrell, M. *Macromolecules* **1989**, 22, 262.
21. Chauveteau, G. *Adv. Chem. Series* **1986**, 213, 227.
22. Lee, J.-J., Fuller, G.G. *J. Colloid Interface Sci.* **1985**, 103, 569.

CHAPTER 3

INVESTIGATION OF FACTORS GOVERNING THE STRUCTURAL INTEGRITY OF PHOTOLITHOGRAPHIC POLYMERS

Photolithographic Materials

Radiation-curable materials succeeded commercially in the early 1970's although photopolymerization has been known for a century. At least one photographic technique was based on the photochemistry of naturally photosensitive materials using sunlight as the source of ultraviolet radiation.¹ Radiation curing is essentially polymerization induced by electromagnetic, beta (electron particles) or nuclear radiation. The source used in the printed circuit industry is almost exclusively high-intensity ultraviolet radiation. Energetic photons cause monomers to react with one another, typically through the action of a photoinitiator. Radiation is absorbed by the photoinitiator causing it to release polymerization-initiating species, such as free radicals. Some initiators rearrange to a high energy state and react directly with monomers. Once the initial reaction takes place, the reacted monomer remains active so it goes on to react with a second monomer. The process continues until most of the monomer is utilized or the active species are consumed or deactivated. Scheme 3.1 shows a simple reaction scheme for a free-radical photopolymerization. The most common UV-curable materials are the dielectric coatings. Dielectric coatings are electrical insulators that are printed or coated over conductors. This area is a natural for UV photochemistry since no opaque fillers need to be used, as is the case with conductive materials.



Scheme 3.1. Simple diagram representing a free-radical initiated photopolymerization process.

Polymers in Photolithography

A large number of commercial UV-curable materials are available. Acrylic groups are the most common reactive moieties in use today. Since acrylics tend to be brittle, this functionality is added to other polymers such as urethanes and epoxies. The products are referred to as acrylated epoxies or urethanes.

Limitations of the Polymeric Photosensitive Materials

UV-reactive polymer binders can produce rapid-cure, no-emission and high resolution, but there are many remaining limitations. The fact that polymerization is occurring on the substrate results in several ramifications. The resulting polymer properties are more variable compared to thermoplastics. The yield of polymerization is less than 100% because the mobility of reactive species is reduced as the polymerization proceeds and the matrix hardens. This means that several percent of unreacted monomer may remain to cause long-range problems. Almost all polymerization reactions cause a reduction in volume, which translates to stress. Thin substrates, like the polyester film

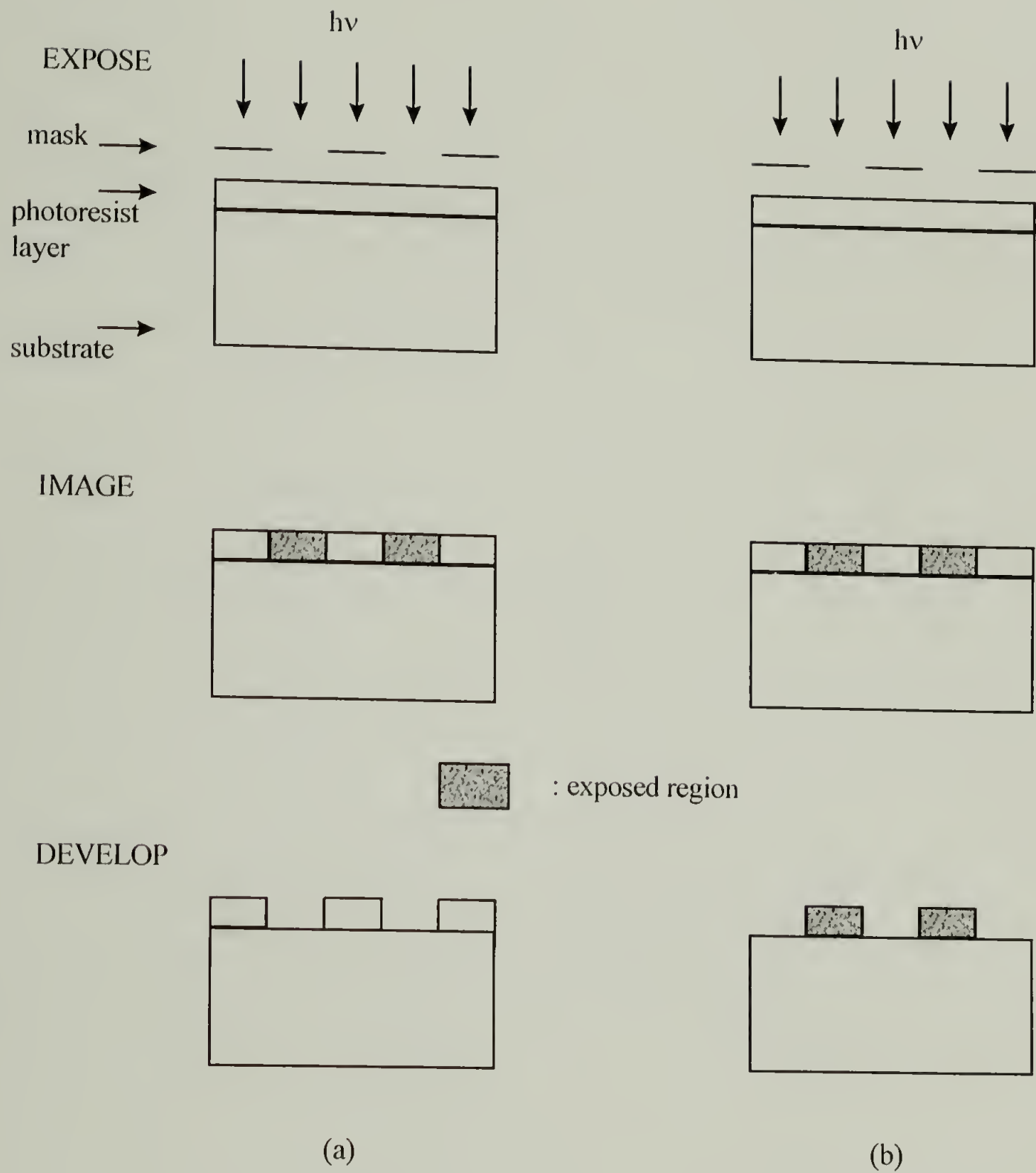
used in circuitry, will respond to the shrinkage by curling. Aside from these problems, UV binder systems are very popular in the electronic polymers arena. We can expect to see continuing progress in the area of radiation-cured materials because of the significant speed and pollution advantages.

Types of Photoresist Coatings

Photoresist coatings are widely used in the electronics industry to manufacture circuit boards and electronic chips. There are two main types of photoresist coatings that are used in industry today. Coatings are termed a positive resist when the exposed area of the film is more soluble than the unexposed. Alternatively, negative resist coatings are processed in the opposite way, where the exposed area is less soluble. The two types of resist coatings are illustrated in Scheme 3.2.² The purpose of these coatings ranges from defining the individual elements of integrated circuit devices to the protection of a given substrate from the harsh environmental conditions to which it may be exposed.

Requirements for Photoresist Polymer Coatings

To carry out these functions, a photoresist coating requires two main properties. First, it must be sensitive to energy (e.g. ultraviolet light) causing polymerization or degradation, allowing for specific patterns to be formed in the coating. Second, it must have the strength and stability to withstand the harsh processing and environmental surroundings to which it will be exposed, such as high and low temperatures, high humidity, and the presence of solvents.



Scheme 3.2. Two different types of photoresists. (a) represents a positive photoresist, and (b) represents a negative photoresist.

Photolithographic Polymers in Adhesive Applications

Polymeric films have had enormous utility in the electronics industry. One specific application is the use of UV and temperature cured polymeric systems that act as an adhesive layer between two different surfaces in a three-laminate system of inkjet printheads. These types of photolithographic polymer materials have been given much attention because of their differences in properties from conventional adhesives. One of their biggest advantages over conventional liquid-like adhesives is their structural integrity creating a solid/solid/solid adhesion that does not plug up the many small ink wells in the printhead cartridge. The purposes of this adhesive layer are (1) to act as a barrier layer for the inks, (2) to serve as an adhesive layer between the orifice layer and the printhead, and (3) to have structural integrity for processing. However, there are problems that arise from using this material. One of the biggest problems is that the polymeric material shows adhesive failure during use. We are interested in investigating the factors that cause this adhesive failure in the three-laminate system. Several approaches can be made in terms of what could be the major contributor in adhesive failure. Some factors include:

- (1) the role residual stress plays on the adhesive failure,
- (2) chemical interaction between the adhesive layer and the other two surfaces,
- (3) structural changes of the polymeric system due to UV and thermal treatment,
- (4) processing conditions of the polymeric system and its effect on its structural integrity,
- and
- (5) the effect of ink swelling on adhesion.

Our research attempts to cover most of these factors and investigates how each of these components affects the material integrity of the photolithographic polymer system.

Residual Stress in Coatings

In a coating, the driving force for failure is the presence of residual stress. When a material is subjected to changes in temperature, chemistry, or solvent used during processing, it is often accompanied by a corresponding dimensional change. If the material is constrained, as in the case of a coating, stress will occur. A photoresist used as a coating will exhibit the same behavior. If a sufficient amount of stress develops, mechanical failure in the form of cracking or delamination can result. The residual stress in a coating is not sufficient to completely characterize its mechanical performance. The mechanical limit of the material, or its strength must be known. Thickness also plays a significant role in the adhesion of these coatings. Stresses that build up during processing add to the energy stored in a coating. This critical energy depends upon the stress in the coating, the elastic constants of the coating, and the thickness. In addition, since the coating will be exposed to various environmental conditions, it is also important to understand how these types of properties will respond to temperature or chemistry changes during cure. Photoresist coatings are unique in that they undergo various processing steps that dramatically change the form of the material in specific regions, leaving the bulk of the coating unaffected. In the past, research on photoresist coatings has focused on the determination of optimum chemical conditions that achieve higher resolution patterns and adequate chemical resistance. With the increasing need for greater density on circuit boards, this line of research has been critical. However, it is equally

important to understand the mechanics of the materials as well. If a coating fails due to poor properties or excessive stresses, the resolution limits of the coating are irrelevant.

There are three experimental techniques available when measuring stresses in polymer coatings.

(1) beam bending, which measures strain or radius of curvature of the system and then correlates the stress by linear elastic assumptions,

(2) membrane deflection, which measures the displacement due to the applied force, and

(3) vibrational holographic interferometry, which measures the response of the material upon vibration.³⁻⁹ Of these techniques, beam bending requires the linear elastic constants of the material to be able to calculate the stress; thus, if the material is not linear elastic, the method provides an approximate value. Also, for a two-dimensional biaxial system, the Poisson's Ratio of the coating is required. The membrane deflection technique can only measure isotropic stresses.

Holographic interferometry is based on the classical theory of membrane vibrations. The governing equation is:

$$\sigma \nabla^2 u = \rho \frac{\partial^2 u}{\partial t^2} \quad (3.1)$$

where σ = biaxial stress in a membrane (N/m²),

u = out-of-plane displacement (m),

ρ = density of the membrane (kg/m²),

t = time (s), and

$$\nabla^2 = \text{Laplacian operator}, \frac{\partial^2}{\partial r^2} + \frac{1}{r} \frac{\partial}{\partial r} + \frac{1}{r^2} \frac{\partial^2}{\partial \theta^2}$$

By applying the boundary condition that the out-of-plane displacement is zero at the edges, $u(r=R) = 0$ (R is the outer radius of the membrane), then the solution for the membrane equation becomes

$$\sigma = 4\pi^2 \rho R^2 \left(\frac{f_{ni}}{Z_{ni}} \right)^2 \quad (3.2)$$

where R = radius of the sample (m),

f_{ni} = resonant frequency for the $(n,i)^{\text{th}}$ mode, and

Z_{ni} = i^{th} zero of the n^{th} order Bessel function.

Here, it can be seen that the only material property that is required is the density of the film. This is an advantage because no linear elastic assumptions are necessary and the elastic constants of the material are not required. Hence, we can measure stresses in films by finding the unique mode patterns, $(n,i)^{\text{th}}$ mode, and their respective frequencies (f_{ni}). The order of the Bessel function is determined from the vibration pattern observed at a specific frequency. Figure 3.1 shows typical patterns that are observed. The number of lines of symmetry in the vibrational pattern determines the order of the Bessel function. For example, the vibration of the zero order shows no nodal lines while vibration of the first order shows one nodal line, etc. The zero of integer order Bessel functions are tabulated in the literature.¹⁰⁻¹² Besides its ability to measure stresses in coatings, the vibrational holographic interferometry can also be employed to determine

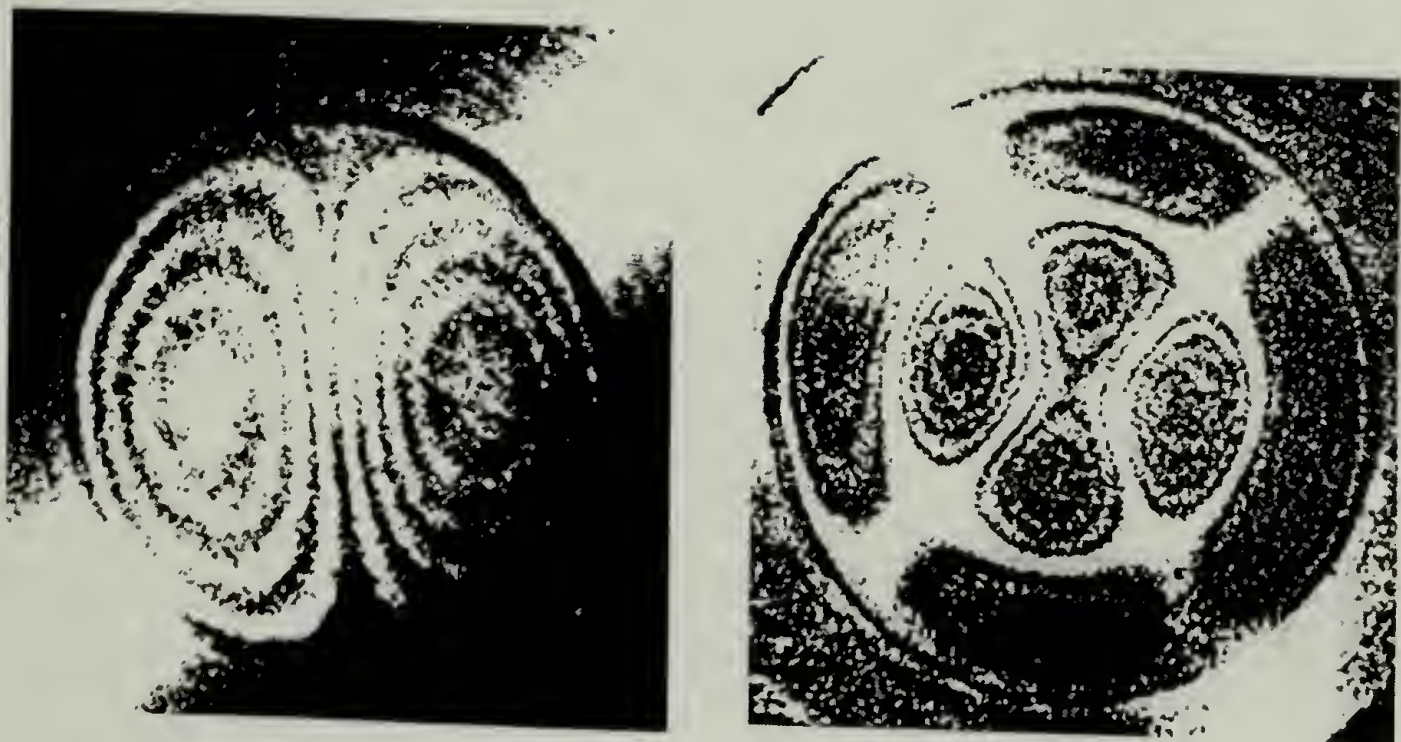


Figure 3.1. Typical holographic patterns observed for constructed membranes. The above sample is a pre-stretched polymer latex sample. Left: (1,1) vibration mode, right: (2,2) vibration mode.

the principal directions and principal stresses in an anisotropic material. Also, by coupling it with other techniques, the orthotropic elasticity coefficients can be fully characterized, and the transport coefficients (thermal and mass diffusion coefficients) can be determined, as well.^{3,4,6,7,9,13} Although it is important to investigate swelling coefficients, the primary mechanical influence of swelling of coatings is the changes in the state of stress that occur on exposure when the material is constrained and not necessarily dimensional changes associated with free swelling. These methods can also be used to determine the orthotropic axis for materials, which can play an important role when materials are analyzed, especially if they are cross-laminated. Using these methods, the state of stress as a function of temperature and environment can be determined for flat coatings, away from the edges or free surfaces normal to the coating plane.

Swelling Stresses and Diffusion of Small Molecules in Polymers

Mass transport properties are another area of interest. The diffusion of small molecules through photolithographic materials is of interest in certain systems where the photolithographic coating is in near contact with certain solvent systems.

Diffusion is the movement of one material, such as a gas or a liquid, in the body of another material. Generally, diffusion behavior depends upon both the characteristics of the polymer (i.e., glass transition temperature, molecular structure, water affinity, etc.) and the characteristics of the penetrant (i.e., molecular size and shape, solubility, etc.).¹⁴ For a planar sheet, the direction of diffusion is usually normal to the plane of polymer film. The general case of one-dimensional diffusion in materials is usually governed by Fick's law as mathematically described in equation 3.3:

$$\frac{\partial C}{\partial t} = D_{eff} \frac{\partial^2 C}{\partial X^2} \quad (3.3)$$

where C = concentration of the penetrant,

t = time,

X = distance in the direction of the diffusion, and

D_{eff} = effective diffusion coefficient.

Applying the following initial and boundary conditions to equation 3.3:

I.C. $C(x,0) = 0$

B.C. $C(0,t) = C_{eq}$

where C_{eq} = equilibrium concentration and

h = film thickness

yields the solution expressed in equation 3.4^{15,16}

$$\frac{M_t}{M_\infty} = 1 - \frac{8}{\pi^2} \sum_{n=0}^{\infty} \frac{1}{(2n+1)^2} \exp\left\{-\frac{D(2n+1)^2 \pi^2 t}{h^2}\right\} \quad (3.4)$$

where M_t , M_∞ = mass uptake at time t and equilibrium, respectively.

The diffusion coefficient can be determined from the plot between M_t/M_∞ vs $t^{1/2}$ which is known as the sorption curve.¹⁷ In some cases, D_{eff} can be calculated from the “reduced” sorption curve which is the plot between M_t/M_∞ vs. $t^{1/2}/h$ as well.

According to the “sorption” curve (unless otherwise specified), the classical Fickian diffusion behavior can be characterized by the following measures¹⁷:

- (1) Both absorption and desorption curves are linear up to $M_t/M_\infty < 0.6$. This means that the mass uptake is proportional to the square root of time.
- (2) Beyond the linear region, both absorption and desorption curves are concave to the abscissa axis and should be identical when superimposed.
- (3) At fixed initial and final concentration, a superimposed single curve is obtained if each absorption (and desorption) curve for films of different thicknesses is re-plotted in the form of a reduced curve.

Note that for criterion (3), films of at least two different thicknesses need to be measured, which may not be practical. Therefore, in these experiments the diffusion behavior is considered as Fickian if criteria (1) and (2) are valid.

However, not every polymer follows Fickian diffusion. Some factors have to be taken into account such as the glass transition temperature (T_g) of the material. According to Alfrey *et al.*'s work¹⁸, at a temperature far above T_g , the diffusion behavior is Fickian. In this region, polymers are soft and rubbery; hence, the motion of polymer chains responds rapidly to the presence of the penetrant. In other words, the relaxation rate is much greater than the diffusion rate. In contrast, "non-Fickian" behavior is observed at temperatures below T_g in which the polymers are hard and glassy. In this case, the motion of polymer chains is not rapid enough to completely homogenize the penetrant; in other words, the rate of diffusion is very fast compared to that of relaxation. In addition, in the vicinity of T_g (10~15°C above T_g) in which the diffusion and relaxation processes are comparable, the diffusion becomes anomalous or "non-Fickian".^{19,20} Examples of "non-Fickian" behavior can be found in the sorption of water by cellulose, keratin, and vinyl acetate.²¹⁻²³

Alfrey, Gurnee, and Lloyd¹⁸ have proposed a simple case for anomalous diffusion so called "case II diffusion" which can be described as follows:

- (1) In contrast to Fickian diffusion, at a temperature well below T_g , a linear relationship exists between the initial mass uptake and time.
- (2) Case II diffusion is associated with swelling behavior in which a sharp boundary separates an outer, swollen, rubbery shell of uniform concentration from an inner glassy core of zero penetrant concentration.

- (3) The swelling front moves through the material at a constant velocity.
- (4) The diffusion rate is very fast compared with the relaxation rate. On the other hand, the diffusion process of Fickian behavior is much slower than the relaxation process.

As mentioned above, from the plot between M_t/M_∞ vs $t^{1/2}$, the diffusion coefficient can be calculated by the initial slope method²⁴ and half-time¹⁵ method as follows:

- (1) initial slope method

$$D_{eff} = \pi \left[\frac{(slope)h}{4} \right]^2 \quad (3.5)$$

- (2) half-time method

$$D_{eff} = \frac{0.0492h^2}{t_{1/2}} \quad (3.6)$$

where $t_{1/2}$ is defined as the time where $M_t/M_\infty=1/2$.

In addition, the diffusion coefficient can also be calculated from the plot between $\log(1 - M_t/M_\infty)$ vs. time by the limiting slope method and the moment method²⁵ as follows:

- (3) limiting slope method

$$D_{eff} = -(slope) \left[\frac{4h}{\pi} \right]^2 \quad (3.7)$$

- (4) moment method

$$D_{eff} = \frac{h^2}{12 \left[\int_0^\infty \left(1 - \frac{M_t}{M_\infty} \right) dt \right]} \quad (3.8)$$

Basically, the diffusion coefficient can be determined by monitoring the mass uptake as a function of time using a conventional gravimetric method such as a Cahn electrobalance. However, it is a very time consuming and tedious method. On the other hand, by applying one-dimensional hygrothermal elasticity theory²⁶, the changes in stress or strain with time at specific relative humidities can be correlated to the mass uptake as shown in equation 3.9.

$$\frac{M_t}{M_\infty} = \frac{\Delta \bar{C}(t)}{\Delta \bar{C}(\infty)} = \left| \frac{\Delta \bar{\sigma}_{xx}(t)}{\Delta \bar{\sigma}_{xx}(\infty)} \right|_e = \left| \frac{\Delta \bar{\epsilon}_{xx}(t)}{\Delta \bar{\epsilon}_{xx}(\infty)} \right|_\sigma \quad (3.9)$$

As a result, the experiments designed to measure stress or strain as a function of time can be employed to determine the diffusion coefficient as well. For example, Sackinger²⁷ developed the force-strain technique to measure swelling stress and swelling strain and then related all these properties to mass uptake. We have developed an Environmental Tensile Tester (ETT) that allows us to measure the swelling stress of polymer films exposed to various types of liquids. The diffusion coefficient can then be determined from the plot between normalized swelling stress (σ_t/σ_∞) vs $t^{1/2}$.

Objective

Our goal is to study two different types of photolithographic polymers used in the fabrication of inkjet printheads that require certain properties desired to be used in the

environment that they experience. Such factors as processing conditions in constructing the printhead assembly include pressure, temperature, and ink exposure are of interest. Moreover, the properties of these photolithographic polymer systems and their residual stress behavior, as well as their swelling and diffusion behavior upon different processing conditions (temperature, pressure, ink exposure, etc.) will be of major interest.

Experimental

Materials. The materials used for this research are quite extensive. The major component of the research will focus on photo-imagable polymer systems.

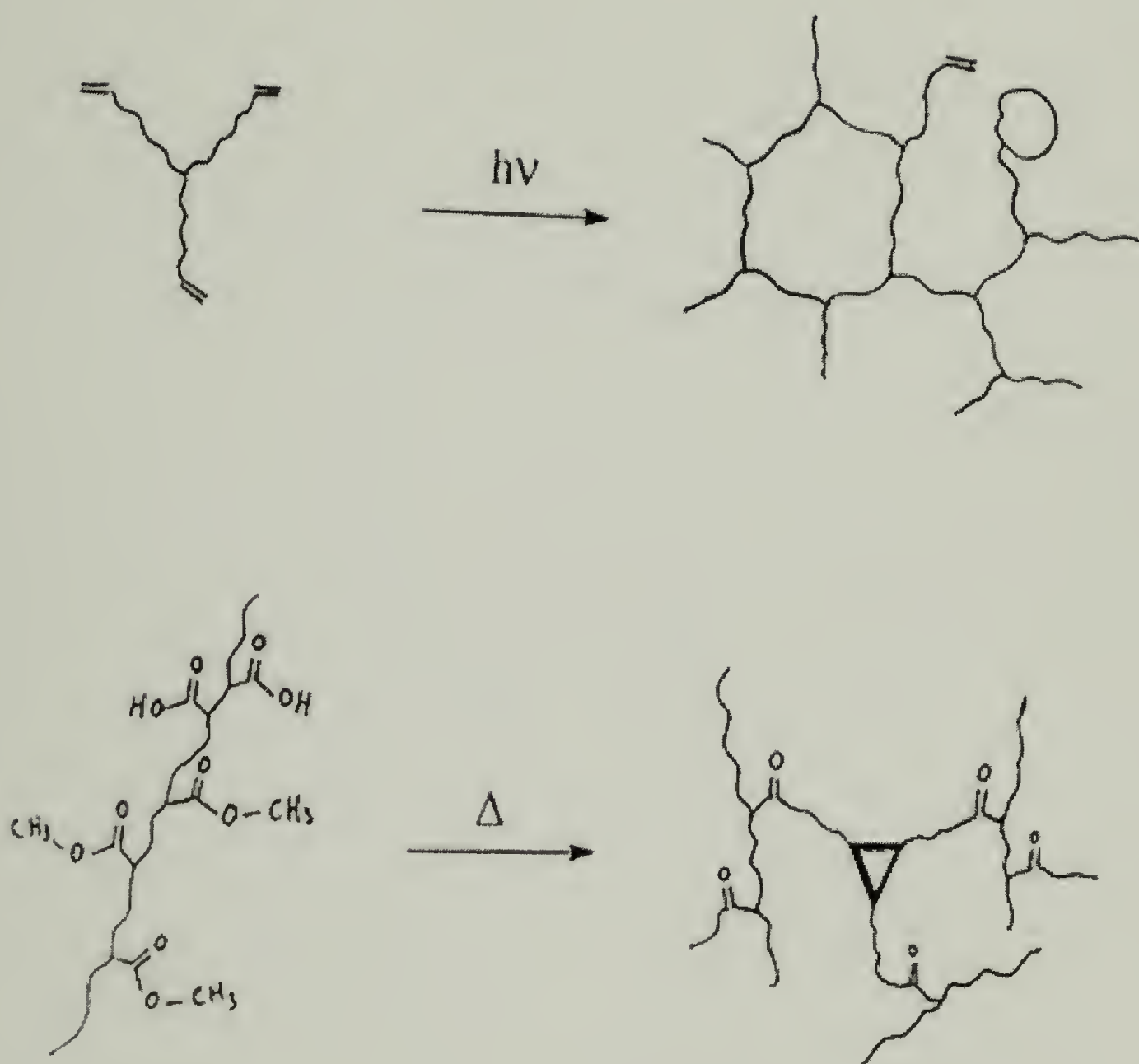
The PUA system, an acrylate-based photoresist, undergoes photopolymerization upon UV exposure. The materials usually consist of a thermoplastic binder, a multi-functional acrylate monomer capable of addition polymerization, and an addition polymerization initiator activatable by UV radiation. Upon UV radiation, the photoinitiator is activated to initiate radical crosslinking polymerization among the C=C double bonds on the multi-functional acrylate monomers. By tailor-making the photopolymerizable acrylate monomers and thermoplastic binder, one can incorporate functional groups that undergo a condensation reaction initiated by elevated temperature either with the photocrosslinked monomer, or between the crosslinked monomer and the thermoplastic binder. A poly(urethane acrylate) system which includes a multi-functional acrylate system along with a copolymer binder which contains acrylic acid functional groups, a ketone-based photoinitiator, a thermally activated poly-melamine crosslinking agent, and an inorganic filler for improved physical and mechanical properties had been

studied in the group previously²⁸. The schematic of the radical and condensation crosslinking reactions of this type of system is shown in Scheme 3.3.

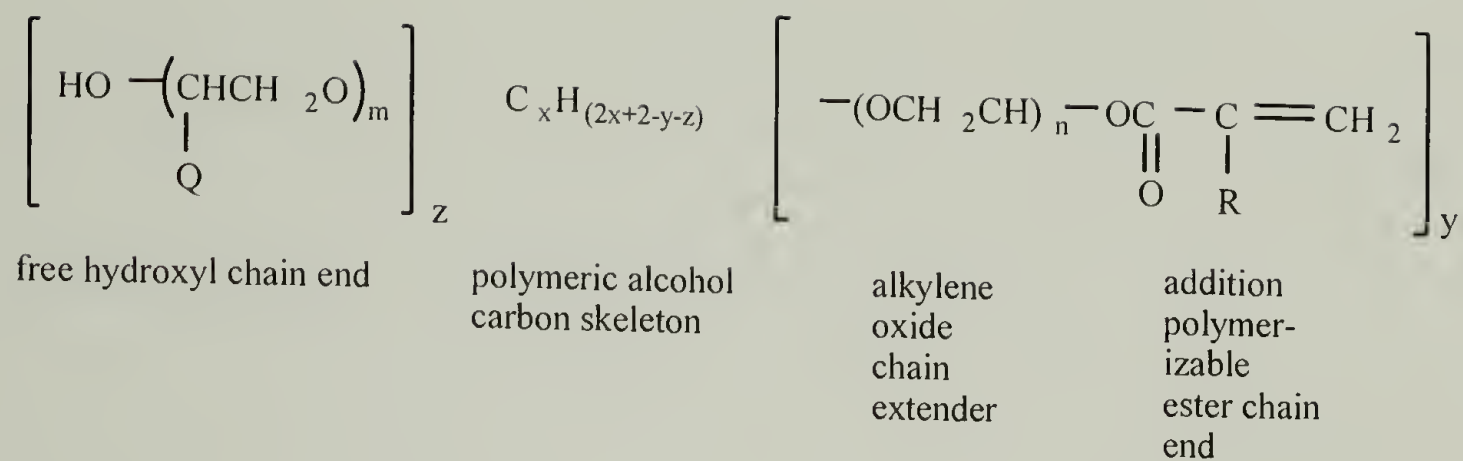
The macromonomer used for this type of poly(urethane acrylate system) is shown in Scheme 3.4.²⁹ This polymer precursor will be abbreviated as PUA (poly(urethane acrylate)). It's monomeric form has no mechanical integrity as a film, and is sandwiched between two different types of "back films" (one linear density polyethylene (LDPE)-based, and the other poly(ethylene terephthalate) (PET)-based). The PUA system, which is a light-blue sticky polymer precursor powder before processing, only shows film properties after a considerable amount of processing either by photo- or thermal crosslinking. Attachment to silicon wafers is achieved by rolling the sandwiched PUA film onto the wafer after peeling off the LDPE back film. After certain processing steps, the PET back film is peeled off, and the PUA film is attached to the wafer. Further processing is done to improve the mechanical integrity of the PUA film. After processing, the average thickness of the PUA film is 25 microns. Processing conditions for the PUA system are shown in Table 3.1.

The HRP system is a class of poly(amic acid) methacrylate esters, These were the first class of patternable organic polyimide precursors. These polymer precursors are synthesized by the addition of hydroxyethylmethacrylate to aromatic acid dianhydride, and its polycondensation of the tetracarboxylic acid diester with aromatic diamines. The polyimide conversion goes through two steps:

1. Photo-crosslinking during UV-radiation, yielding intermediates with high solubility differences between the exposed and non-exposed regions.
2. Thermal conversion of the intermediate into a polyimide.



Scheme 3.3. Processing of the poly(urethane acrylate) (PUA) system. The first step involves a photocrosslinking of the multi-arm structure of the PUA macromonomer. The second step is a thermal condensation reaction with the photocrosslinked PUA macromonomer and a polymer binder which contains acrylic acid functional groups.



where:

Q: H, CH₃, or C₂H₅ R: H, CH₃

x: 3, 4, 5, or 6, being equal or greater than y+z

y: 2, 3, 4, 5, or 6

z: 0, 1, 2, or 3, and y+z is greater than 2

m: 0, 1 and more, n: 1 and more

Scheme 3.4. Chemical compositions of the poly(urethane acrylate) (PUA) macromonomer.

Table 3.1. Processing conditions for the poly(urethane acrylate) (PUA) and the poly(amic acid) methacrylic ester (HRP) films

	PUA system	HRP system
Attachment to wafer	Laminate at 70°C	Spin coat 600 rpm for 35 seconds (x2)
Soft bake	none	60°C (5 min.)/80°C (2 min.)
Align-expose	20-40 mJ*	800mJ/cm ² at 365 nm (1 minute)*
Post-expose bake	125°C for 1 min.	125°C for 30 sec.
Develop	NMP/DEG (10°C, 1 min.)-rinse (DI)	NMP (60 sec.)-IPA (20 sec.)
UV cure	1.75 J/cm ² at 50°C*	none
Hard bake	220°C, 150 psi, 30 min.	260°C for 30 min.

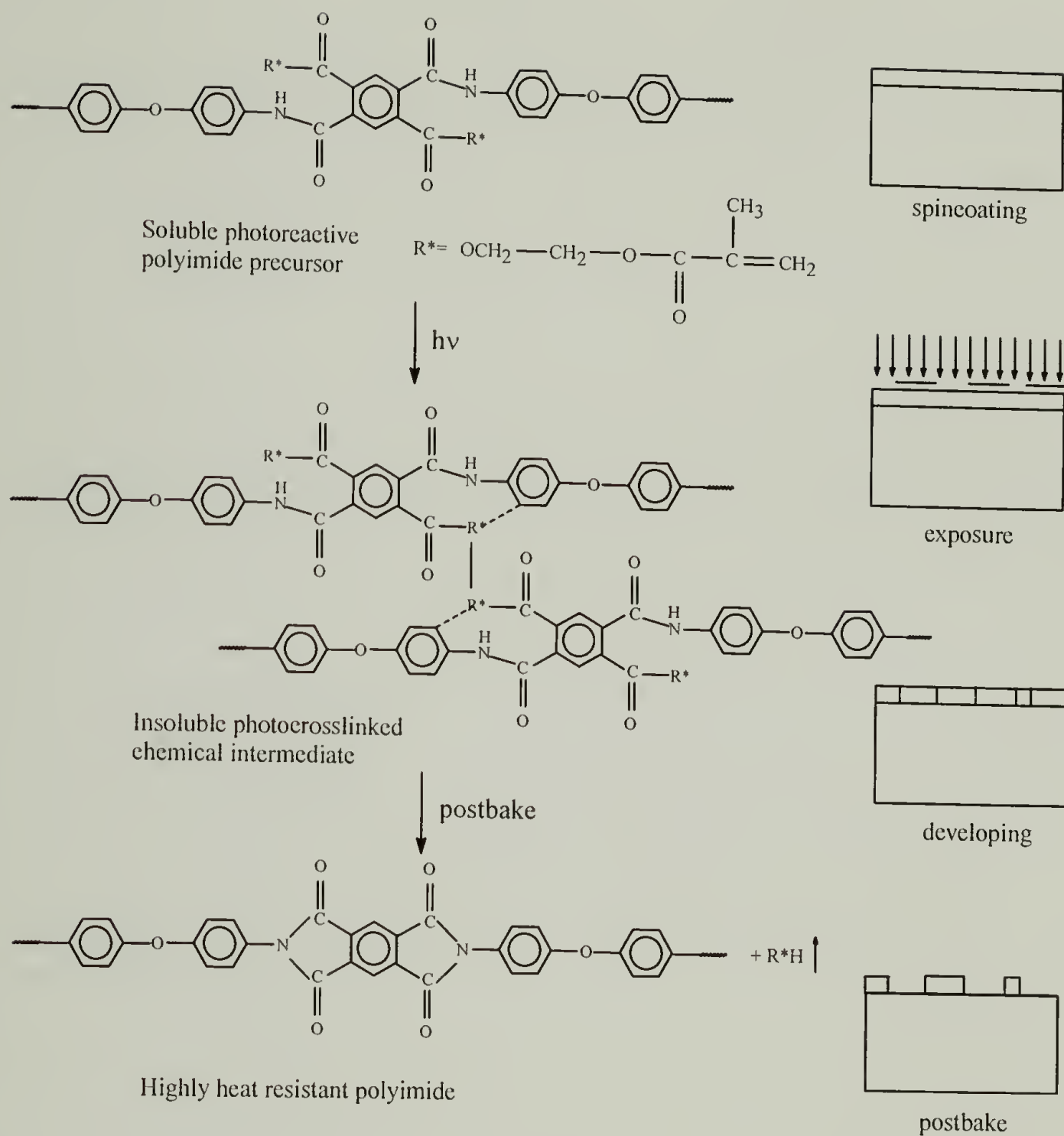
*: Either done in-house (dual mirror deep-UV lightsource, OAI) or received.

This process is shown schematically in Scheme 3.5.³ The poly(amic acid) methacrylate ester used in this research is a viscous liquid (20 wt%) in N-methyl pyrrolidinone (NMP). This polymer precursor will be abbreviated as HRP (high-resolution polyimide). Attachment to silicon wafers is achieved by spin-coating the material onto the wafer. Further processing steps follow to give the HRP its mechanical integrity. After processing, the average thickness of the HRP film is 14 microns.

Processing steps for the HRP film is shown in Table 3.1.

For both PUA and HRP systems, processing conditions were varied to investigate the effect processing has on the thermomechanical performance of the two films.

Thermomechanical Studies In addition to using methods to directly investigate phase behavior, several standard characterization methods were used to study the



Scheme 3.5. Chemical composition of the poly(amic acid) methacrylic ester (HRP) and its photoresist processing.

materials as a function of process history and ink exposure. These methods include Thermo-Gravimetric Analysis (TGA), Differential Scanning Calorimetry (DSC), Dynamic Mechanical Thermal Analysis (DMTA), Thermo-Mechanical Analysis (TMA), and mechanical properties measurements using an Instron tensile tester. We also attempted to determine if the observed phase morphology is highly dependent upon processing conditions and how these observations relate to characteristics of the systems performance.

TGA Studies. Thermal degradation and weight loss studies were carried out using a DuPont Thermogravimetric Analyzer (TGA 2950) for both the PUA and the HRP films at different processing steps. The films were freeze-milled using a SPEX 6700 freezer mill under liquid nitrogen to obtain the films in powder form. All experiments were carried out under a nitrogen purge, and the ramp rate was at 10°C/min.

Differential Scanning Calorimetry (DSC). Thermal characterization was done using a DuPont Differential Scanning Calorimeter (DSC2910) for the PUA and HRP films obtained at different processing steps. The films were freeze-milled using a SPEX 6700 freezer mill under liquid nitrogen to reduce the films in powder form. All experiments were carried out under a nitrogen purge, and the ramp rate was at 10°C/min.

Dynamic Mechanical Thermal Analysis (DMTA). DMTA measurements were done using a Rheometric Scientific MkIV for the PUA and HRP films obtained at

different processing steps. The films were cut into strips (W 5 mm x L 25 mm) and were tested at 1 Hz, 5°C/min. at 0.1% strain under a nitrogen purge.

Thermo-Mechanical Analysis (TMA). Thermal expansion studies were carried out using a DuPont ThermoMechanical Analyzer (TMA 2940) for the PUA and HRP films obtained at different processing steps. Samples were cut into strips 5 mm wide with a length that was approximately 13 mm. A small force of 0.001 N was applied, and all experiments were run at 10°C/min. under a nitrogen purge. Typically the test involved two heat/cool cycles.

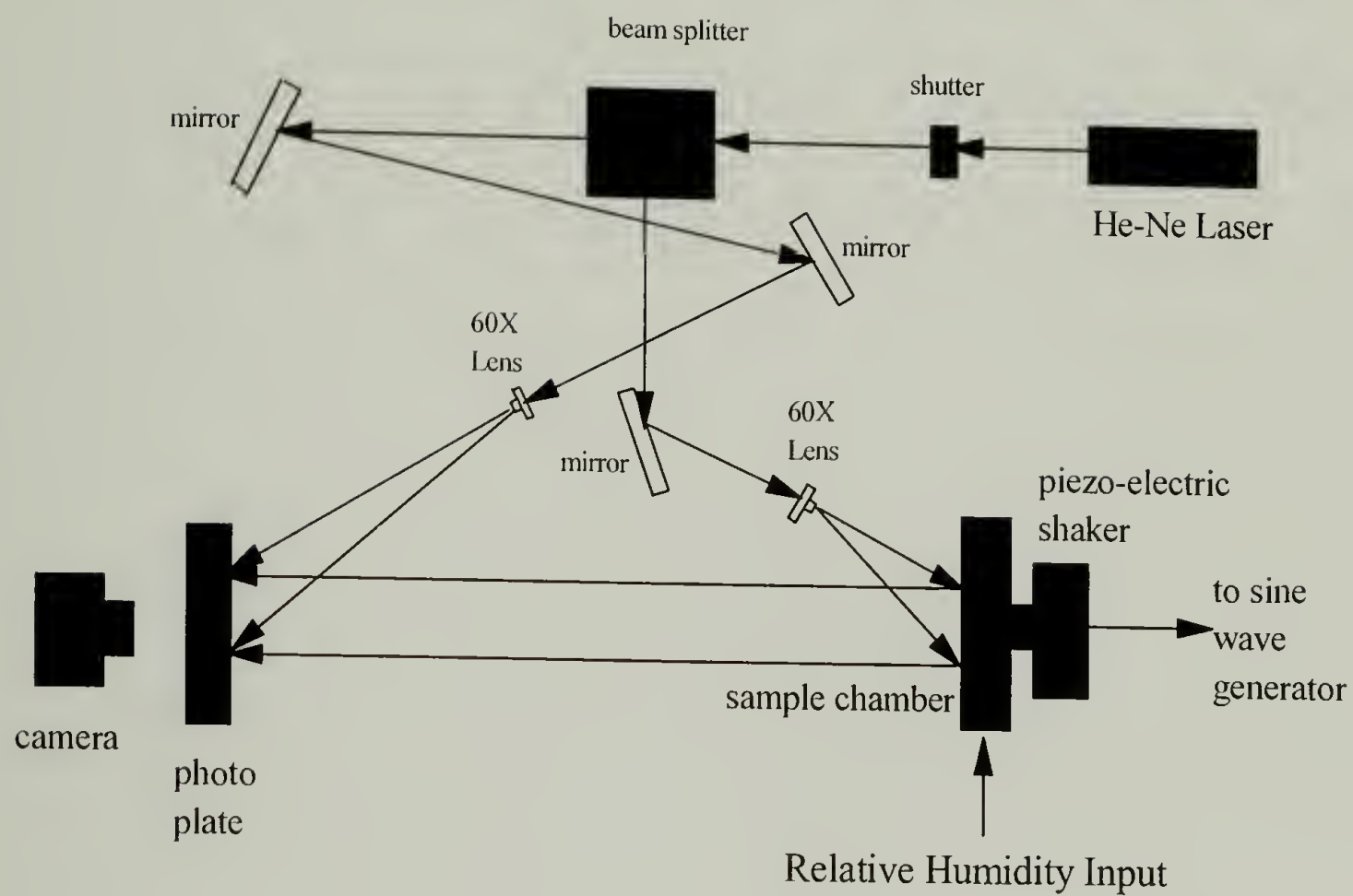
Mechanical Properties. Mechanical properties were measured for the PUA and HRP films obtained at different processing steps using an Instron tensile tester. Samples were cut up into 5 mm x 65 mm rectangular strips and then glued with an instant adhesive to manila paper tabs which ensured a specimen length of exactly 50 mm. A strain rate of 5 mm/min was used. At least 5 samples were tested for each set of materials.

Phase Structure. Microstructural changes were monitored using a JEOL 100 CX Transmission Electron Microscope (TEM) operated at 100kV accelerating voltage for the PUA and HRP film samples obtained at different processing steps. All samples were microtomed in a Reichert-Jung cryo-ultramicrotome. Sections approximately 300~800 Å were cut with a Diatome diamond knife at a sample temperature of -110 °C and a knife temperature of -90 °C. The sections were stained in osmium tetroxide (OsO₄)

or ruthenium oxide (RuO_4) vapors for approximately 2 hours, which selectively stains double bonds.

Residual Stress Measurements. The residual stress state for the materials in question was investigated as a function of process history. The methods to investigate the state of stress, developed over the years, include time-averaged vibrational holographic interferometry shown in Scheme 3.6.³ The holographic samples were made by detaching the processed films (both PUA and HRP) from the silicon wafer at different stages of processing. Once the films went through their desired state during the processing step, a rigid steel washer (ID 4.1 cm) was attached to the assembly using an industrial grade cyanoacrylate adhesive. The whole assembly was immersed into a water bath (80°C) for a prolonged period of time (usually 8 hours or less), resulting in the film detaching itself from the wafer, but it remained bonded to the steel washer. This ensured that we still have conserved the residual strain within the coating while processed on the wafer. The membrane sample is then let to air-dry for at least 24 hours before characterization.

The holographic equipment is a typical two-beam holographic interferometry. The coherent light source is a 5 mW He-Ne laser (wavelength = 632.8 nm). The laser beam is split into two beams by a variable beam splitter as the reference beam and the object beam. The variable beam splitter can be adjusted for different intensity ratios of the two split beams. The two beams are superimposed on a thermoplastic holographic plate. It is used to record the interference patterns of the two beams as a hologram. The thermoplastic plate can be developed in-situ by electronic charging of a holographic

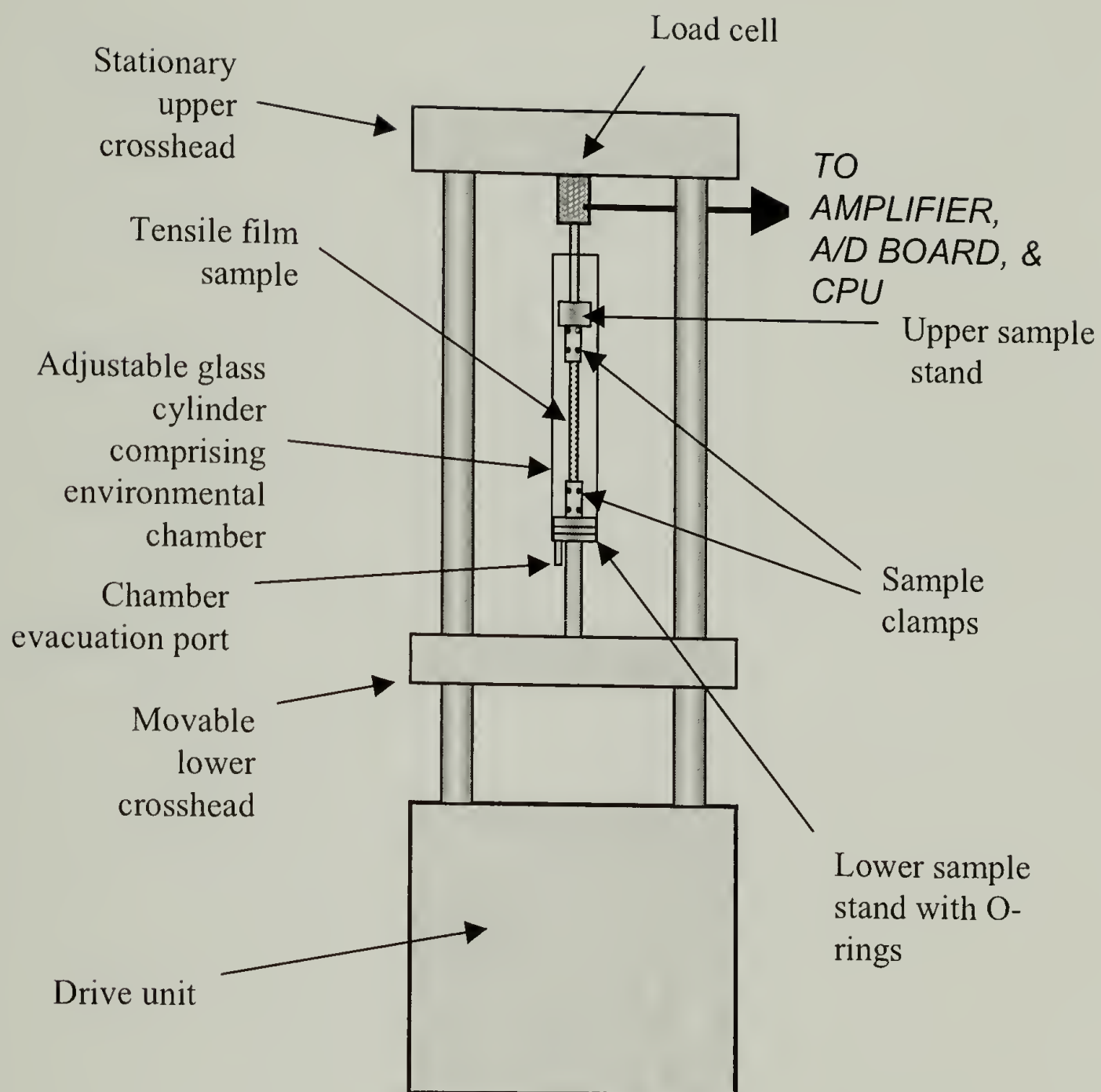


Scheme 3.6. Schematic set-up for the holographic interferometry.

camera (Newport Research Corporation, HC301). All results were performed under reduced pressure conditions (<20 torr).

The film sample on a constraining steel washer is rigidly mounted inside a vacuum chamber. The entire chamber is connected to a piezoelectric shaker (Wilcoxon Research), driven by a frequency generator (Wavetek, Model 190). The frequency generator produces sinusoidal vibration with various frequencies and adjustable amplitudes. A hologram is taken on the thermoplastic holographic plate as the static image of the sample. The sample is then excited by the piezoelectric shaker. The excited image of the vibrating sample is superimposed on the hologram recorded on the thermoplastic plate. Once the driving frequencies coincide with one of the natural frequencies of the sample, the vibration amplitude reaches its maximum and a characteristic interference pattern appears. The interference pattern can be viewed by a TV monitor through a CCD video camera set up behind the thermoplastic plate. The resonant frequency is read off a digital frequency counter (Bruel & Kjaer Precision, 180). The frequencies recorded can be inserted into equation 3.2 to calculate the residual stress in a given sample. Density measurements needed for this residual stress analysis were performed by cutting a film sample of known volume and weighing the sample.

Swelling Stress and Stress Relaxation Behavior upon Ink Exposure. The use of custom equipment in conjunction with tensile testing equipment for swelling investigations is shown in Scheme 3.7. Named the environmental tensile tester (ETT), the instrument allows us to monitor the swelling stress and stress relaxation behavior of samples submerged in a liquid environment. The experimental procedure for stress



Scheme 3.7. Schematic set-up of the environmental tensile tester (ETT).

relaxation behavior is similar to that of measuring mechanical properties. Both PUA and HRP samples taken at different processing steps were cut up into 5 mm x 65 mm rectangular strips and then glued with an instant adhesive to aluminum tabs which ensured a specimen length of exactly 50 mm. The motor driving the movable crosshead was stopped at a given elongation before the sample broke. The samples were left under constant strain until the film fully relaxed. The ink formulation of interest was then introduced to the sample by pouring it into the glass cylinder surrounding the sample. The relaxation behavior of the film versus time was measured. This later relaxation is due to ink swelling. Ink pen type WB60, which contains about 60% water, was received from Hewlett-Packard, and was used in the experiments. The ink (without the dye) consists of a high percentage of water, and other components such as surfactant, polar solvent, and certain diols. The pH values of the inks vary over a wide range, from acidic to basic.

Results and Discussions

TGA Results. Figure 3.2 shows the thermal degradation behavior of the PUA films obtained at different processing steps. As can be seen, the processing alters the thermal behavior of the film. Upon UV cure, we see that the transition at ~200 °C that is prominent in the non-UV cured, non-thermally cured PUA macromonomer is greatly depressed. This suggests that the transition at ~200 °C is not thermal degradation of the PUA sample, but is related to the crosslinking mechanism that the PUA undergoes upon

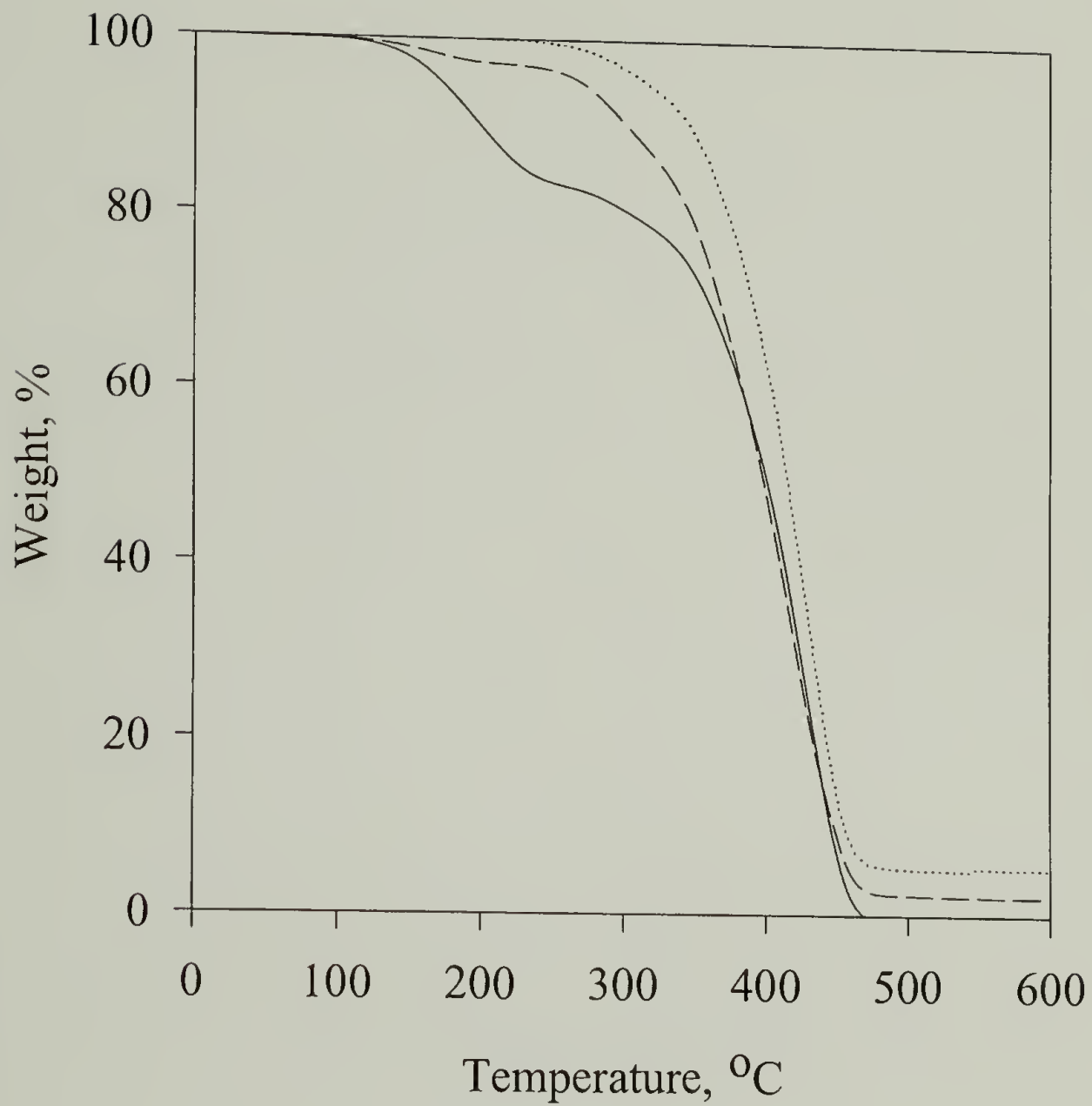


Figure 3.2. TGA thermograms of poly(urethane acrylate) (PUA) films obtained under different processing conditions. Solid line: non-UV, non-thermally cured PUA macromonomer, large dotted line: PUA film UV cured at 5.0 J/cm², small dotted line: PUA film thermally cured at 220 °C for 30 min.

curing. The thermally cured PUA film (at 220 °C for 30 min.) shows even less of a transition at these lower temperatures (up to 300 °C), which suggests that there are fewer reaction sites for crosslinking after the thermal curing step is performed, and ultimately shows little to no transition related to crosslinking at these lower temperatures.

Degradation starts to occur for these PUA samples above ~300 °C.

We also observe upon processing the PUA film that additional crosslinking enhances the thermal stability of the PUA film. This behavior is obvious by analyzing the remaining residuals after heating to 600 °C. The percent residuals for the varying PUA films are 0, 2, and 5% for the PUA macromonomer, UV cured PUA film, and the thermally cured PUA film, respectively.

Figure 3.3 shows TGA thermograms of PUA films obtained under different UV cure conditions. Although there is a considerable difference between non-UV cured and UV cured, there is not a discernable difference between different UV cured PUA films. Minimal, or no, enhancement in thermal stability is achieved by higher UV curing conditions.

Similar results for the HRP film were obtained. The amount of polymer precursor in solution (20 wt% HRP in NMP) is verified with the TGA thermogram of the solution shown in Figure 3.4. Figure 3.5 compares HRP films thermally cured at different temperatures. Transitions up to 500 °C that are not apparent in the TGA thermogram for the HRP film cured at 260 °C suggest that the transitions at the temperatures below 500 °C are related to transitions that take place for the poly(amic acid) methacrylic ester by first crosslinking to form the intermediate insoluble network for photoresist development, and finally at high curing temperatures, breaking the bond to imidize into a polyimide.

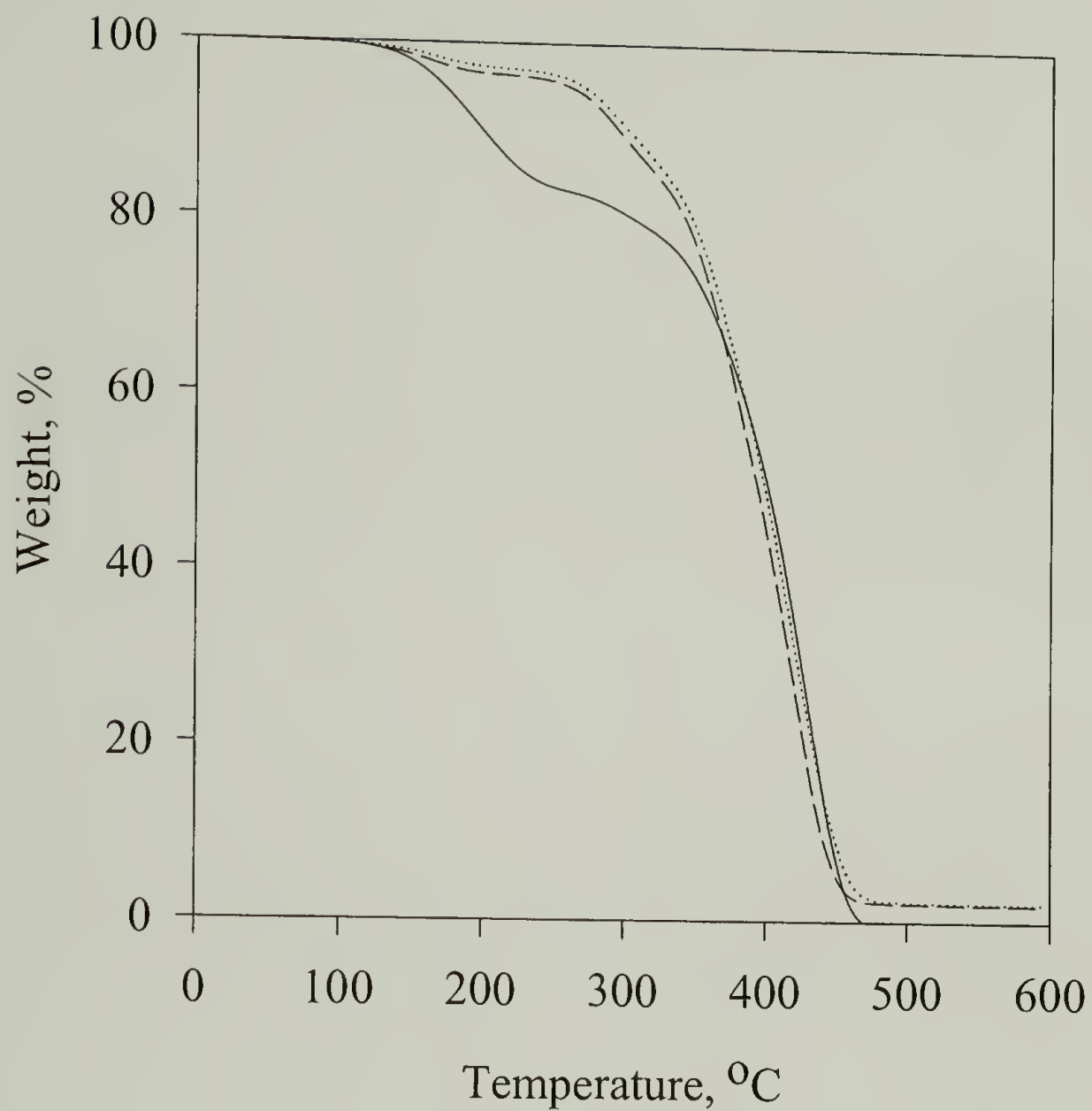


Figure 3.3. TGA thermograms of poly(urethane acrylate) (PUA) films obtained under different UV curing conditions. Solid line: non-UV, non-thermally cured PUA macromonomer, large dotted line: PUA film UV cured at 1.5 J/cm², small dotted line: PUA film UV cured at 5.0 J/cm².

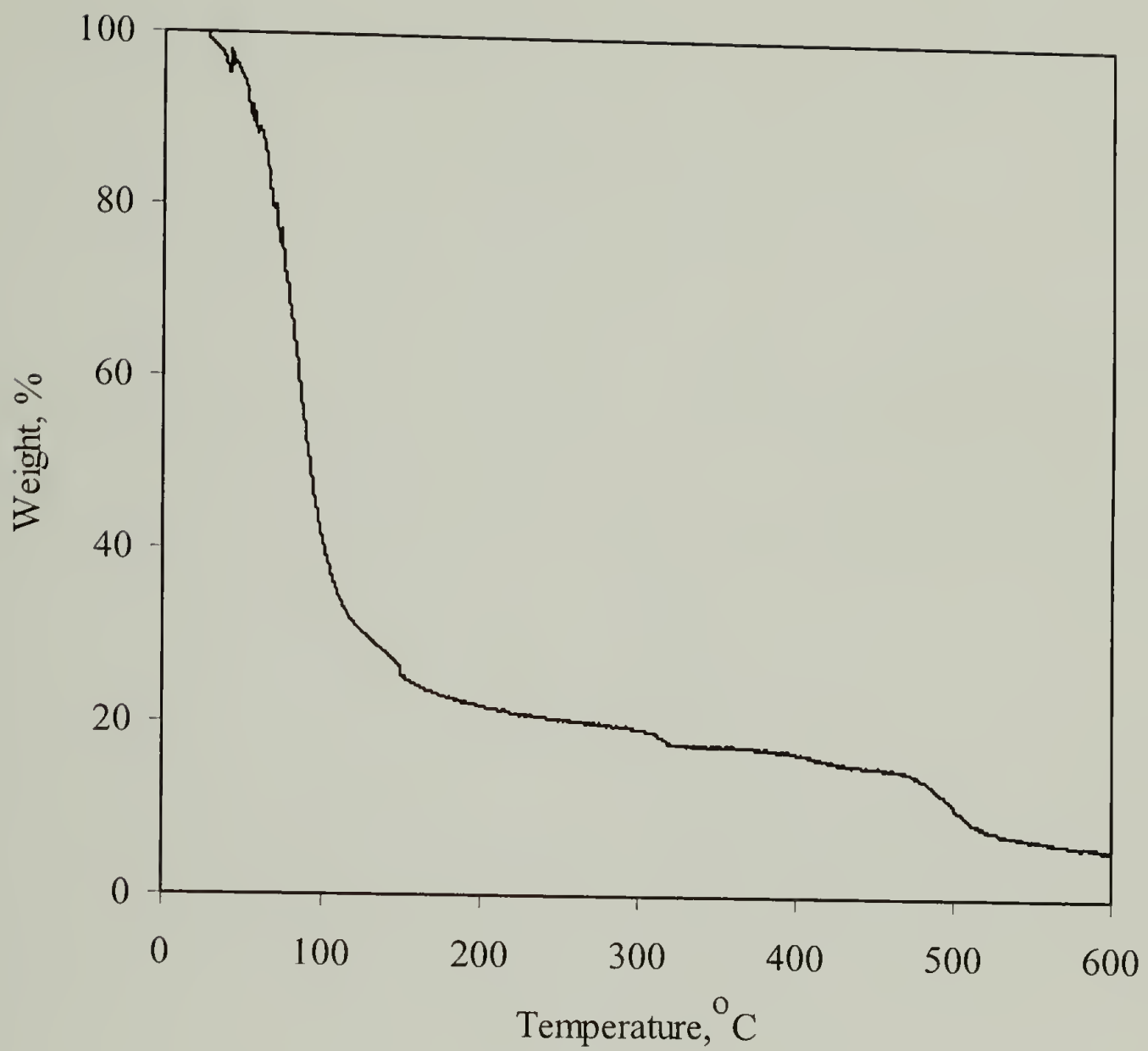


Figure 3.4. TGA thermogram of the poly(amic acid) methacrylic ester (HRP) solution (20 wt%) in N-methyl pyrrolidinone (NMP).

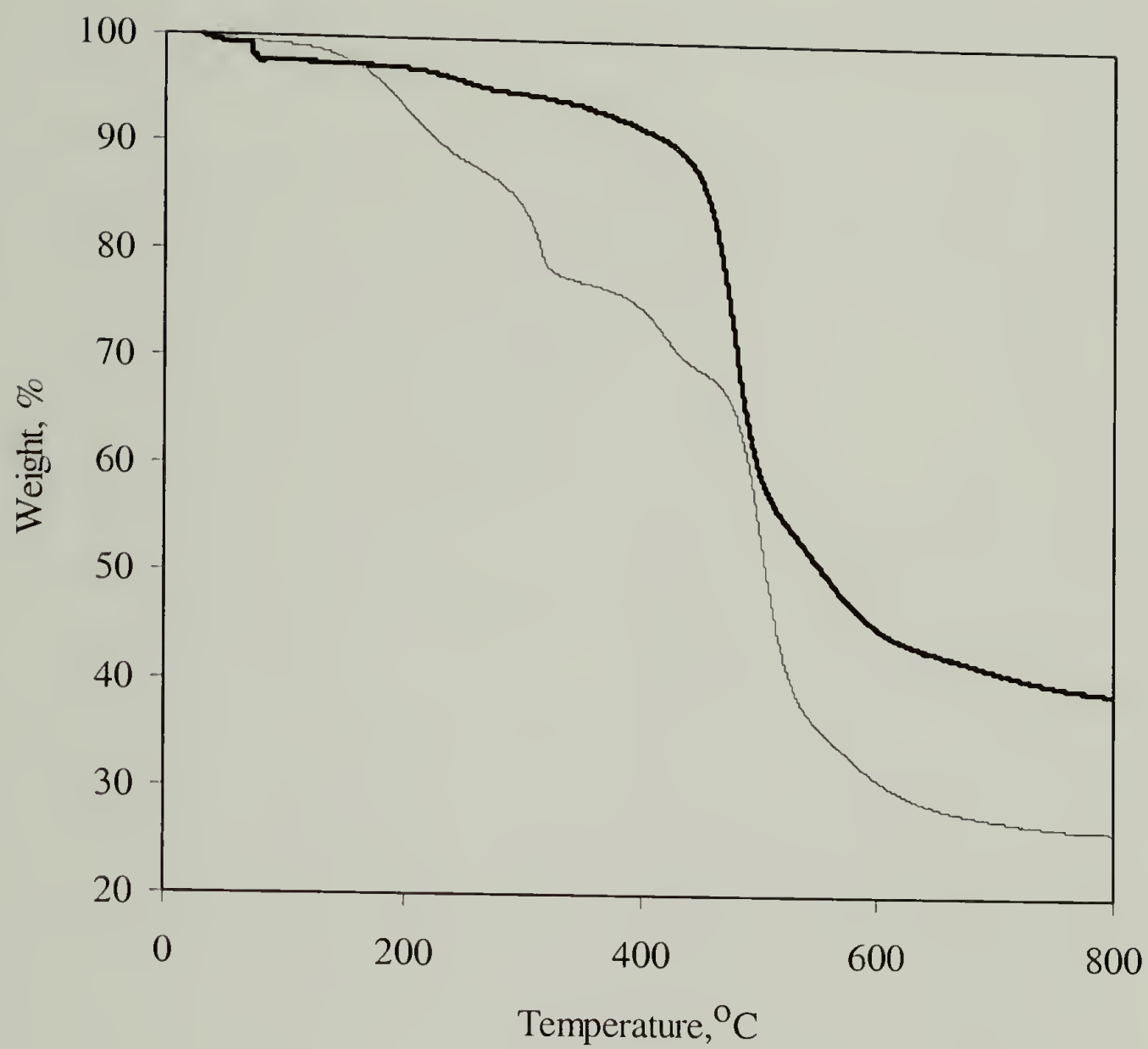


Figure 3.5. TGA thermogram of the poly(amic acid) methacrylic ester (HRP) film. Thin line: cured at 125 °C for 1 hour, thick line: cured at 260 °C for 30 min.

The first transition below 300 °C in Figure 3.5 is due to residual solvent (NMP) present in the films. Figure 3.5 also suggests that the thermal stability of the HRP film is greatly enhanced upon imidization by comparing the film cured at 260 °C to the film cured at 125 °C. This can be shown by analyzing the residuals for the two films at 800 °C (25% for the 125 °C cured HRP film, and 40% for the 260 °C cured HRP film). Note that 125 °C is a soft bake condition prior to imidization. Imidization is achieved by curing at temperatures above 260 °C.

Comparing the two different photolithographic films, we see that the HRP film has better thermal stability than the PUA film. This is expected due to the nature of the superior thermal stability that polyimides have over acrylic polymer films.

DSC Results. To verify that the results shown by TGA for these lower temperature transitions are being related to crosslinking reactions and not thermal degradation, DSC was performed. Figure 3.6 shows DSC thermograms for PUA films obtained under different UV cure conditions. Data from Figure 3.3 showing the TGA thermograms of these materials at different UV curing conditions are also shown. Upon UV cure, we see that the two exothermic transition peaks at 170 °C and 280 °C are greatly diminished. Both peaks are indicative of the crosslinking mechanism upon UV cure. We also see that the higher UV cure completely diminishes the residual exothermic peak at 280 °C shown for the 1.5 J/cm² UV-cured PUA sample. Hence, we conclude that higher UV curing conditions enhance the probability of completing the photocrosslinking process for the PUA film. Further thermal curing of the PUA film induces no transition at the temperatures of interest.

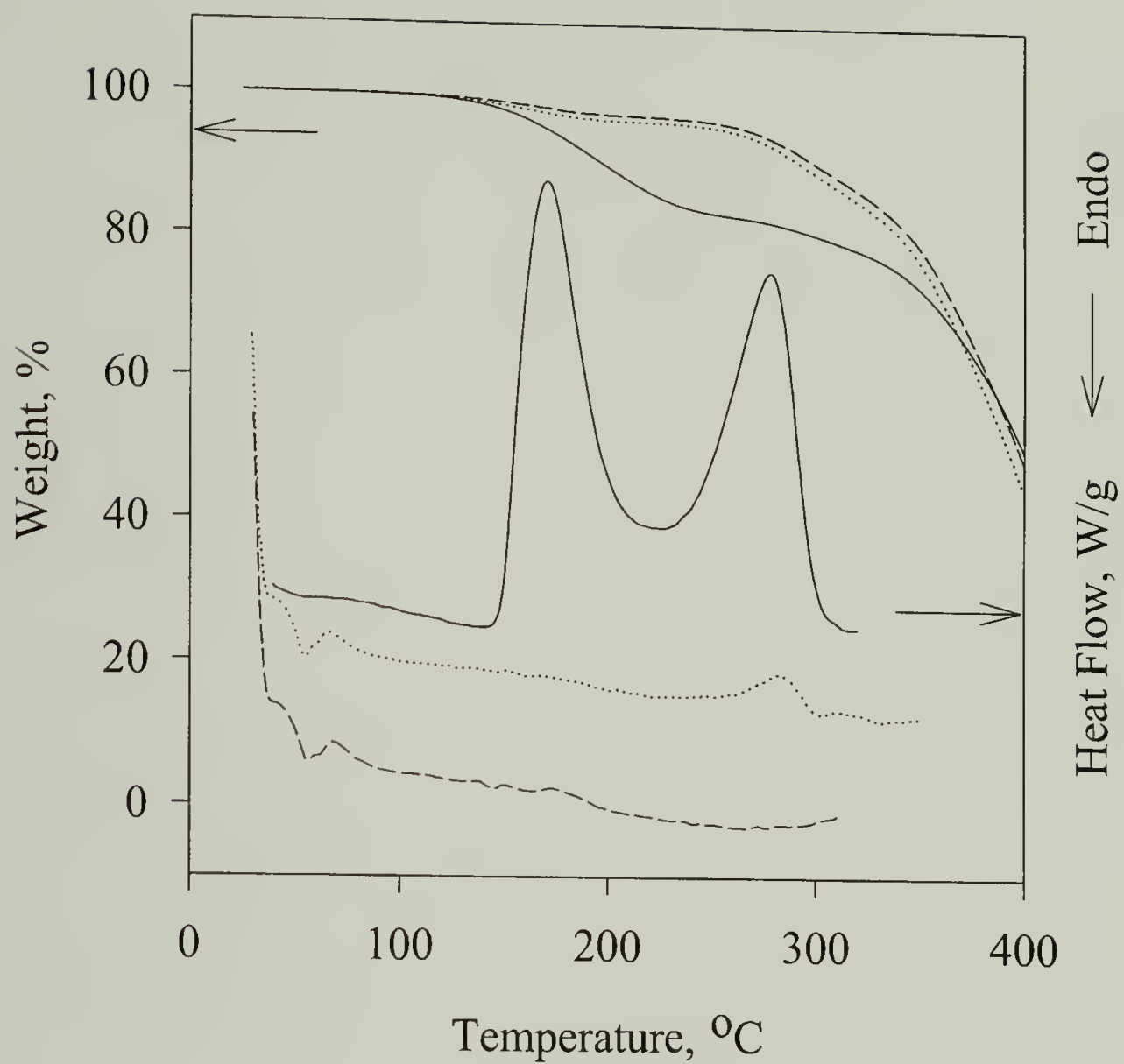


Figure 3.6. DSC thermogram for poly(urethane acrylate) (PUA) macromonomer. Top three lines: TGA thermograms (data extracted from Figure 3.2). Solid curve: DSC thermogram for poly(urethane acrylate) (PUA) macromonomer, small dotted curve: PUA film UV cured at 1.5 J/cm^2 , large dotted curve: PUA film UV cured at 5.0 J/cm^2 .

Figure 3.6 suggests that there is a transition at $\sim 60^{\circ}\text{C}$, aside from the transition peaks that are related to the crosslinking reactions for the PUA film. TGA thermograms suggest that there is no weight loss associated with that particular peak at 60°C . Figure 3.7 shows a low temperature DSC thermogram for PUA films obtained at different UV curing conditions. The endothermic peak at 60°C appears consistently in UV cured PUA samples, regardless of the amount of UV cure. However, the endothermic peak disappears after the second run. This likely indicates that the endothermic peak at 60°C is related to a thermal transition present in the PUA film. As will be seen in the following DMTA results section, the peak is not related to any secondary transition of the PUA film. Figure 3.8 shows the effect of thermal cure for different times on the UV cured PUA film that has the endothermic peak. Upon thermal cure, the endothermic peak diminishes in intensity for all the thermally cured PUA films. However, the peak does not completely disappear.

Figure 3.9 shows an interesting observation involving the endothermic peak at 60°C . Upon stretching the sample to a certain degree (in Figure 3.9, 31.6%), we see that the endothermic peak increases. Upon re-heating the PUA sample on the second run, the peak diminishes. This led us to believe that the endothermic peak may be involved with a transition involving strain (or stress)-induced crystallization. For this reason, we have attempted to see if there are any crystalline peaks that are present upon stretching the PUA film by X-ray scattering. X-ray scattering of PUA film samples were performed using a Siemens D500 diffractometer operating with a Ni filtered $\text{CuK}\alpha$ radiation in the transmission mode. Results of the X-ray scattering are shown in Figure 3.10. From the diffractogram, we conclude that there is no strong evidence of crystalline formation

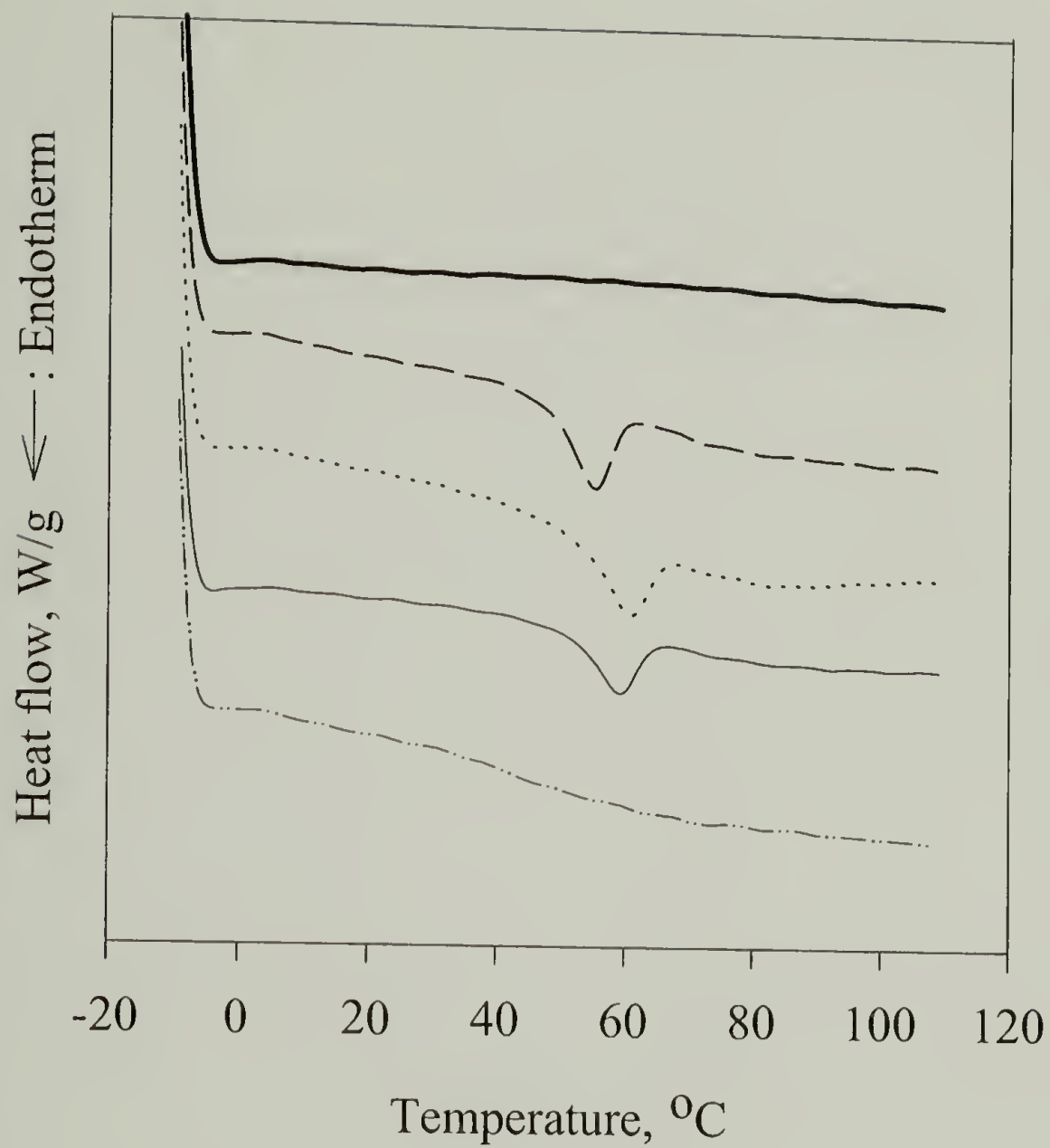


Figure 3.7. DSC thermogram of PUA film obtained at different processing steps. Thick solid curve: PUA film UV cured at 3.0 J/cm^2 (no thermal cure), large dotted curve: PUA film UV cured at 1.5 J/cm^2 , small dotted curve: PUA film UV cured at 3.0 J/cm^2 , thin solid curve: PUA film UV cured at 5.0 J/cm^2 , double dotted curve: PUA film, 2nd run.

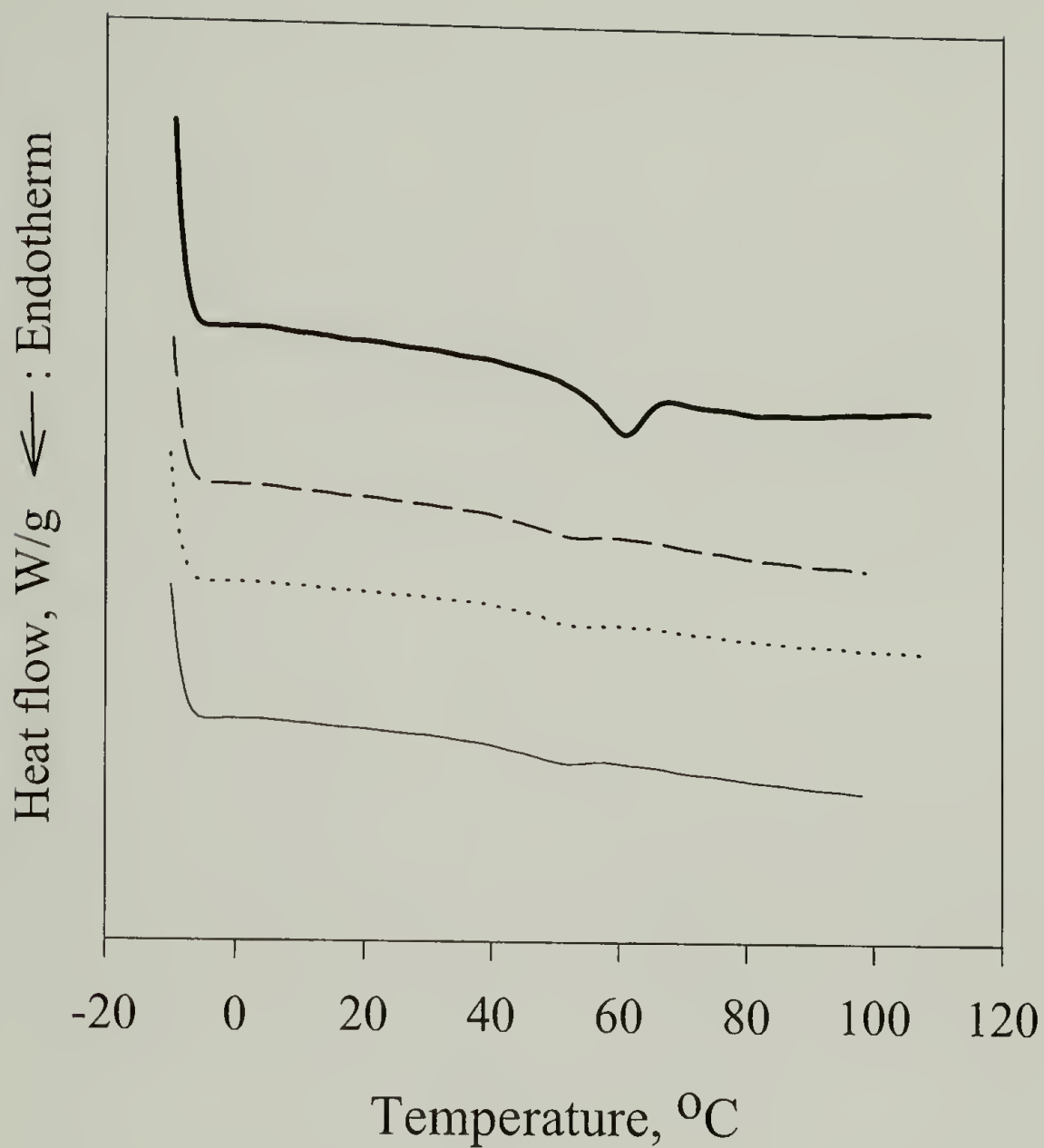


Figure 3.8. DSC thermogram of PUA film obtained at different processing steps. Thick solid curve: PUA film UV cured at 3.0 J/cm^2 (no thermal cure), large dotted curve: PUA film UV cured at $3.0 \text{ J/cm}^2 + 220 \text{ }^\circ\text{C}$ for 30 min., small dotted curve: PUA film UV cured at $3.0 \text{ J/cm}^2 + 220 \text{ }^\circ\text{C}$ for 60 min., thin solid curve: PUA film UV cured at $3.0 \text{ J/cm}^2 + 220 \text{ }^\circ\text{C}$ for 90 min.

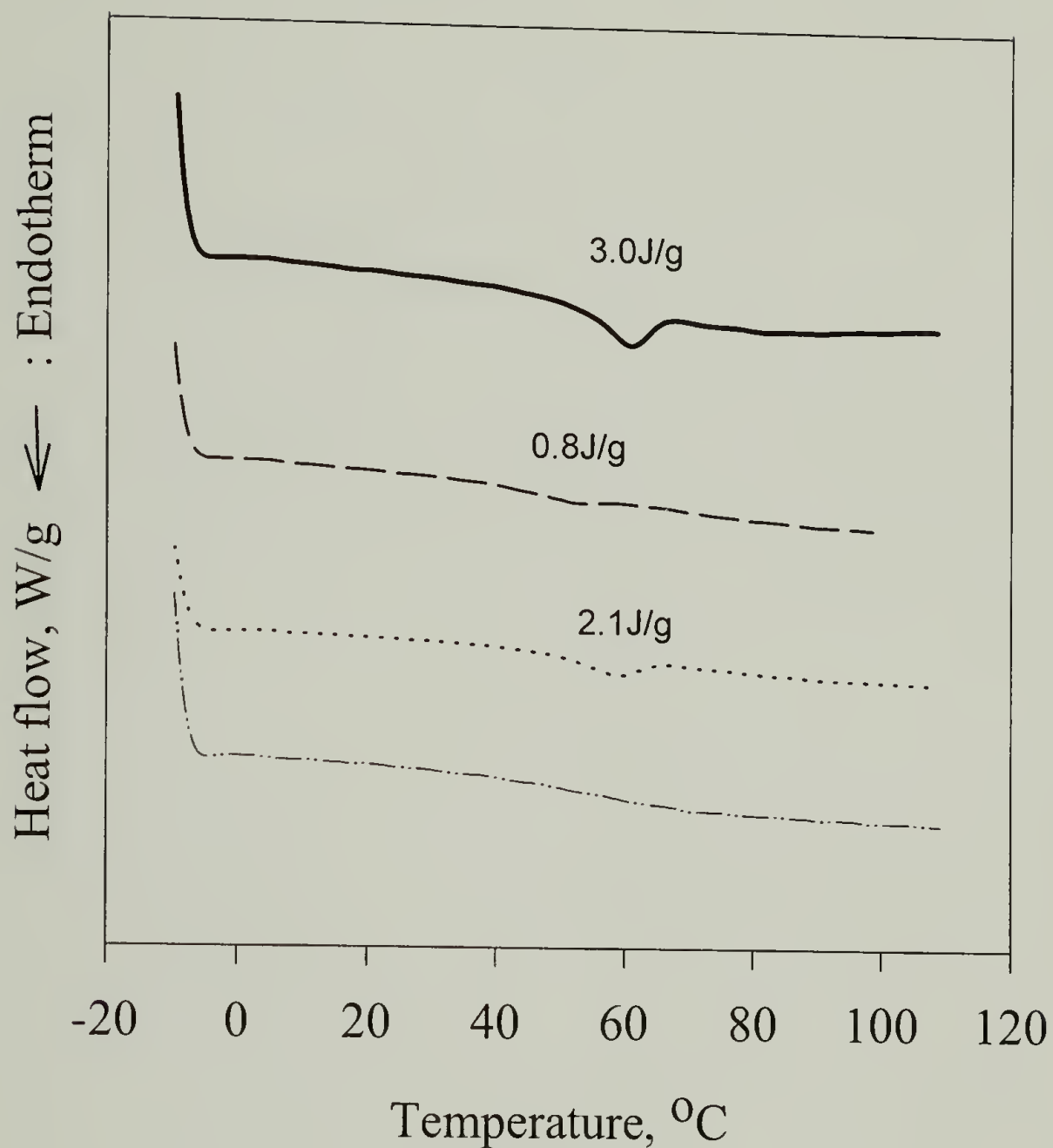


Figure 3.9. DSC thermograms of PUA film obtained under different processing conditions. Solid curve: PUA film UV cured at 3.0 J/cm², large dotted curve: PUA film UV cured at 3.0 J/cm² + 220 °C for 30 min., small dotted curve: PUA film UV cured at 3.0 J/cm² + 220 °C for 30 min. stretched 31.6%, double dotted curve: stretched PUA sample, 2nd run.

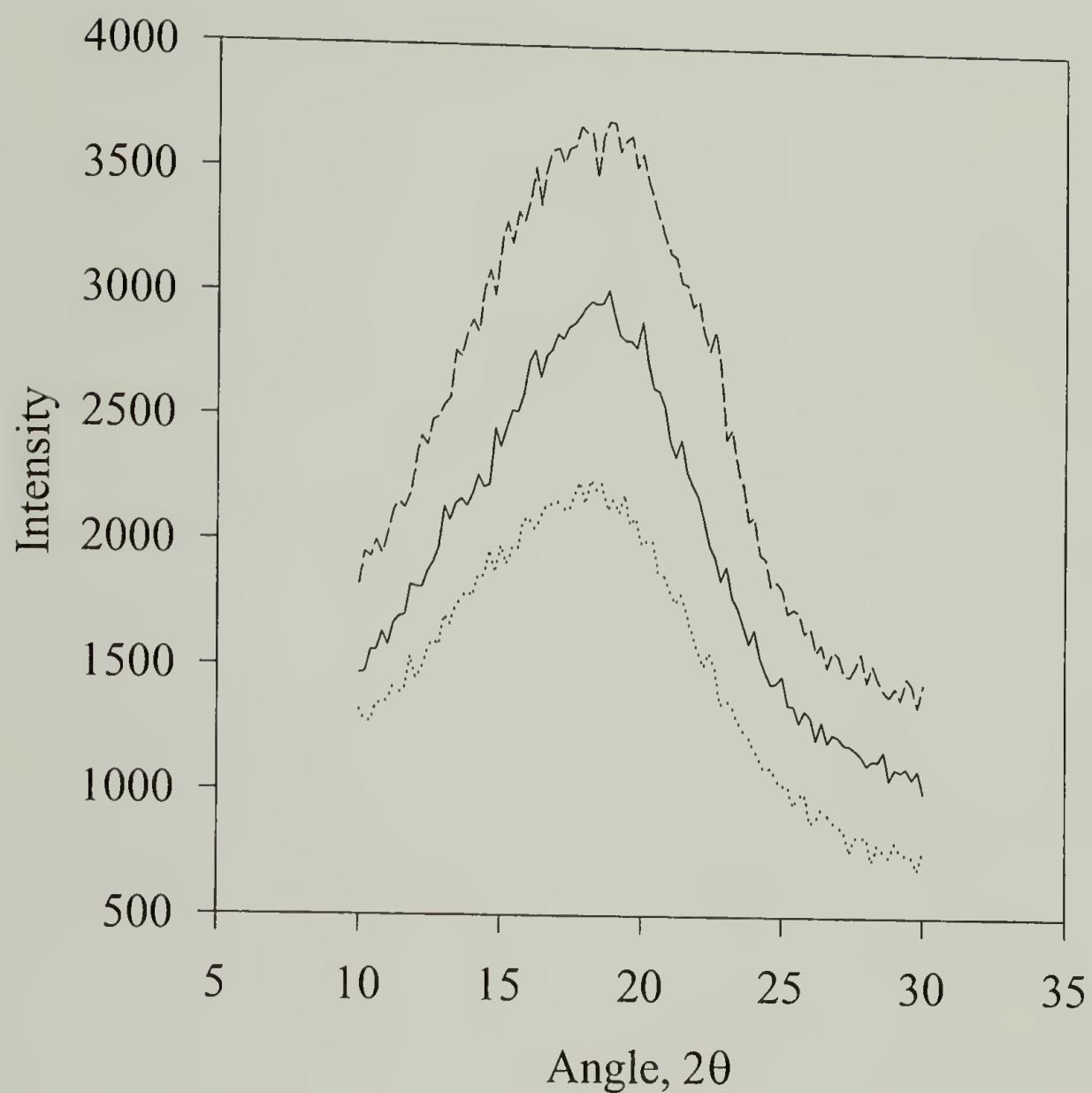


Figure 3.10. X-ray diffractograms of PUA films obtained at different processing steps. Top large dotted curve: PUA film UV cured at 3.0 J/cm^2 , solid curve: PUA film UV cured at $3.0 \text{ J/cm}^2 + 220^\circ\text{C}$ for 30 min., small dotted curve: PUA film UV cured at $3.0 \text{ J/cm}^2 + 220^\circ\text{C}$ for 30 min. stretched at 31.6%.

within the PUA film, for the peaks are too broad to be considered due to a significant crystalline component.

Further analysis of the endothermic peak at 60 °C was done on the stretched samples using a polarized optical microscope. Polarized optical microscopy was performed using an Olympus BX60 microscope. PUA film samples were observed in the transmission mode and taken at their minimum (0°) and maximum (45°) polarization angles for comparison. Results are shown in Figure 3.11. There is an obvious shear banding that becomes more apparent upon stretching the PUA film samples (from 10% to 40%). We conclude that the endothermic peak at 60 °C is related to some type of relaxation phenomena in the PUA film that is triggered by either the UV curing process, or mechanically deforming the PUA films.

Figure 3.12 shows a DSC thermogram of the poly(amic acid) methacrylic ester (HRP) film processed at 125 °C. The thermogram suggests that a small exothermic transition at ~170 °C, which is likely related to the imidization of the poly(amic acid) methacrylic ester. Figure 3.13 shows a DSC thermogram of the HRP film thermally cured to 260 °C, which shows no exotherm at 170 °C, but an endotherm. The reason for the endotherm is likely due to (1) residual methacrylic ester side groups that did not evaporate out of the film upon imidization, and degrading within the film at high temperatures, or (2) residual solvent bound by secondary interactions (i.e., hydrogen bonding) within the film evaporating out at higher temperatures.

DMTA Results. Figures 3.14 through 3.16 show DMTA thermograms of the PUA film obtained at different processing conditions. No noticeable trend is

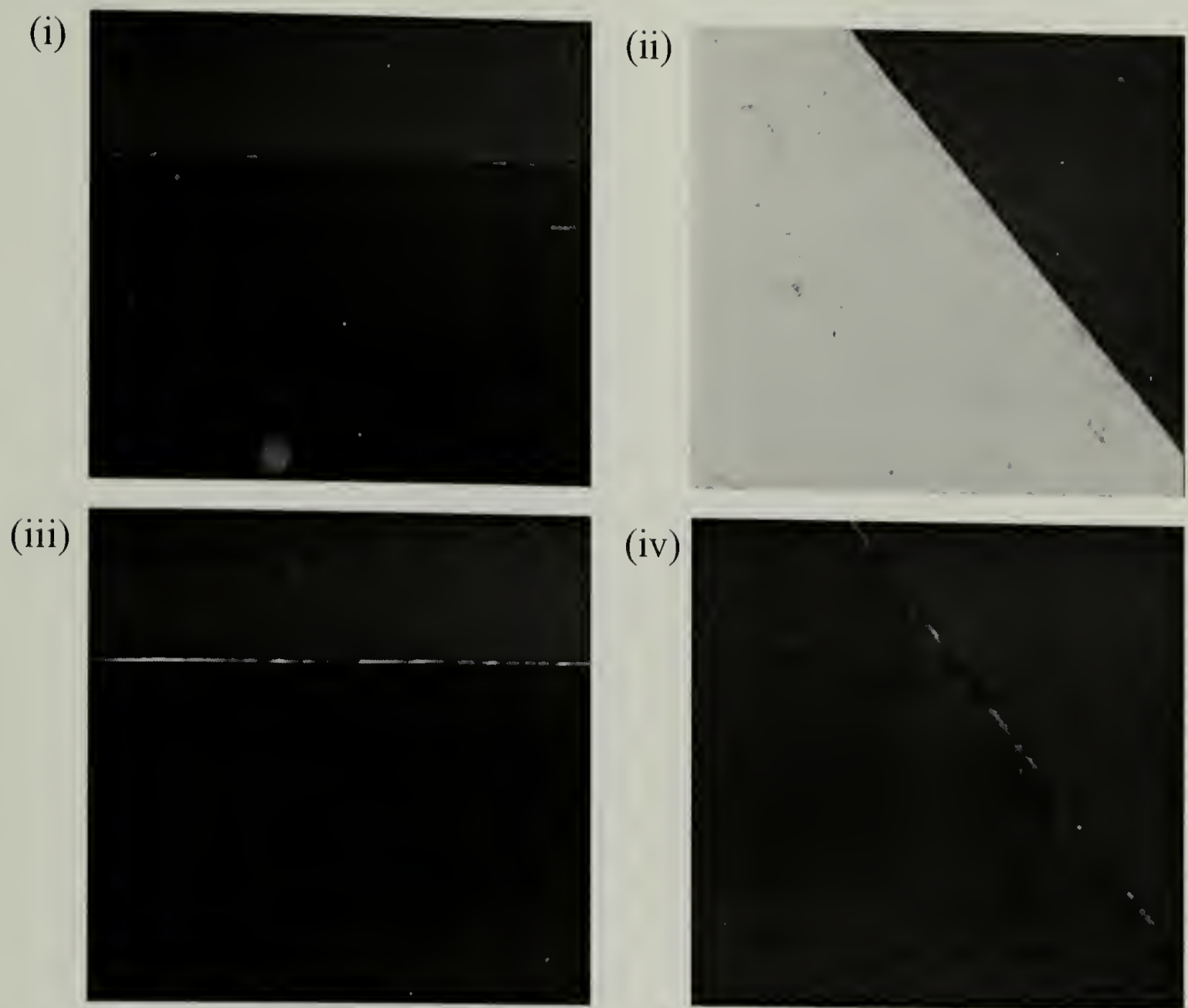


Figure 3.11. Polarized optical micrographs of PUA film cured at 220 °C, 150 psi, 30 min.
(i) 0° polarization and (ii) 45° polarization for a 40% elongated sample; (iii) 0° polarization and (iv) 45° polarization for a 10% elongated sample.

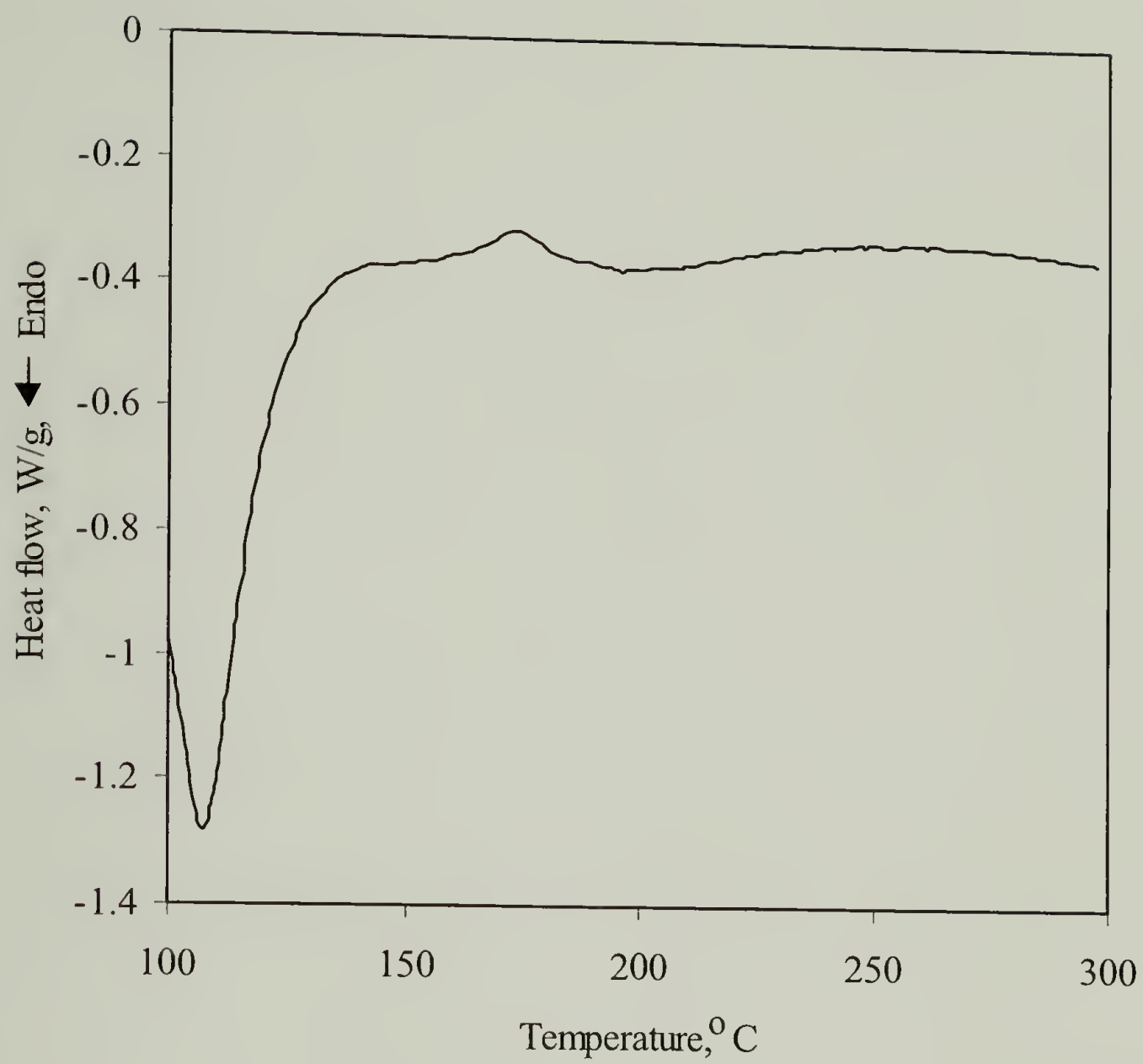


Figure 3.12. DSC thermogram of HRP film obtained after the 125 °C thermal cure.

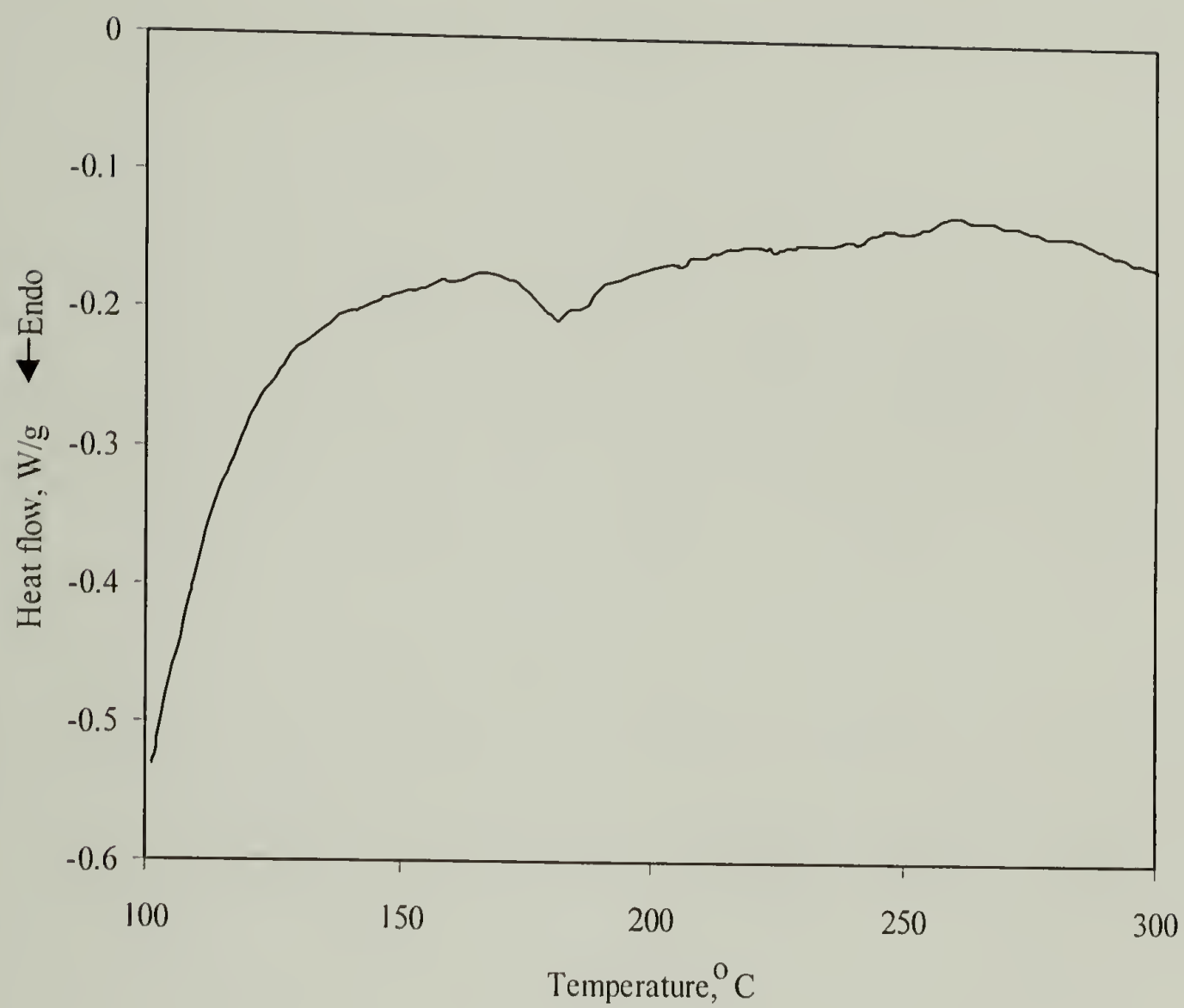


Figure 3.13. DSC thermogram of HRP film obtained after the 260 °C thermal cure.

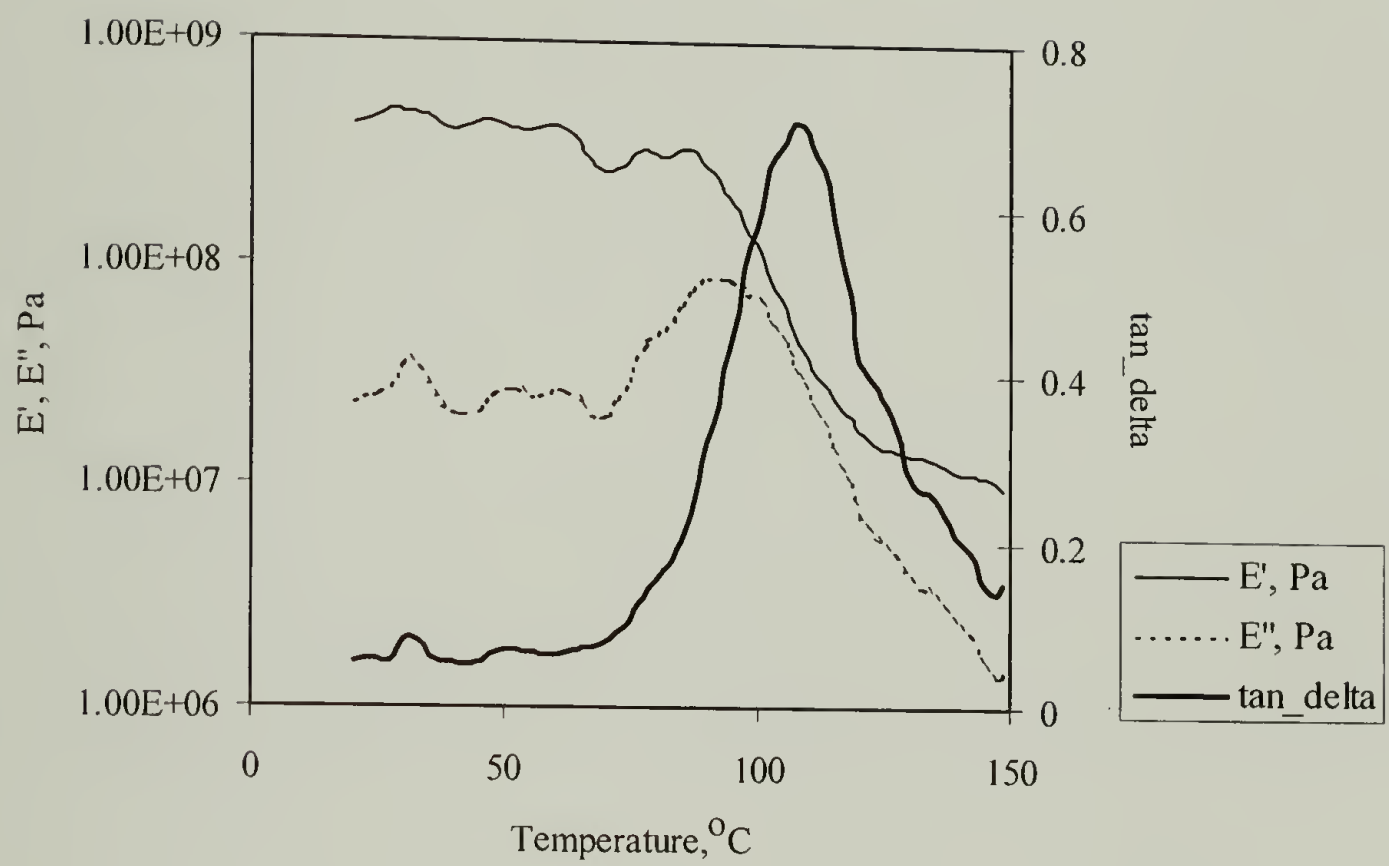


Figure 3.14. DMTA thermogram of poly(urethane acrylate) (PUA) polymer film UV cured at 3.0 J/cm².

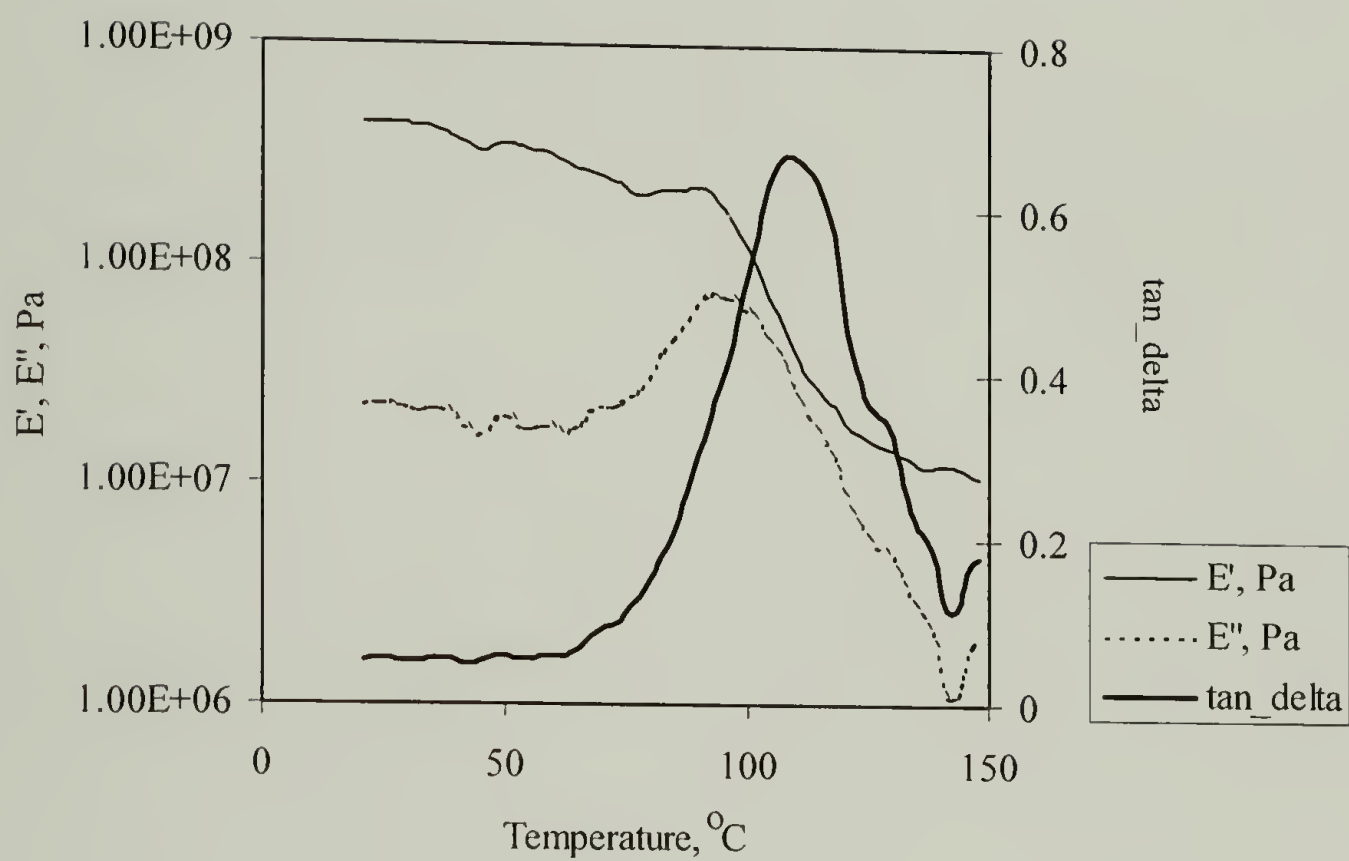


Figure 3.15. DMTA thermogram of poly(urethane acrylate) (PUA) polymer film UV cured at 5.0 J/cm².

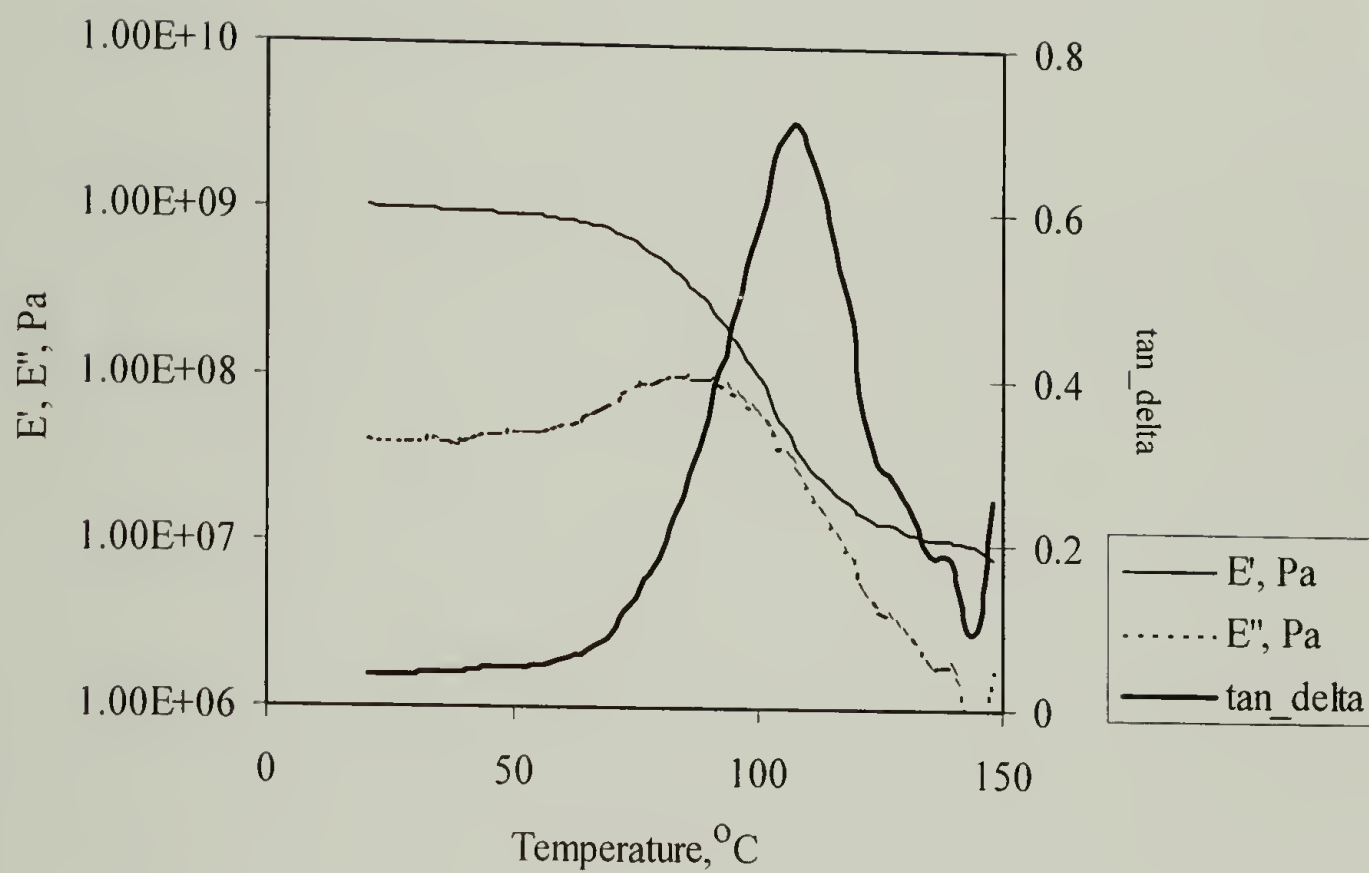


Figure 3.16. DMTA thermogram of poly(urethane acrylate) (PUA) polymer film UV cured at 3.0 J/cm² + thermally cured (220 °C, 150 psi., 30 min.).

observed upon different UV cure or thermal cure besides the observation that the signals are more pronounced for the thermally cured samples. All samples show a transition around 110 °C upon heating. This is most likely the glass transition temperature (T_g) of the PUA polymer film. This transition is also noticed for the PUA film samples through TMA analysis (see following TMA Results section). Hence, we see that neither the UV nor thermal cure affects the T_g of the PUA polymer film significantly.

Figure 3.17 shows the DMTA thermogram of the fully cured HRP film. We see that there is no noticeable transition in the film sample. The HRP film, therefore, most probably exhibits a higher T_g than the range tested, which is what would be expected from polyimides that usually show very high, or questionable, T_g ranges.

TMA Results. Perhaps one of the most important properties to measure in determining the residual stress of coatings is the coefficient of thermal expansion (CTE). Different mismatches in CTE's for coatings, especially when the substrate has a very different CTE than the coating, can result in high residual stresses. TMA allows one to measure CTE. Figure 3.18 shows a typical TMA thermogram of a processed PUA polymer film. An interesting observation, aforementioned in the DMTA Results section, is for the transition of the slope around 110 °C for all thermograms. This, along with the DMTA Results reported earlier, strongly indicates that the PUA polymer film has a glass transition temperature around 110 °C. The glass transition temperature does not significantly change upon UV cure or thermal cure.

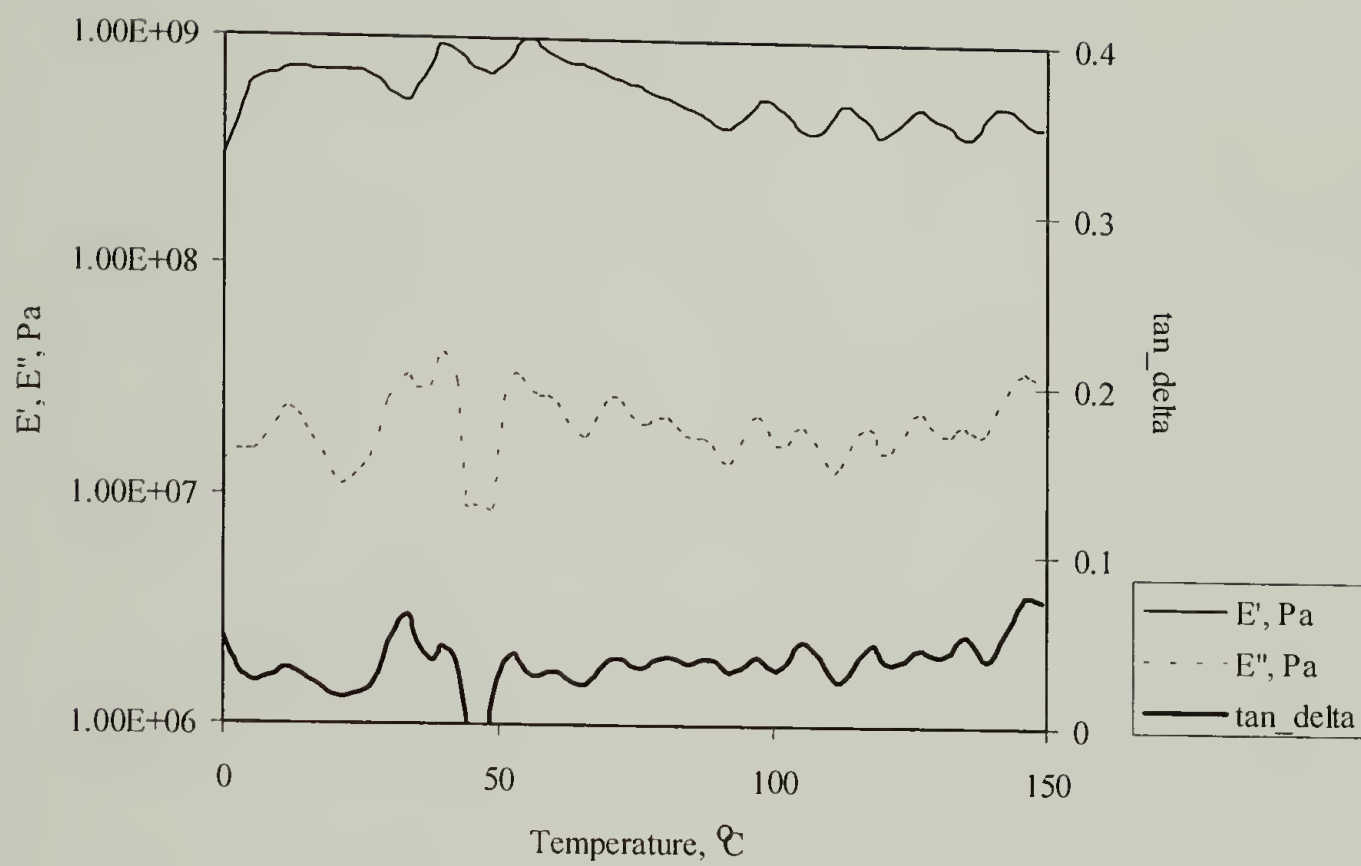


Figure 3.17. DMTA thermogram of poly(amic acid) methacrylic ester (HRP) polymer film, thermally cured.

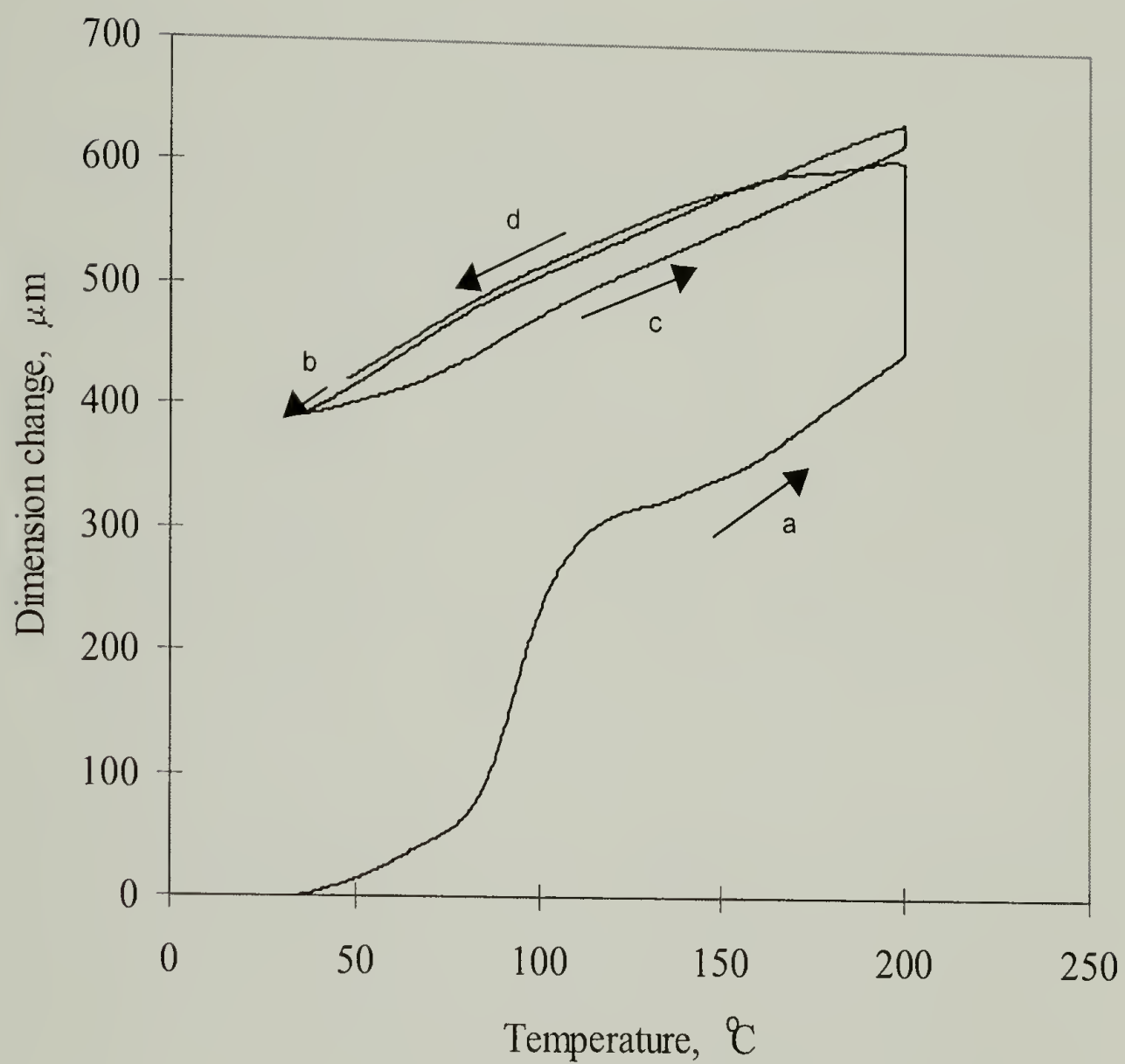


Figure 3.18. TMA thermogram of poly(urethane acrylate) (PUA) polymer film UV cured at 3.0 J/cm^2 + thermal cure at 220°C , 150 psi. for 30 min. Step a: first heating, b: first cooling, c: second heating, d: second cooling ($\text{CTE} = 149 \mu\text{m/m/}^{\circ}\text{C}$).

UV cure does not affect the overall coefficient of thermal expansion of the PUA material. This is shown in Table 3.2. Neither different cure times at 220 °C (Table 3.3) nor different final cure temperatures (Table 3.4) show any significant trend for the CTE values of the PUA polymer film. After a considerable amount of thermal cure is performed, the PUA polymer film shows relatively comparable thermal behavior.

Figure 3.19 shows the TMA thermogram of the HRP film. Much lower coefficient of thermal expansion (CTE) values compared to the PUA polymer films ($56 \mu\text{m}/\text{m}/^\circ\text{C}$ vs. $\sim 180 \mu\text{m}/\text{m}/^\circ\text{C}$) are reported. Hence, the HRP film is much more thermally stable in terms of dimensional stability. This CTE value is slightly higher than commercial polyimide CTE's that show CTE values in the $20 \mu\text{m}/\text{m}/^\circ\text{C}$ range.³⁰ Also, no discernable transition is noticed for the HRP film (unlike the PUA films at low temperatures below 150 °C).

Instron Tensile Testing. Figure 3.20 shows a representative graph of the stress-strain curve of PUA polymer films obtained under different processing conditions. As can be seen, the Young's moduli of the PUA film (UV cured only, $3.0 \text{ J}/\text{cm}^2$), and the PUA film (UV cured - $3.0 \text{ J}/\text{cm}^2$ and thermally cured (220 °C, 150 psi., 30 min. with minimal air contact) show identical values. Both samples show a yield point at 3% strain, 35 MPa. The major difference upon thermal cure is the elongation to break. Unlike the non-thermally cured PUA polymer film (7%), the thermally cured PUA film shows a large increase (37%). This indicates that the thermal cure, which induces further crosslinking of the PUA system, changes the mechanical properties of the PUA film, allowing the PUA film to behave more like a thermoplastic than a brittle polymer.

Table 3.2. Coefficient of thermal expansion measurements (TMA) for poly(urethane acrylate) (PUA) films processed at different UV cure conditions.

Material	Coefficient of thermal expansion ($\mu\text{m}/\text{m}/^{\circ}\text{C}$)
PUA 1.5 J/cm ² UV cure	159
PUA 3.0 J/cm ² UV cure	149
PUA 5.0 J/cm ² UV cure	151

Table 3.3. Coefficient of thermal expansion measurements (TMA) for poly(urethane acrylate) (PUA) films UV cured at 3.0 J/cm², thermally cured (220°C) at different cure times.

PUA film 3.0 J/cm ² UV cured + 220°C for	Coefficient of thermal expansion ($\mu\text{m}/\text{m}/^{\circ}\text{C}$)
15 min.	187
30 min.	203
45 min.	177
60 min.	258

Table 3.4. Coefficient of thermal expansion measurements (TMA) for poly(urethane acrylate) (PUA) films UV cured at 3.0 J/cm², thermally cured (30 min.) at different cure temperatures.

PUA film 3.0 J/cm ² UV cured + thermally cured for 30 min. at	Coefficient of thermal expansion ($\mu\text{m}/\text{m}/^{\circ}\text{C}$)
150°C	182
200°C	196
250°C	192

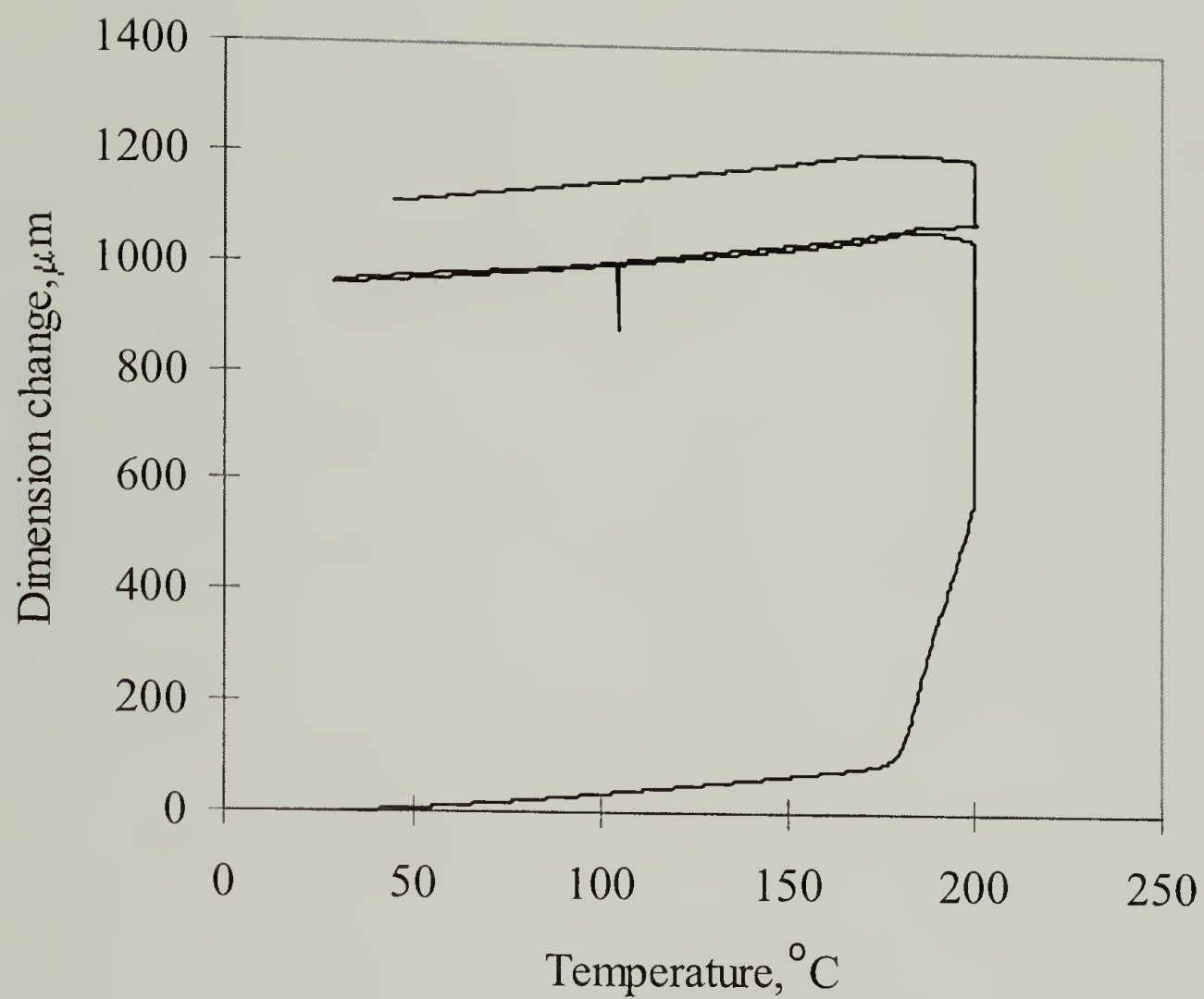


Figure 3.19. TMA thermogram of poly(amic acid) methacrylic ester (HRP) polymer film fully cured (CTE = $56 \mu\text{m}/\text{m}/^{\circ}\text{C}$).

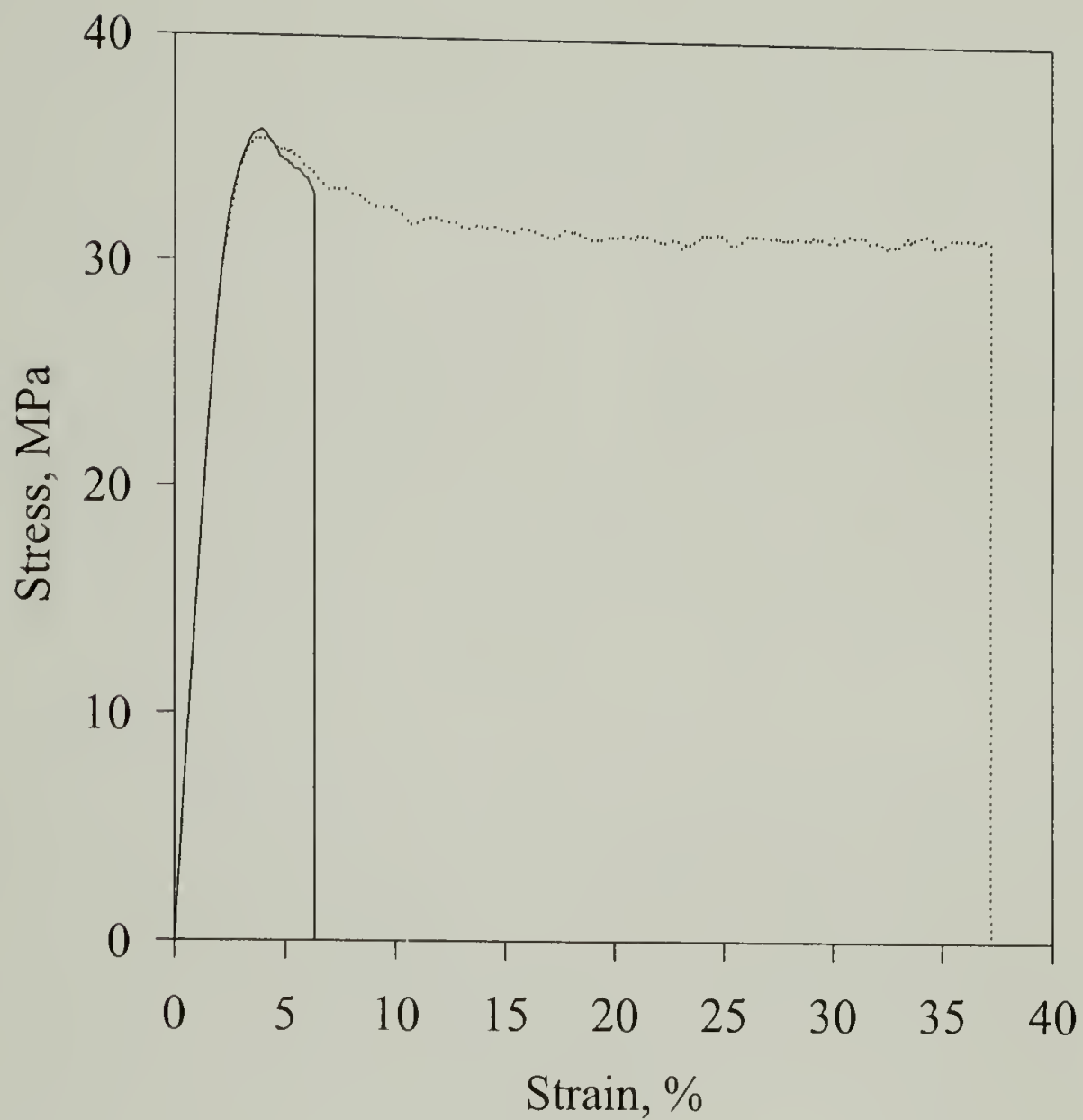


Figure 3.20. Stress-strain curve of poly(urethane acrylate) (PUA) films obtained at different processing conditions. Solid line: UV cured at 3.0 J/cm^2 , dotted line: UV cured at 3.0 J/cm^2 + thermally cured at 220°C , 150 psi., 30 min. (no air contact).

The minimal air contact is noted during thermal cure for good reason. Table 3.5 shows the difference in mechanical behavior of the PUA polymer film processed under different thermal conditions. The first set of data were obtained with samples that had contact with air (oven flushed with N₂), whereas the other set of samples had minimal contact with air (vacuum oven). The mechanical properties of the air-contacted PUA films are indicated by inferior values compared to the non-air contact PUA films. This is due to the oxidation of the PUA film upon thermal cure, which attacks the carbonyl groups present in the PUA polymer film. Oxygen, with the aid of high temperatures, breaks the highly crosslinked network, and hence, creates weak links within the system. This behavior, especially for photolithographic polymers, is well documented.³¹

Table 3.5. Mechanical properties of poly(urethane acrylate) (PUA) film UV cured at 3.0 J/cm² obtained at different thermal cure conditions. i: 220°C, 150 psi, 30 min., N₂ purge, ii: 220 °C, 150 psi, 30 min., vacuum oven.

PUA 3.0 J/cm ² UV cured	Stress at break (MPa)	Young's modulus (GPa)	Strain at break (%)
+ thermal cure with air contact ⁱ	29.0	2.1	1.2
+ thermal cure without air contact ⁱⁱ	33.4	1.6	38.3

Figure 3.21 shows the stress-strain curve of the fully cured poly(amic acid) methacrylic ester (HRP) film. The film shows higher mechanical properties than the PUA film, with a higher yield stress and comparable strain at break.

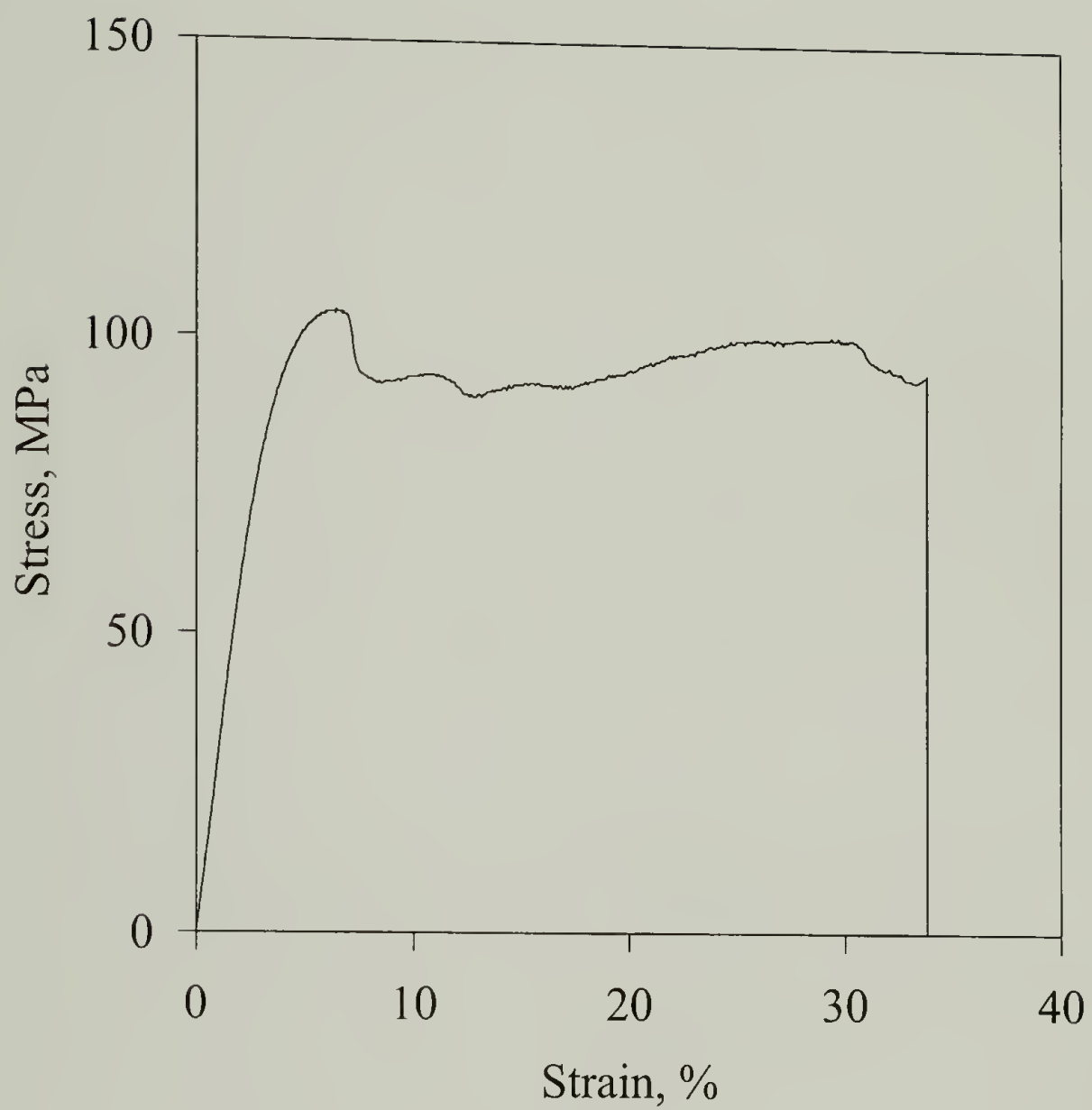


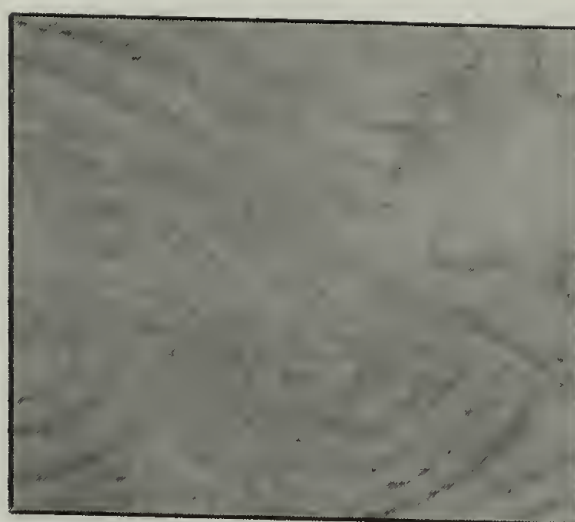
Figure 3.21. Stress-strain curve of the fully cured poly(amic acid) methacrylic ester (HRP) film.

Phase Structure Studies. Figure 3.22 shows the change in morphology of the PUA polymer film after different UV cure conditions. It is shown that UV curing changes the morphology of the PUA film. This is correlated to the carbon-carbon double bonds (unreacted crosslinkable side chain) and carbonyl bonds (within the ester group) that are available for staining, and their availability and distribution for staining upon the increased chemistry that occurs at higher UV curing conditions.

When further chemistry is completed with a thermal cure (220 °C, 150 psi., 30 min.), the morphology is non-existent (see Figure 3.23). This is an indication that the crosslinking has come to near completion, thus not having a significant number of pendant carbon-carbon double bonds left (especially) in the PUA polymer after thermal cure. The faint, but regular, grainy morphology in the thermally cured PUA polymer film may arise from homogeneously distributed carbonyl groups still present in the ester groups of the PUA polymer film. This behavior for thermally cured PUA film samples is shown in all UV cured PUA polymer samples.

The poly(amic acid) methacrylic ester (HRP) samples show no interesting change in morphology upon thermal cure. All samples were dark after staining. No TEM micrographs are reported.

Residual Stress Measurements upon Processing. Figure 3.24 shows residual stress values for poly(urethane acrylate) (PUA) polymer films obtained at different UV cure conditions. One thing to note is the decrease in density upon increasing UV cure dosage ($\rho = 1.15$ (1.5 J/cm²), 1.09 (3.0 J/cm²), and 1.07 (5.0 J/cm²) kg/m³). The residual stress within the PUA polymer films, however, increased with increasing UV cure.



— 0.5 μ



— 1.0 μ



— 0.1 μ

Figure 3.22. TEM micrographs of poly(urethane acrylate) (PUA) films processed at different UV cure conditions. Top: 1.5 J/cm², middle: 3.0 J/cm², bottom: 5.0 J/cm².

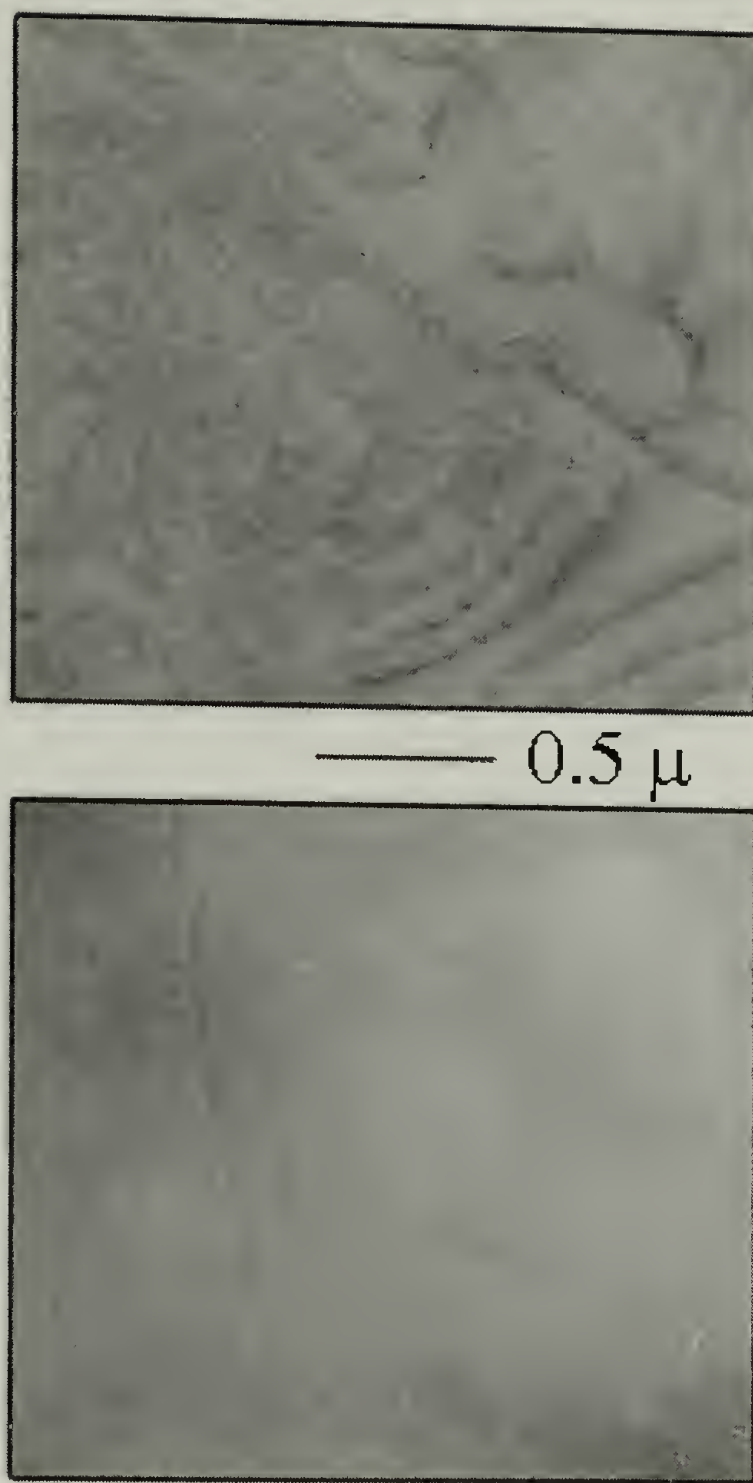


Figure 3.23. TEM micrographs of poly(urethane acrylate) (PUA) film processed at different conditions. Top: PUA film UV cured at 1.5 J/cm^2 , bottom: PUA film UV cured at 1.5 J/cm^2 + thermally cured (220°C , 150 psi, 30 min.).

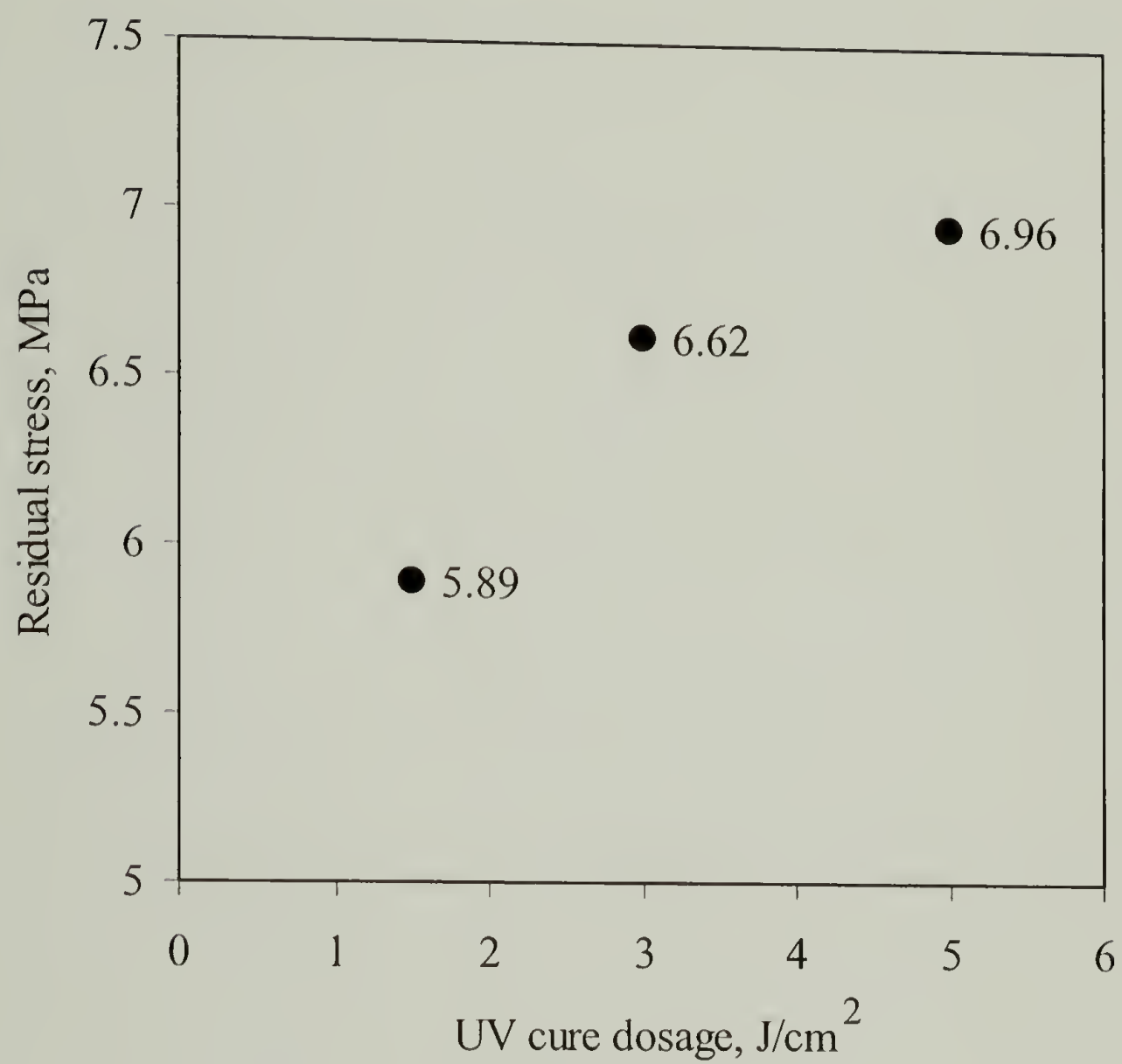


Figure 3.24. Residual stress measurements (holographic interferometry) for poly(urethane acrylate) (PUA) film UV cured at 1.5, 3.0, 5.0 J/cm².

Thermally cured PUA samples (to 220 °C) using an air-contact oven were tested. The residual stress values decreased to 2.46 MPa. This may be due to one of two reasons:

(1) Thermal annealing allows the PUA film to relax, alleviating some of the residual stress built up within the system, or

(2) Degradation behavior occurred with thermal oxidation for semi-insulated environments, resulting in a less than desirable film sample for analysis.

Swelling Stresses and Small Molecule Diffusion. Figure 3.25 shows the calibration curve for the Environmental Tensile Tester (ETT). The output measured is voltage (V), so converting the voltage read-out to load is necessary. Further calibration to verify the ETT voltage readings and correlate it with Instron tensile tests for identical samples were performed, and gave highly comparable results.

Figure 3.26 and 3.27 show the stress vs. time upon introducing the WB60 ink to the fully cured poly(urethane acrylate) (PUA) and fully cured poly(amic acid) methacrylic ester (HRP) film, respectively. We see in the graphs that the PUA film is more prone to relaxation more than the HRP film, which is anticipated when comparing solvent swelling of a low T_g -like material to a polyimide-like material. The PUA film relaxes approximately 12 MPa to its apparent equilibrium, whereas the HRP film relaxes to approximately 6 MPa.

Using the initial slope method to determine the diffusion coefficient of ink (WB60) through the two films, we see that the diffusion coefficient in the PUA film (1.759×10^{-9}) is larger than that in the HRP film (9.206×10^{-10}). Hence, the ink diffuses more rapidly into the PUA film than the HRP film.

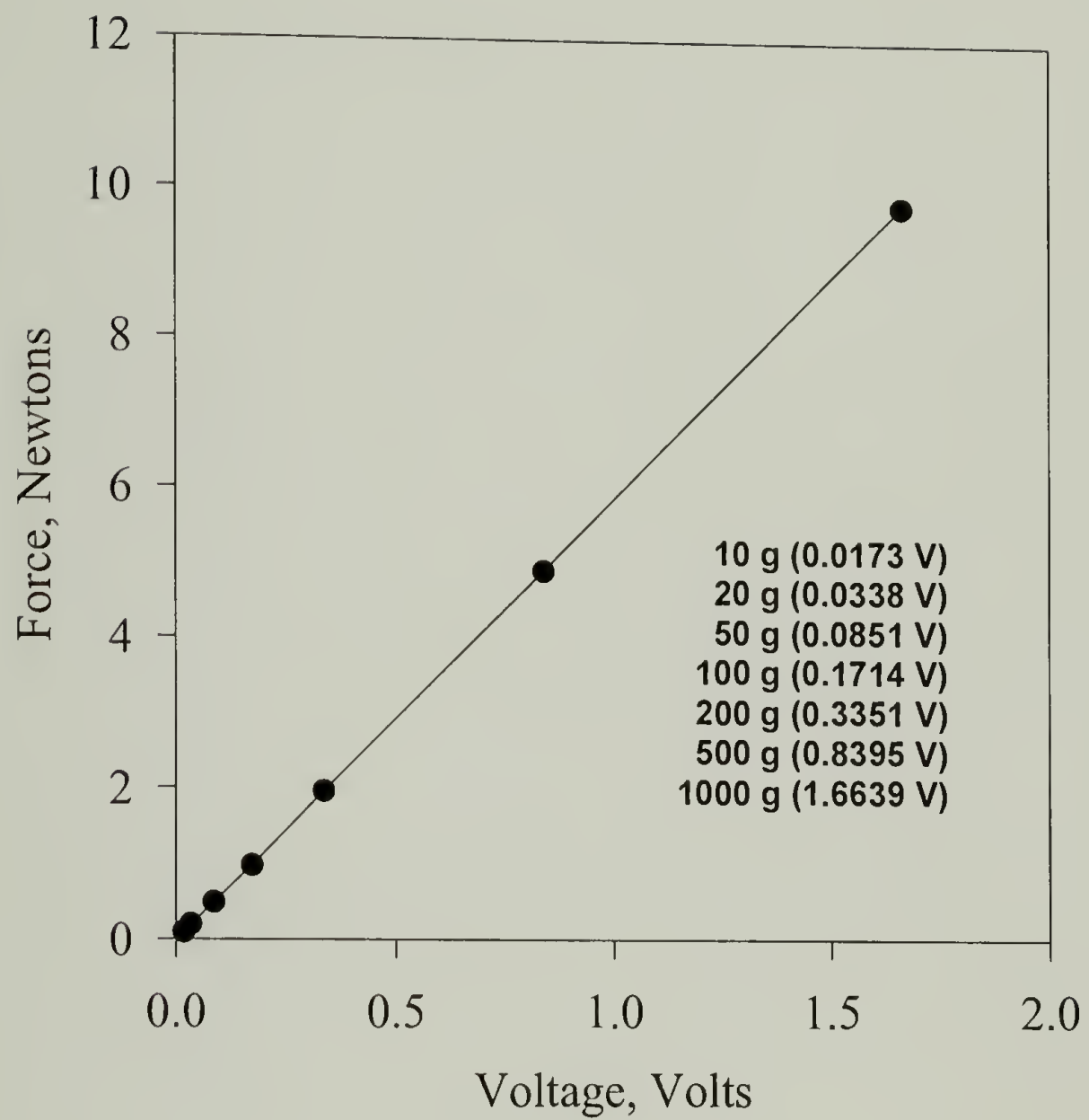


Figure 3.25. Calibration curve for the Environmental Tensile Tester (ETT).

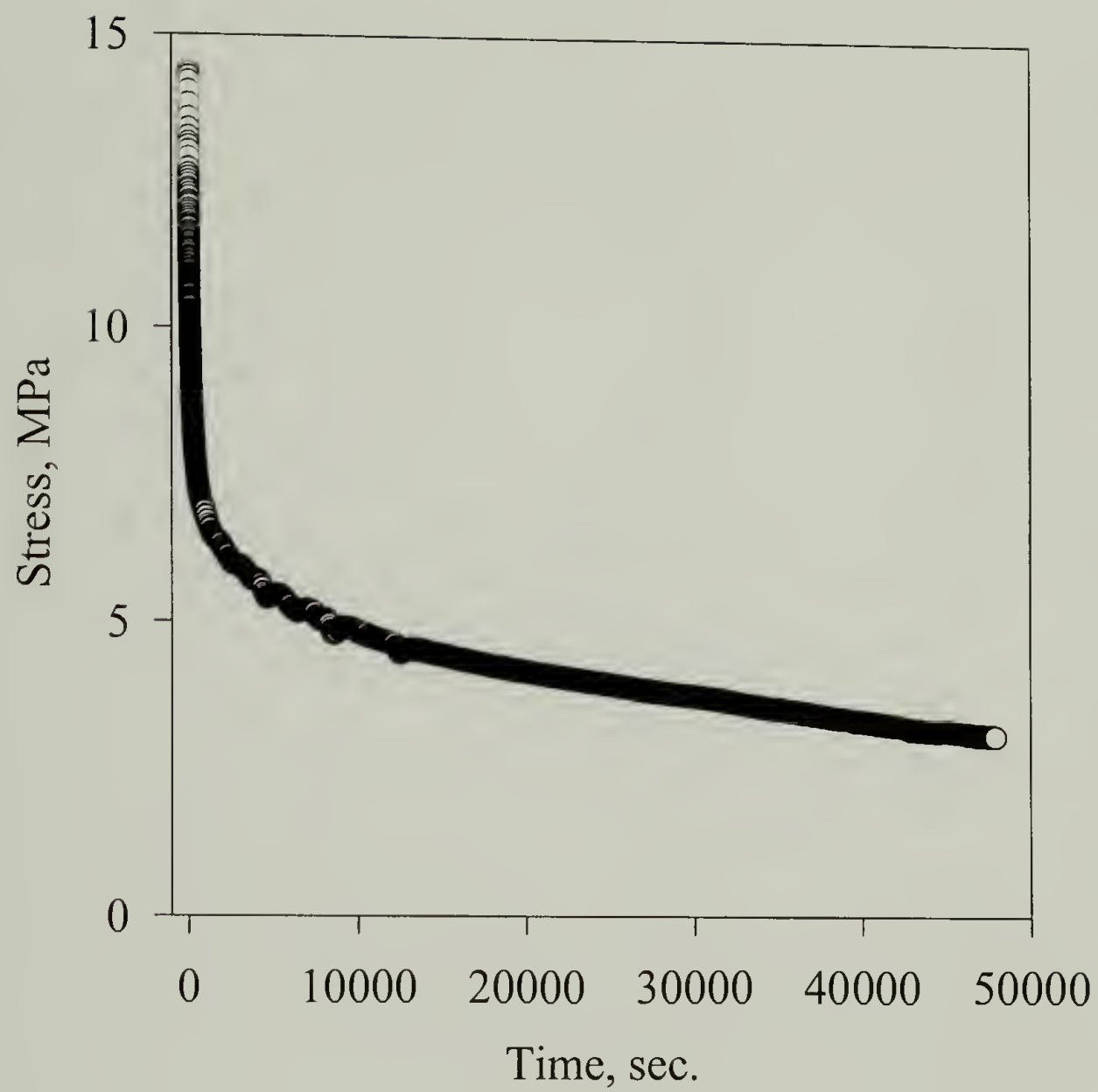


Figure 3.26 Stress relaxation behavior of fully cured poly(urethane acrylate) (PUA) film upon introduction of WB60 ink.

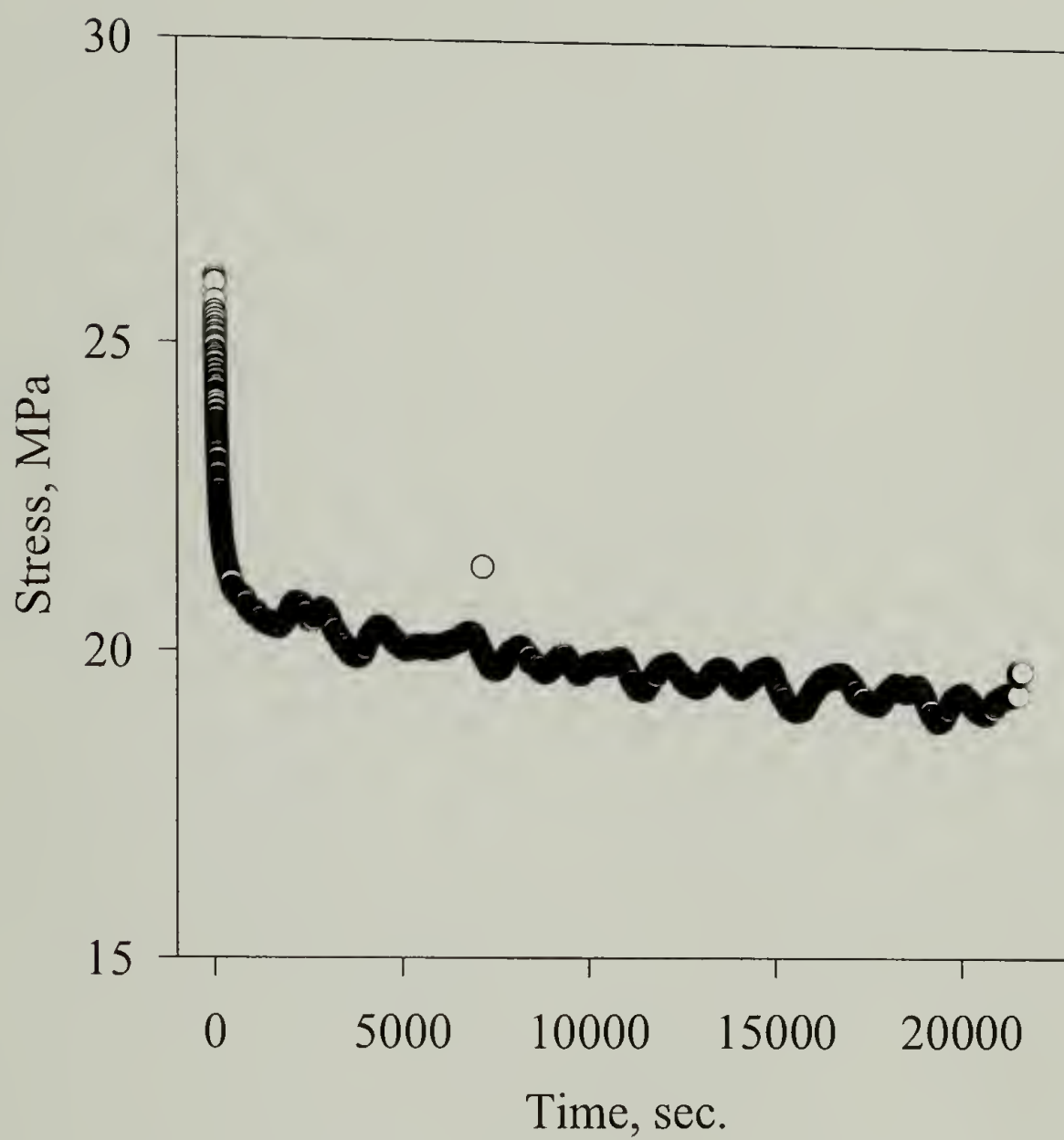


Figure 3.27. Stress relaxation behavior of fully cured poly(amic acid) methacrylic ester (HRP) film upon introduction of WB60 ink.

Conclusions

Two photolithographic polymer systems have been investigated to assess their integrity as possible barrier layers in an inkjet printhead environment. A series of tests were conducted to fully understand the materials. Such techniques include thermomechanical measurements, mechanical measurements, microscopic investigations, and other in-house characterization techniques which include vibrational holographic interferometry for residual stress measurements, and environmental tensile testing (ETT) for swelling stress and diffusion measurements.

Comparing the two different photolithographic films, we see that the HRP film has better thermal stability than the PUA film from TGA results.

DSC results show that there are two distinct peaks that correlate with the photocrosslinking and the thermal crosslinking of the PUA film, whereas the HRP film only has one exothermic peak, most likely correlated to the imidization of the HRP film. Both films show interesting endothermic peaks that may be related to small crystalline materials not detectable by X-ray diffraction, or, as is the case for PUA films, related to stored energy induced by stress (or strain) during processing.

DMTA shows a transition around 110 °C for the PUA film samples. This is due to the glass transition of the PUA film, which does not change significantly with processing. HRP films do not show a transition in the temperature range of interest.

TMA results show that the PUA samples have a higher coefficient of thermal expansion ($\sim 180 \mu\text{m}/\text{m}/^{\circ}\text{C}$) than that for the HRP film ($56 \mu\text{m}/\text{m}/^{\circ}\text{C}$). The TMA thermograms for PUA films reinforce the results obtained with DMTA concerning the transition at 110 °C.

Mechanical properties of PUA films show that different processing conditions change the mechanical stability. Thermal cure with minimal oxygen exposure improves the mechanical properties, while thermal cure with oxygen exposure gives unfavorable mechanical properties. Fully cured HRP films show better mechanical properties than fully cured PUA films.

TEM results show that the PUA films adopt different morphologies upon different UV cure. This is an indication primarily of the extent of crosslinking reaction that take place during UV curing. No morphology was obtained after thermal cure was performed. No morphology was observed with the HRP film.

Holography shows that upon increasing UV cure, there is an increase in residual stress for PUA films. Note that there is a decrease in density upon increasing UV cure. Thermally cured PUA film with oxygen exposure decreases the residual stress, which is most likely either due to (1) thermal relaxation of the PUA film, or (2) thermal degradation (oxidation) of the PUA film.

Using the environmental tensile tester (ETT), we see that the stress relaxation and the diffusion characteristics are larger for the fully cured PUA film than the fully cured HRP film upon ink exposure. This is expected when comparing a low T_g polymeric system to a polyimide-like system, and their solvent swelling and diffusion behavior.

Future Work

The environmental tensile tester (ETT) results show an interesting phenomenon. Even after a long period of time, the experiment does not seem to reach equilibrium for either polymer system. The stress curve continues to decrease with time. This is due to

the selective diffusion characteristics of the separate components in the WB60 ink. The ink (without the dye) consists of a high percentage of water, and other components such as surfactant, polar solvent, and certain diols. The pH values of the inks vary over a wide range, from acidic to basic. It may well be that some components of the ink diffuse faster into the polymer film, while other components tend to diffuse more slowly into the polymer film. Separate components and their diffusion through these photolithographic polymer films at different pH values may elucidate different diffusion and swelling characteristics that would be worthwhile investigating.

Processing the HRP film was difficult to carry out. This may be due to the degradative nature of the HRP film. The HRP solution has a finite shelf life, where after a certain period of time, the solution increases in viscosity, and gels. This gelation results in unwanted side reactions within the film. The gelation also makes it difficult to analyze the material for step-by-step processing. Obtaining pinhole-free films with good reproducible results was much harder for the HRP film than for the PUA films, which also has a finite shelf life, but seems to behave more predictably. Development of the PUA film for lithographic patterning showed better results compared to the HRP film (see Appendix). Further studies involving the effect of processing towards the properties of the HRP film should reveal interesting aspects of the HRP film that may serve as a unique advantage over the PUA film.

The ultimate goal of this research is to study the adhesion of these photolithographic polymer systems towards various surfaces. Studying the effect of adhesion upon different processing conditions for the PUA and HRP film on various surfaces (i.e., Si, Te, Au, polyimide, etc.) is very important for the feasibility of a

particular photolithographic polymer system to be used as part of an inkjet printhead construction. The effect of ink on the adhesion of these photolithographic polymer films towards various substrates should shed light on the interaction the polymer films have on these various substrates.

References

1. Kirby, P. *PTF-A Review of Polymer Thick Film Technology* Patinel, England, 1990.
2. Bowden, M. J., Turner, S.R. *Polymers for High Technology*; American Chemical Society: Washington, D.C., 1988.
3. Vrtis, J.K., Ph.D., *Polymer Science and Engineering*, 1995.
4. Maden, M.A., Ph.D., *Polymer Science and Engineering*, 1992.
5. Perera, D.Y., Eynde, D.V. *Journal of Coatings Technology* 1987, 59, 55.
6. Maden, M.A., Farris, R.J. *Experimental Mechanics* 1991, 31, 178.
7. Farris, R.J., Vrtis, J.K., Jou, C., Chen, M.J., Sheth, K.C., *Adv. Coatings Tech. Conf.-Eng. Soc.*, 1994.
8. Jennings, R.M., Taylor, J.F., Farris, R.J. *Journal of Adhesion* 1995, 49, 57.
9. Vrtis, J.K., Farris, R.J., *MRS Symp. Proc.* 1994, 338, 527.
10. Gray, A., Matthews, G.B. *Bessel Functions and Their Applications to Physics*, 1952.
11. Watson, G.N. *A Treatise on the Theory of Bessel Functions*, 1962.
12. Arfken, G. *Mathematical Methods for Physicists*; 3rd ed.; Academic Press: New York, 1985.
13. Sheth, K.C., Ph.D., *Polymer Science and Engineering*, 1996.
14. Jou, C.S. Ph.D., *Polymer Science and Engineering*, 1993.
15. Crank, J., Park, G.S., *Trans. Faraday Soc.* 1949, 45, 240.

16. Thomas, A.M., Gent, W.L., *Proc. Phys. Soc. Lond.* **1945**, 57, 324.
17. Crank, J., *Diffusion in Polymers*, Academic Press, New York, 1968.
18. Alfrey, T., Gurnee, E.F., Lloyd, W.G., *J. Polym. Sci., Part C.* **1966**, 12, 249.
19. Hopfenberg, H.B., Frisch, H.L., *J. Polym. Sci., Part B.* **1969**, 7, 405.
20. Vrentas, J.C., Duda, J.L., *AIChE J.* **1979**, 25, 1.
21. Newns, A.C., *Trans. Faraday Soc.* **1956**, 52, 1533.
22. King, G. *Trans. Faraday Soc.* **1945**, 41, 325.
23. Long, F.A., Thompson, L.J., *J. Polym. Sci.* **1955**, 15, 413.
24. Crank, J., *The Mathematics of Diffusion*, Clarendon Press, Oxford, 1956.
25. Felder, R.M., Huvar, G.S., *Methods of Experimental Physics*, Academic Press, New York, 1980.
26. Sih, G.C., Michopoulos, J.G., Chou, S.C., *Hygrothermoelasticity*, Martinus Nijhoff Publishers, Boston, 1986.
27. Sakinger, S.T., Ph.D., *Polymer Science and Engineering*, **1989**.
28. Tong, Q.K., Ph.D., *Polymer Science and Engineering*, **1993**.
29. Torchin, N.G., Brown, J.T., Smith, R.H., U.S. Patent 3,380,831, 1968.
30. Kapton E film: CTE = $17 \mu\text{m/m}^\circ\text{C}$, Kapton KN film: CTE = $17 \mu\text{m/m}^\circ\text{C}$ (results released from DuPont), Kapton H film: CTE = $20 \mu\text{m/m}^\circ\text{C}$ (results from *Polymer Handbook*).
31. Woods, R.J., Pikaev, A.K., *Applied Radiation Chemistry: Radiation Processing*, Wiley Interscience, New York, 1994.

APPENDIX A

XPS AND DYNAMIC CONTACT ANGLE DATA FOR THE POLYELECTROLYTE MULTILAYERS ASSEMBLED ONTO FUNCTIONALIZED ALUMINUM OXIDE

element	%C(15/75)	%O(15/75)	%N(15/75)	%S(15/75)	%Al(15/75)	%Si(15/75)	adv/rec CA
clean Al	47.54/32.03	40.01/51/05			10.54/16/33	1.92/0/58	93/9
Al- NH3+	63.28/51/81	21.64/28/64	5.03/6.45		4.39/6.23	5.66/6.87	50/8
1 layer	68.12/60.03	19.59/24.67	2.88/3/32	1.4/1.68	3.03/6.3	4.98/4.00	
2 layers	49.99/42.11	36.65/42.44	1.66/1.59	0.78/0.63	8.9/11.47	2.031/76	
3 layers	68.56/62.39	20.11/22.55	4.20/5.38	3.08/3.59	1.43/4.31	2.62/1.79	65/10
4 layers	52.49/47.00	33.07/37.14	2.73/2.84	1.06/1.3	8.19/9.97	2.46/1.75	
5 layers	64.73/58.99	22.14/26.56	3.25/4.00	1.932.33	5.36/6.00	2.59/2.11	
6 layers	71.11/65.94	16.52/19.93	6.36/6.86	3.27/3.07	0.95/2.46	1.78/1.74	89/9
9 layers	68.22/65.22	21.04/24.21	6.17/5.2	3.32/3.65	0.00/0.00	1.25/1.72	45/6
10 layers	75.45/70.65	14.17/16.74	6.35/7.39	3.42/3.93	0.00/0.77	0.61/0.52	
12 layers	70.44/73.53	14.98/16.05	2.44/2.42	1.28/1.35	1.98/2.85	3.26/1.76	87/13
15 layers	69.38/73.20	21.20/17.06	3.94/5.00	4.17/4.74	1.06/0.00	0.24/0.00	44/14
18 layers	69.21/68.43	19.23/19.13	4.85/5.81	3.36/3.30	1.92/1.92	1.44/1.41	79/16
21 layers	74.38/73.35	15.91/16.32	4.62/5.60	4.52/4.72	0.58/0.00	0.00/0.00	58/14
24 layers	71.55/72.75	17.5/16.27	5.68/6.34	3.62/3.85	1.16/0.68	0.5/0.12	72/11
25 layers	69.76/70.45	19.31/18.54	4.85/5.33	3.80/4.24	0.47/0.80	1.82/0.64	61/16
27 layers	73.24/72.70	17.25/17.47	4.18/4.68	4.75/4.97	0.00/0.00	0.58/0.18	58/13
29 layers	69.86/70.86	20.51/18.86	4.38/5.23	3.72/4.26	0.52/0.54	1.02/0.26	
30 layers	74.92/75.53	14.54/13.72	6.48/6.88	3.61/3.86	0.00/0.00	0.45/0.00	95/18
50 layers	73.10/73.50	17.04/16.62	6.15/7.04	2.00/2.56	0.90/0.00	0.82/0.29	125/17
75 layers	68.53/71.66	20.05/17.70	4.76/5.51	4.38/4.85	0.31/0.06	1.97/0.22	59/14
99 layers	71.63/71.82	17.75/17.26	5.17/6.37	3.89/4.55	0.00/0.00	1.56/0.00	57/8
100 layers	71.05/69.49	18.1/19.05	4.67/5.89	2.59/3.57	1.79/2.00	1.80/0.00	102/9
5th layer	kinetic	data					
element	%C(15/75)	%O(15/75)	%N(15/75)	%S(15/75)	%Al(15/75)	%Si(15/75)	
10 min.	66.41/63.96	20.58/22.84	4.79/4.99	2.87/3.68	2.36/3.13	2.98/1.40	
20 mn.	67.76/67.56	20.08/20.21	4.964.82	3.6/3.95	1.82/2.67	1.78/0.79	
30 min	67.1/64.84	20.65/22.18	4.65/4.95	3.74/4.10	1.78/3.43	2.08/0.5	
40 min.	68.02/68.08	20.42/20.38	4.32/4.48	3.37/4.14	1.63/2.36	2.24/0.56	
50 mn.	70.52/67.17	17.77/19.82	4.54/5.78	3.35/3.60	1.96/2.97	1.86/0.67	
60 min.	67.22/65.94	20.7/21.40	4.82/5.01	3.10/3.75	2.05/3.10	2.12/0.81	

APPENDIX B

DERIVATION OF THE RELATIONSHIP BETWEEN NORMALIZED STRESS, STRAIN, AND MASS UPTAKE

From linear elastic theory, the stress-strain relationship of a homogeneous, elastic, isotropic material is:

$$E[d\epsilon_{ij} - \delta_{ij} (\beta dC + \alpha(T - T_o))] = (1 + \nu)d\sigma_{ij} - \nu d_{ij}d\sigma_{kk} \quad (B.1)$$

For a one dimensional stress and strain:

$$\sigma_{xx} = E[\epsilon_{xx} - \alpha\Delta T(x, y, z, t) - \beta\Delta C(x, y, z, t)] \quad (B.2)$$

At isothermal conditions:

$$\sigma_{xx} = E(\epsilon_{xx} - \beta\Delta C(x, y, z, t)) \quad (B.3)$$

For the average property through the volume:

$$\bar{\Gamma} = \frac{1}{V} \int \Gamma(x, y, z, t) dV \quad (B.4)$$

where $\bar{\Gamma} = \epsilon_{xx}, \sigma_{xx},$ or ΔC , and $V =$ volume of the sample

The average mass uptake per unit volume is:

$$\Delta\bar{C}(t) = \frac{1}{V} \int \Delta C(x, y, z, t) dV \quad (B.5)$$

The total amount of moisture absorbed by the film is:

$$M_t(t) = V\Delta\bar{C}(t) = \int \Delta C(x, y, z, t) dV \quad (B.6)$$

Integrate equation (3) through the volume:

$$\bar{\sigma}_{xx}(t) = E[\bar{\epsilon}_{xx}(t) - \beta \Delta \bar{C}(t)] \quad (\text{B.7})$$

Therefore, at constant stress, $\Delta \bar{\sigma}_{xx}(t) = 0$:

$$\Delta \bar{\epsilon}_{xx}(t) = \beta \Delta \bar{C}(t) \quad (\text{B.8})$$

where $\Delta \bar{\epsilon}_{xx}(t) = \bar{\epsilon}_{xx}(t) - \bar{\epsilon}_{xx}(0)$

Analogously, at constant strain, $\Delta \bar{\epsilon}_{xx}(t) = 0$:

$$\Delta \bar{\sigma}_{xx}(t) = -E\beta \Delta \bar{C}(t) \quad (\text{B.9})$$

where $\Delta \bar{\sigma}_{xx}(t) = \bar{\sigma}_{xx}(t) - \bar{\sigma}_{xx}(0)$

By normalizing equation (6), (8), and (9):

$$\frac{M_t}{M_\infty} = \frac{\Delta \bar{C}(t)}{\Delta \bar{C}(\infty)} = \frac{\Delta \bar{\sigma}_{xx}(t)}{\Delta \bar{\sigma}_{xx}(\infty)} = \frac{\Delta \bar{\epsilon}_{xx}(t)}{\Delta \bar{\epsilon}_{xx}(\infty)} \quad (\text{B.10})$$

APPENDIX C

OPTICAL MICROGRAPHS (REFLECTIVE MODE) OF FULLY PROCESSED POLY(URETHANE ACRYLATE) (PUA) AND POLY(AMIC ACID) METHACRYLIC ESTER (HRP) LITHOGRAPHIC PATTERNS

Figure C.1. Fully processed PUA lithographic patterns.

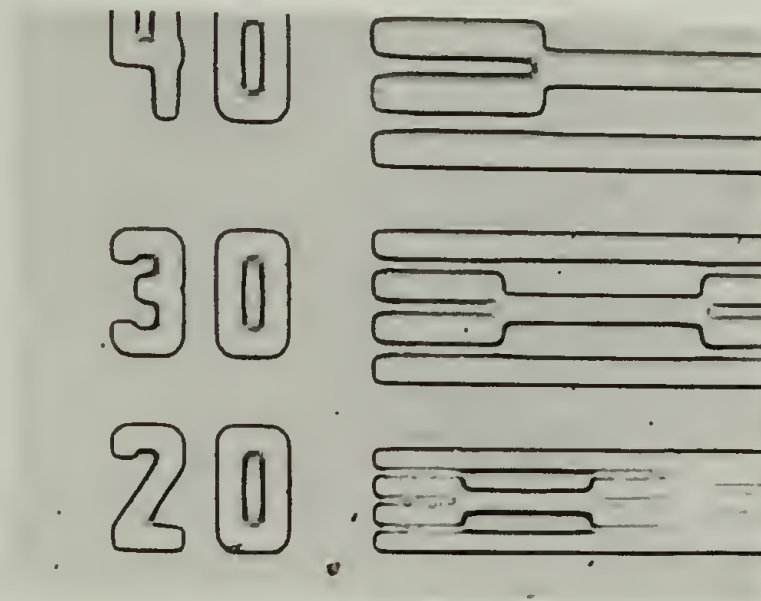


Figure C.2. Fully processed HRP lithographic patterns.



BIBLIOGRAPHY

- Alfrey, T., Gurnee, E.F., Lloyd, W.G., *J. Polym. Sci., Part C* **1966**, *12*, 249.
- Andrade, J.D., Gregonis, D.E., Smith, L.M., *Surface and Interfacial Aspects of Biomedical Polymers*, Plenum Press, New York, 1986.
- Arenholz, E., Heitz, J., Wagner, M., Baeuerle, D., Hibst, H., Hagenmeyer, A., *Appl. Surf. Sci.* **1993**, *69*, 16.
- Arfken, G. *Mathematical Methods for Physicists*; 3rd ed.; Academic Press: New York, 1985.
- Atkinson, J., Goh, C.J., Phan-Tien, N. *J. Chem. Phys.* **1984**, *80*, 6305.
- Avny, Y., Reubenfeld, L., *J. Appl. Polym. Sci.* **1986**, *32*, 4009.
- Bagassi, M., Chauveteau, G., Lecourtier, J., Englert, J., Tirrell, M. *Macromolecules* **1989**, *22*, 262.
- Berndt, P., Kurihara, K., Kunitake, T., *Langmuir* **1992**, *8*, 2486.
- Bertrand, P., DePuydt, Y., Beuken, J.M., Lutgen, P., Feyder, G., *Nucl. Instrum. Methods Phys. Res., Sect. B* **1987**, *B19-20*, 887.
- Besio, G. J., Prud'homme, R.K., Benziger, J.B. *Macromolecules* **1988**, *21*, 1070.
- Blaakmeer, J., Böhmer, M.R., Cohen Stuart, M.A., Fleer, G.J. *Macromolecules* **1990**, *23*, 2301.
- Boerio, F.J., Gosselin, C.A., *36th Ann. Conf. Reinf. Plast/-Composites Inst.*, SPI Paper 2G, 1981.
- Böhmer, M. R., Evers, O.A., Scheutjens, J.M.H.M. *Macromolecules* **1990**, *23*, 2288.
- Bowden, M. J., Turner, S.R. *Polymers for High Technology*; American Chemical Society: Washington, D.C., 1988.
- Bùi, L.N., Thompson, M., McKeown, N.B., Romaschin, A.D., Kalman, P.G., *Analyst* **1993**, *118*, 463.
- Caruso, F., Niikura, K., Furlong, D.N., Okahata, Y. *Langmuir* **1997**, *13*, 3422.
- Caruso, F., Niikura, K., Furlong, D.N., Okahata, Y. *Langmuir* **1997**, *13*, 3427.
- Chauveteau, G. *Adv. Chem. Series* **1986**, *213*, 227.

- Chen, W., McCarthy, T.J. *Macromolecules* **1997**, 30, 78.
- Cheung, J. H., Stockton, W.B., Rubner, M.F. *Macromolecules* **1997**, 30, 2712.
- Clark, D.T., Thomas, H.R., *J. Polym. Sci., Polym. Chem. Ed.* **1977**, 15, 2843.
- Cohen, Y. *Macromolecules* **1988**, 21, 494.
- Collin, R.J., U.S. Pat. 2,955,954, 1964.
- Cosgrove, T., Obey, T.M., Vincent, B. *J. Colloid Interface Sci.* **1986**, 111(2), 409.
- Crank, J., Park, G.S., *Trans. Faraday Soc.* **1949**, 45, 240.
- Crank, J., *The Mathematics of Diffusion*, Clarendon Press, Oxford, 1956.
- Crank, J., *Diffusion in Polymers*, Academic Press, New York, 1968.
- Dave, J., Kumar, R., Srivastava, H.C., *J. Appl. Polym. Sci.* **1987**, 33, 455.
- Decher, G., Hong, J.D., *Ber Bunsenges. Phys. Chem.* **1991**, 95, 1430.
- Decher, G., Hong, J. -D., Schmitt, J. *Thin Solid Films* **1992**, 210, 831.
- Decher, G., Schmitt, J. *Progr. Colloid. Polym. Sci.* **1992**, 89, 160.
- Decher, G., Hong, J.D., European Patent 0472 990 A2, 1992.
- Decher, G., Lvov, Y., Schmitt, J. *Thin Solid Films* **1994**, 244, 772.
- Decher, G., Ed., *Multilayer Films(Polyelectrolytes)*; CRC Press: Boca Raton; 1996, p. 4540.
- Decher, G., Eckle, M., Schmitt, J., Struth, B *Current Opinion in Colloid & Interface Science* **1998**, 3, 32.
- Delcorte, A., Bertrand, P., Arys, X., Jonas, A., Wischerhoff, E., Mayer, B., Laschewsky, A. *Surface Science* **1996**, 366, 149.
- Delcorte, A., Bertrand, P., Wischerhoff, E., Laschewsky, A. *Langmuir* **1997**, 13, 5125.
- Desai, N.P., Hubbell, J.A., *Macromolecules* **1992**, 25, 226.
- Dias, A. J., McCarthy, T.J. *Macromolecules* **1987**, 20, 2068.

- Evers, O. A., Fler, G.J., Scheutjens, J.M.H.M., Lyklema, J. *J. Colloid Interface Sci.* **1986**, *111*(2), 446.
- Farris, R.J., Vrtis, J.K., Jou, C., Chen, M.J., Sheth, K.C., *Adv. Coatings Tech. Conf.- Eng. Soc.*, **1994**.
- Felder, R.M., Huvard, G.S., *Methods of Experimental Physics*, Academic Press, New York, 1980.
- Ferreira, M., Cheung, J.H., Rubner, M.F. *Thin Solid Films* **1994**, *244*, 806.
- Ferreira, M., Rubner, M.F. *Macromolecules* **1995**, *28*, 7107.
- Fou, A. C., Rubner, M.F. *Macromolecules* **1995**, *28*, 7115.
- Fou, A. C., Onitsuka, O., Ferreira, M., Rubner, M.F., Hsieh, B.R. *J. Appl. Phys.* **1996**, *79*, 7501.
- Gettings, M., Kinloch, A.J., *J. Mater. Sci.* **1977**, *12*, 2511.
- Gettings, M., Kinloch, A.J., *Surface Interface Analysis* **1979**, *1*, 189.
- Gramain, P., Myard, P. *Macromolecules* **1981**, *14*, 180.
- Gray, A., Matthews, G.B. *Bessel Functions and Their Applications to Physics*, 1952.
- Hammond, P. T., Whitesides, G.M. *Macromolecules* **1995**, *28*, 7569.
- Hopfenberg, H.B., Frisch, H.L., *J. Polym. Sci., Part B.* **1969**, *7*, 405.
- Huh, C., Mason, S.G. *J. Colloid Interface Sci.*, **1977**, *60*, 11.
- Jennings, R.M., Taylor, J.F., Farris, R.J. *Journal of Adhesion* **1995**, *49*, 57.
- Johnson, R.E., Dettre, R.H. *J. Phys. Chem.* **1964**, *68*, 1744.
- Jou, C.S. Ph.D., Polymer Science and Engineering, **1993**.
- Keller, A., Odell, J.A. *Colloid Polymer Sci.* **1985**, *263*, 181.
- King, G. *Trans. Faraday Soc.* **1945**, *41*, 325.
- Kinloch, A.J., Dukes, W.A., Glandhill, R.A. *Adhesion Science and Technology*, Plenum Press, New York, 1975.
- Kirby, P. *PTF-A Review of Polymer Thick Film Technology* Patinel, England, 1990.

- Kleinfield, E. R., Ferguson, G.S. *Science* **1994**, 265, 370.
- Kleinfield, E. R., Ferguson, G.S. *Chem. Mater.* **1995**, 7, 2327.
- Laschewsky, A., Bayer, B., Wischerhoff, E., Arys, X., Bertrand, P., Delacorte, A., Jonas, A. *Thin Solid Films* **1996**, 284, 334.
- Laurent, D., Schlenoff, J.B. *Langmuir* **1997**, 13, 1552.
- Lee, J. J., Fuller, G.G. *Macromolecules* **1984**, 17, 375.
- Lee, J.-J., Fuller, G.G. *J. Colloid Interface Sci.* **1985**, 103, 569.
- Leväsalmi, J.-M., McCarthy, T.J. *Macromolecules* **1997**, 30, 1752.
- Long, F.A., Thompson, L.J., *J. Polym. Sci.* **1955**, 15, 413.
- Lvov, Y., Decher, G., Sukhorukov, G. *Macromolecules* **1993**, 26, 5397.
- Lvov, Y., Decher, G., Möhwald, H. *Langmuir* **1993**, 9, 481.
- Lvov, Y., Haas, H., Decher, G., Möhwald, H., Kalachev, A. *J. Phys. Chem.* **1993**, 97, 12835.
- Lvov, Y., Ariga, K., Kunitake, T. *Chem. Lett.* **1994**, 2323.
- Lvov, Y., Haas, H., Decher, G., Möhwald, H. *Langmuir* **1994**, 10, 4232.
- Lvov, Y., Ariga, K., Ichinose, I., Kunitake, T. *Langmuir* **1996**, 12, 3038.
- Maden, M.A., Farris, R.J. *Experimental Mechanics* **1991**, 31, 178.
- Maden, M.A., Ph.D., Polymer Science and Engineering, **1992**.
- Marra, J., van der Schee, H.A., Fleer, G.J., Lyklema, J., Ed., *Adsorption from Solution*; Academic Press: New York; 1983, p.245.
- Muilenberg, G.E., *Handbook of X-ray Photoelectron Spectroscopy*, Perkin-Elmer Corp., 1979.
- Newns, A.C., *Trans. Faraday Soc.* **1956**, 52, 1533.
- Onoda, M., Yoshino, K. *Jpn. J. Appl. Phys.* **1995**, 34, L260.
- Onoda, M., Lvov, Y., Ariga, K., Kunitake, T. *J. Ferment. Bioeng.* **1996**, 82, 502.

- Papenhuijzen, J., Fleer, G.J., Bijsterbosch, B.H. *J. Colloid Interface Sci.* **1985**, *104*, 530.
- Patrick, R.L., Brown, J.A., Cameron, N.M., Gehman, W.G., *Appl. Polym. Symp.* **1971**, *12*, 87.
- Perera, D.Y., Eynde, D.V. *Journal of Coatings Technology* **1987**, *59*, 55.
- Phuwanartnuruks, V., McCarthy, T.J. *Polym. Prepr. (Am. Chem. Soc. Div. Polym. Chem.)* **1997**, *38(1)*, 961.
- Plueddemann, E.P., *Silane Coupling Agents*, 2nd ed., Plenum Press, New York, 1990.
- Roberts, G. G., *Langmuir-Blodgett Films*, Plenum Press, New York, 1990.
- Robinson, R.A., *CRC Handbook of Chemistry and Physics*, CRC Press, Boca Raton, 1986.
- Sakinger, S.T., Ph.D., Polymer Science and Engineering, **1989**.
- Schmitt, J., Grunewald, G., Decher, G., Pershan, P.S., Kjaer, K., Losche, M. *Macromolecules* **1993**, *26*, 7058.
- Sheth, K.C., Ph.D., Polymer Science and Engineering, **1996**.
- Sih, G.C., Michopoulos, J.G., Chou, S.C., *Hygrothermoelasticity*, Martinus Nijhoff Publishers, Boston, 1986.
- Stepp, J., Schlenoff, J.B. *J. Electrochem. Soc.* **1997**, *144*, L155.
- Stockton, W. B., Rubner, M.F. *Macromolecules* **1997**, *30*, 2717.
- Strobel, M., Lyons, C.S., Strobel, J.M., Kapaun, R.S., *J. Adhes. Sci. Technol.* **1992**, *6*, 429.
- Sukhorukov, G. B., Schmitt, J., Decher, G. *Ber. Bunsenges. Phys. Chem.* **1996**, *100*, 948.
- Thomas, A.M., Gent, W.L., *Proc. Phys. Soc. Lond.* **1945**, *57*, 324.
- Tong, Q.K., Ph.D., Polymer Science and Engineering, **1993**.
- Torchin, N.G., Brown, J.T., Smith, R.H., U.S. Patent 3,380,831, 1968.
- Tsukruk, V. V., Rinderspacher, F., Bliznyuk, V. *Langmuir* **1997**, *13*, 2171.

- van der Schee, H. A., Lyklema, J. *J. Phys. Chem.* **1984**, 88, 6661.
- Vrentas, J.C., Duda, J.L., *AIChE J.* **1979**, 25, 1.
- Vrtis, J.K., Farris, R.J., *MRS Symp. Proc.* **1994**, 338, 527.
- Vrtis, J.K., Ph.D., Polymer Science and Engineering, **1995**.
- Wang, J., Feng, D., Wang, H., Remhold, M., Fritz, T., *J. Appl. Polym. Sci.* **1993**, 50, 585.
- Watanabe, S., Regan, S.L. *J. Am. Chem. Soc.* **1994**, 116, 8855.
- Watson, G.N. *A Treatise on the Theory of Bessel Functions*, 1962.
- Werner, E., Janocha, S., Hopper, M.J., MacKenzie, K.J., *Encyclopedia of Polymer Science and Engineering*, John Wiley & Sons, New York, 1989.
- Woods, R.J., Pikaev, A.K., *Applied Radiation Chemistry: Radiation Processing*, Wiley Interscience, New York, 1994.
- Yao, Z.P., Rånby, B., *J. Appl. Polym. Sci.* **1990**, 41, 1459.
- Zisman, W.A., *Adv. Chem. Ser.* **1964**, 68, 1744.

